The analysis of $\bar{p}p \rightarrow \pi^+\pi^-\pi^\circ\pi^\circ\pi^\circ$ in the $\pi^+\pi^-6\gamma$ Final State Part 2: The Spin Parity Analysis

Curtis A. Meyer
Universität Zürich

15 April, 1993

Abstract

This document is a detailed description of the spin parity analysis of $\bar{p}p \rightarrow \pi^+\pi^-\pi^\circ\pi^\circ\pi^\circ$. In addition to this, We find the that $\pi^+\pi^-\pi^\circ\pi^\circ\pi^\circ$ represent 0.091 ± 0.004 of all annihilations at rest. Excluding ω and η intermediate states, we find $\pi^+\pi^-\pi^\circ\pi^\circ\pi^\circ$ to represent 0.067 ± 0.004 of all annihilations at rest. From the spin parity analysis, we learn that much of the $\pi^+\pi^-\pi^\circ\pi^\circ\pi^\circ$ final state proceeds through an isoscaler ($J^{PC} = 0^{++}$) object decaying into $\rho^+\rho^-$. This f_0 object has a mass of 1437±13 MeV/c^2 and a width of 352±43 MeV/c^2. We find that

$$BR\left[\bar{p}p \rightarrow f_0\pi^\circ \rightarrow \rho^+\rho^-\pi^\circ \rightarrow (\pi^+\pi^\circ)(\pi^-\pi^\circ)\pi^\circ\right] = 0.022 \pm 0.004$$

We also see evidence for this f_0 decaying into $\sigma\sigma$.

$$BR\left[\bar{p}p \rightarrow f_0\pi^\circ \rightarrow \sigma\sigma\pi^\circ \rightarrow (\pi^+\pi^-)(\pi^\circ\pi^\circ)\pi^\circ\right] \approx 0.006$$

In addition to this 0^{++} object, we find evidence for a large contribution from $^3S_1$ initial state proceeding through probably two $J = 1$ objects. These may be the $b_1(1235) \rightarrow \rho\sigma$ and the $\rho^\circ{}' \rightarrow \rho^+\rho^-$. We find the ρ' to have a mass of 1530 MeV/c^2 and a width of 300 MeV/c^2. We find rather odd parameters for the $b_1(1235)$, mass 1350 MeV/c^2 and width 680 MeV/c^2. This is not completely understood.

We have also looked for the $f_2(1520) \rightarrow \rho^+\rho^-$. The data are consistent with a small contribution from this decay,

$$BR\left[\bar{p}p(^1S_0) \rightarrow f_2(1520)\pi^\circ \rightarrow \rho^+\rho^-\pi^\circ \rightarrow (\pi^+\pi^\circ)(\pi^-\pi^\circ)\pi^\circ\right] \leq 0.00201,$$

but certainly do not require this contribution.

Contents

List of Figures

List of Tables

1 Introduction

In this note, I describe in detail the spin parity analsysis of the $\pi^+\pi^-\pi^\circ\pi^\circ\pi^\circ$ final state. This analysis is quite different from preexisting crystal barrel analysises due to the large number of final state particles. It is not possible to carry out a Dalitz plot analysis as has usually been done. Rather, an unbinned maximum liklihood fit in the 8–dimensional $\pi^+\pi^-\pi^\circ\pi^\circ\pi^\circ$ phase space has been performed.

This document is part 2 of a detailed description of the analysis of the $\pi^+\pi^-\pi^\circ\pi^\circ\pi^\circ$ final state. It is assumed throughout that the reader is familar with part 1 of this document[1]. All details of how the data have been reconstructed are described in the previous document, and will not be repeated here. The starting point for this description will be the 38266 7–C fit $\pi^+\pi^-\pi^\circ\pi^\circ\pi^\circ$ events obtained in the previous document. Also used are a sample of 569787 Monte Carlo, CBGEANT, events which yield a sample of 72997 7–C fit $\pi^+\pi^-\pi^\circ\pi^\circ\pi^\circ$ Monte Carlo events at 15% confidence level.

2 Survey of the Data

Before continuing, it is necessary to identfy the obvious features in the data. If we assume that the $\pi^+\pi^-\pi^\circ\pi^\circ\pi^\circ$ final state is reached through a series of quasi two–body processes, then we need to identify potential 4π, 3π and 2π objects. The following decay chains are possible:

$$\begin{aligned}
\bar{p}p &\rightarrow A\pi, A \rightarrow BC, B \rightarrow \pi\pi, C \rightarrow \pi\pi \\
\bar{p}p &\rightarrow A\pi, A \rightarrow B\pi, B \rightarrow C\pi, C \rightarrow \pi\pi \\
\bar{p}p &\rightarrow AB, A \rightarrow C\pi, B \rightarrow \pi\pi, C \rightarrow \pi\pi.
\end{aligned}$$

2.1 The 4π Invariant Mass

In order to identify what the A, B and C objects could be, I have produced both *invariant mass* plots, and *difference* plots. The best example of both of these is shown in figure 2.1. In this figure are shown two invariant mass plots, that for $\pi^+\pi^-\pi^\circ\pi^\circ$ which contains 3 entries per event, and that for $\pi^\pm\pi^\circ\pi^\circ\pi^\circ$, which contains 2 entries per event. The difference plot defined as the former minus the latter, and is also shown. The idea behind this is that if there is something in the former spectra, but not in the latter spectra, then the latter is a good measure of the bad combinations in the former. By subtracting the two, one is left with only the *good* combination. It is important to note that we have subtracted 2 entries per event from 3 entries per event, which yields 1 entry per event. The resulting difference spectra is also shown more clearly in figure 2.2. In this figure, I have labeled a structure near 1200 as the b_1. This is the b_1° decaying to $\omega\pi^\circ$. It is not possible to have a charged b_1 here, as both charged particles are needed to form the ω. There is also a large peak near 1500 labeled the ζ and a peak near the end of the spectra labeled accpetance. The latter peak is an artifact of the fact that we have a lower momentum cut–off for neutral pions than that for charged pions. Finally the ζ peak is what as been seen in $\bar{p}d$ and fit to both a 0^{++} and 2^{++} object [2] ,[3],[4], [5],[6], [7]. In order to indicate that these peaks are significant, I have also provided the corresponding Monte Carlo plots from $\pi^+\pi^-\pi^\circ\pi^\circ\pi^\circ$ phase space. Figures 2.3 and 2.4 show that the previous peaks cannot be generated by simple phase space.

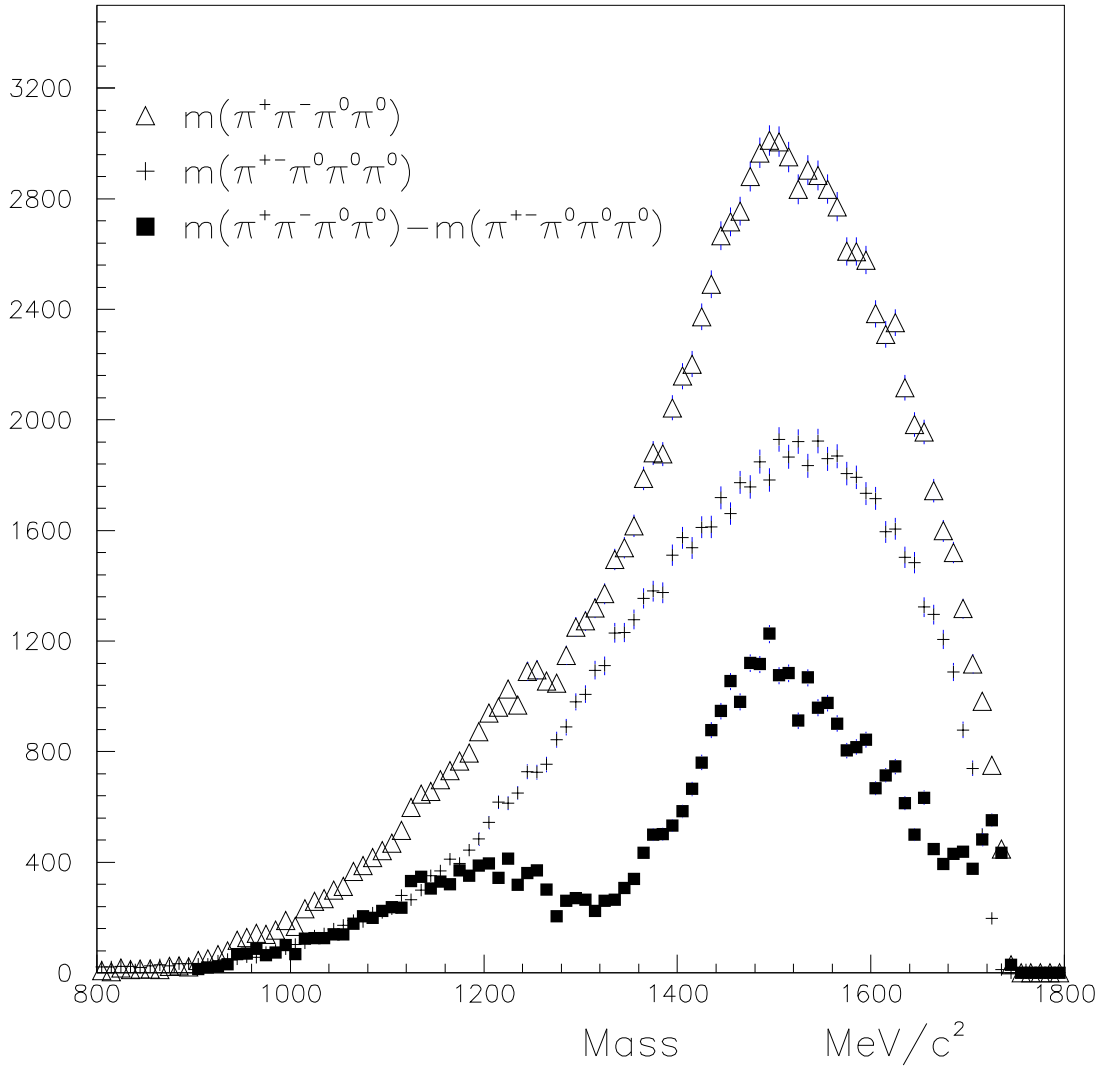

Figure 2.1: The 4π invariant mass spectrum. The $\triangle$ show the $\pi^+\pi^-\pi^\circ\pi^\circ$ invariant mass, (three entries per event). The $+$ show the $\pi^\pm\pi^\circ\pi^\circ\pi^\circ$ invariant mass, (two entries per event). The $\blacksquare$ show the difference between the two previous spectra.

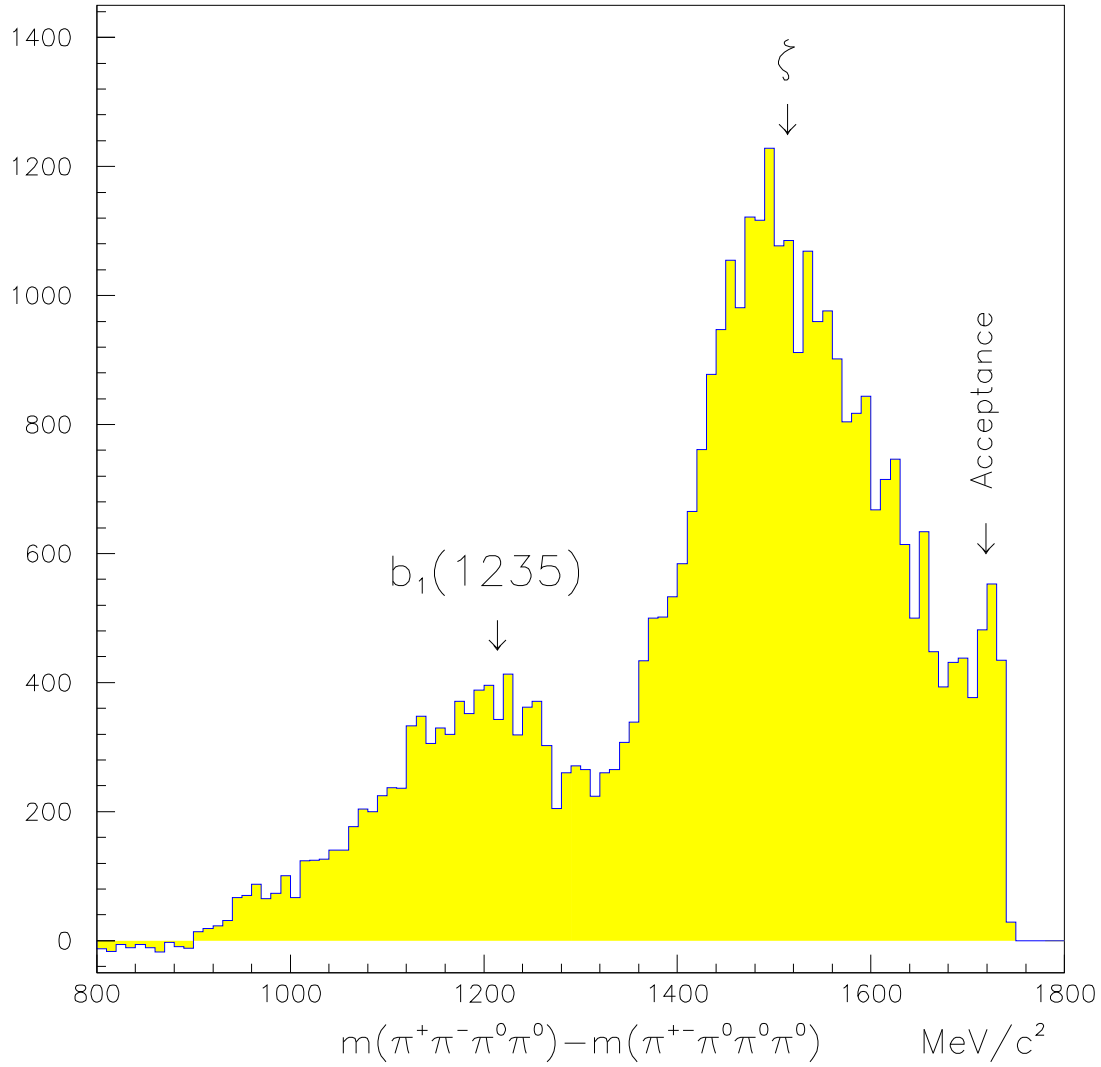

Figure 2.2: The difference spectra between the 3 $\pi^+\pi^-\pi^\circ\pi^\circ$ combinations and the 2 $\pi^\pm\pi^\circ\pi^\circ\pi^\circ$ combinations per event. The lower peak labeled b_1 arises from the $b_1 \rightarrow \omega\pi^\circ$ decay. The peak labled *Acceptance* arises from the difference in acceptance between the charged and neutral π's.

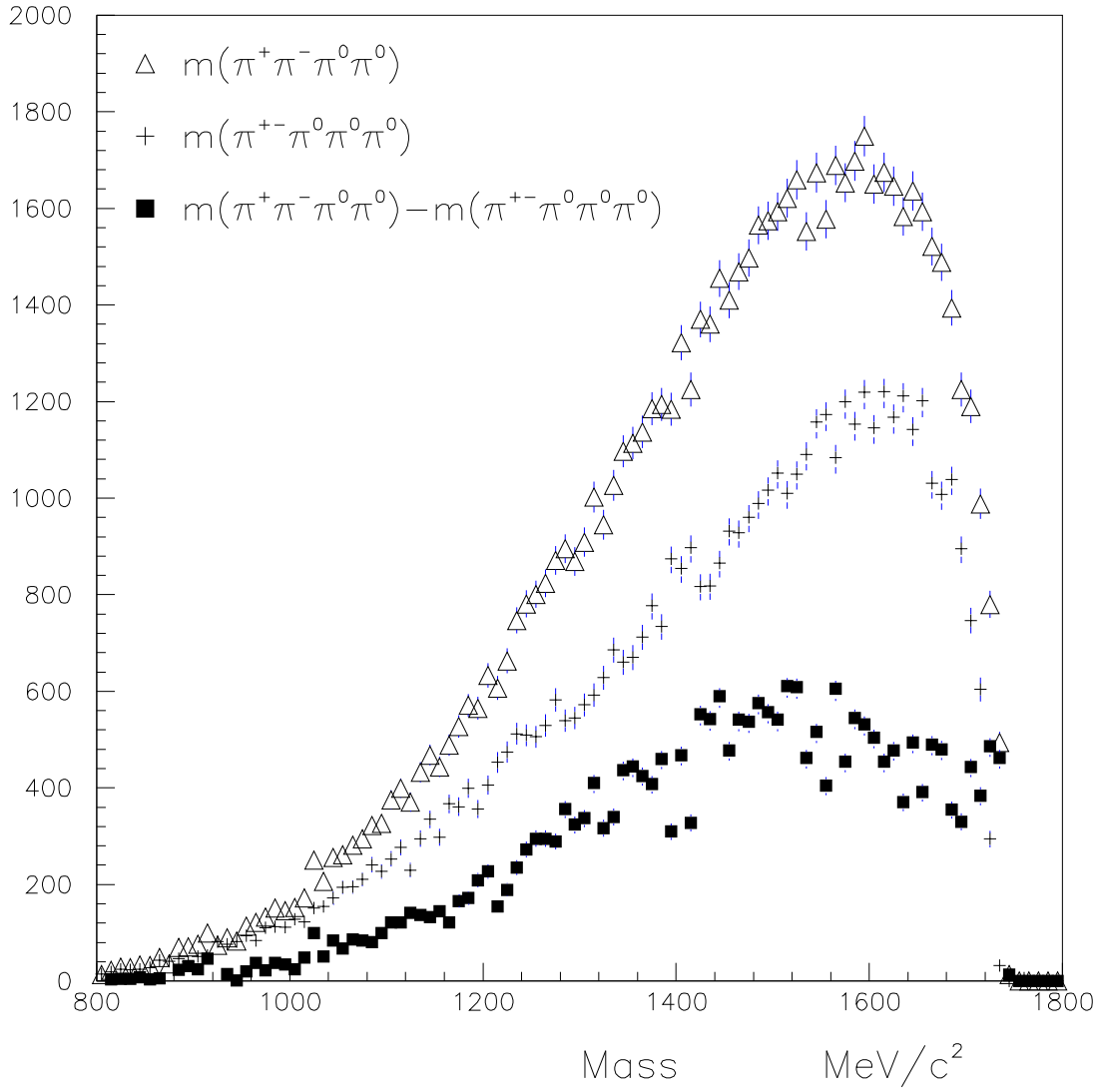

Figure 2.3: The 4π invariant mass spectrum for Monte Carlo. The $\triangle$ show the $\pi^+\pi^-\pi^\circ\pi^\circ$ invariant mass, (three entries per event). The $+$ show the $\pi^\pm\pi^\circ\pi^\circ\pi^\circ$ invariant mass, (two entries per event). The $\blacksquare$ show the difference between the two previous spectra.

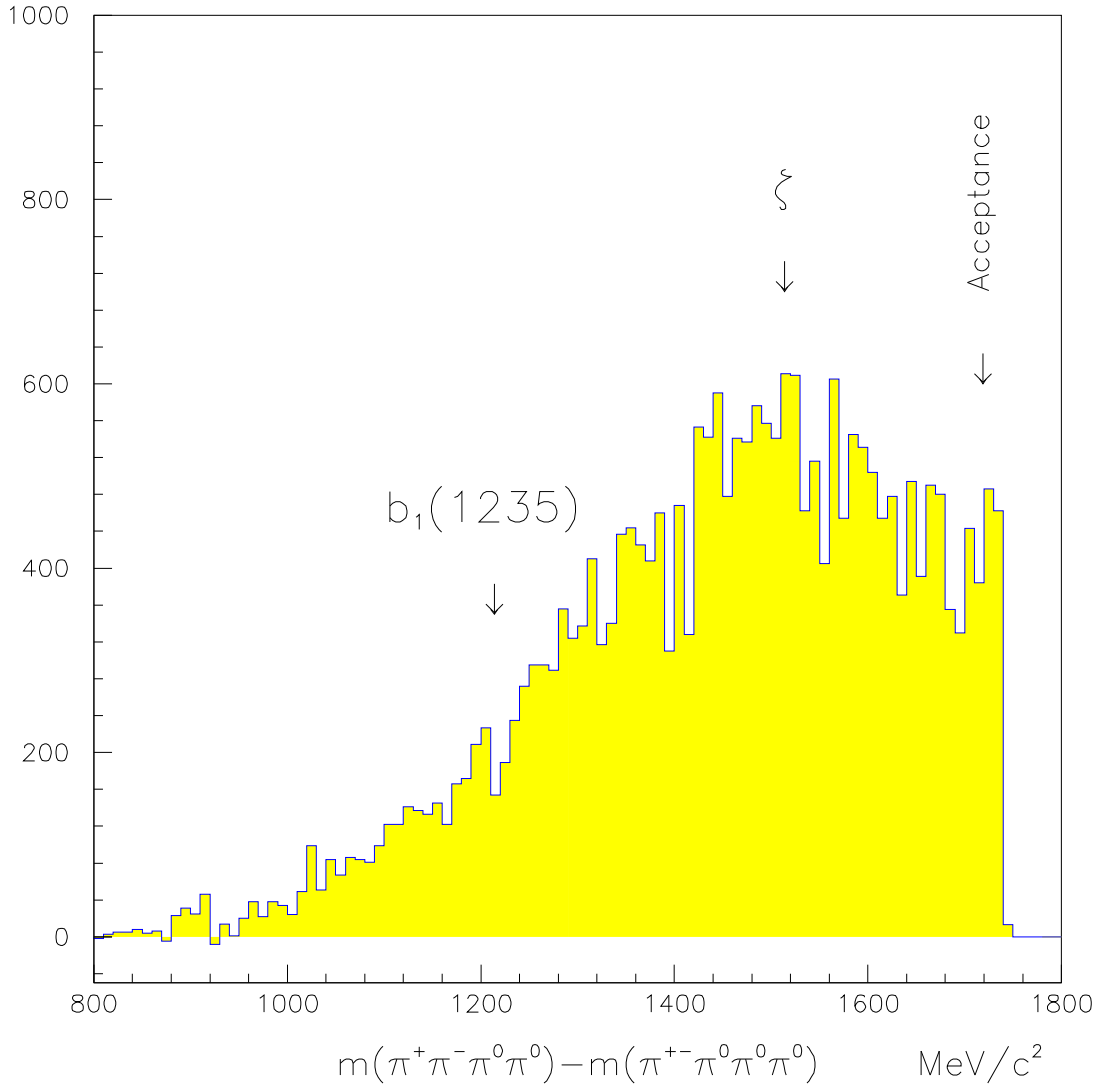

Figure 2.4: The difference spectra between the 3 $\pi^+\pi^-\pi^\circ\pi^\circ$ combinations and the 2 $\pi^\pm\pi^\circ\pi^\circ\pi^\circ$ combinations per event. The lower peak labeled b_1 arises from the $b_1 \rightarrow \omega\pi^\circ$ decay. The peak labled *Acceptance* arises from the difference in acceptance between the charged and neutral π's.

2.2 The 3π Invariant Masses

We next consider the 3π invariant masses. The four possible masses are shown in figure 2.5. In these spectra, the only obvious structures are the η and ω as discussed in the previous note, ([1]). As a comparison, the 3π mass spectra formed from Monte Carlo $\pi^+\pi^-\pi^\circ\pi^\circ\pi^\circ$ phase space are shown in figure 2.6. As with the real data, the locations of the η and ω are marked. However, in principle the η and ω are not the only 3π objects in the mass range from 400 to 1500 MeV/c. We might expect to see the following mesons via their $\rho\pi$ decays.

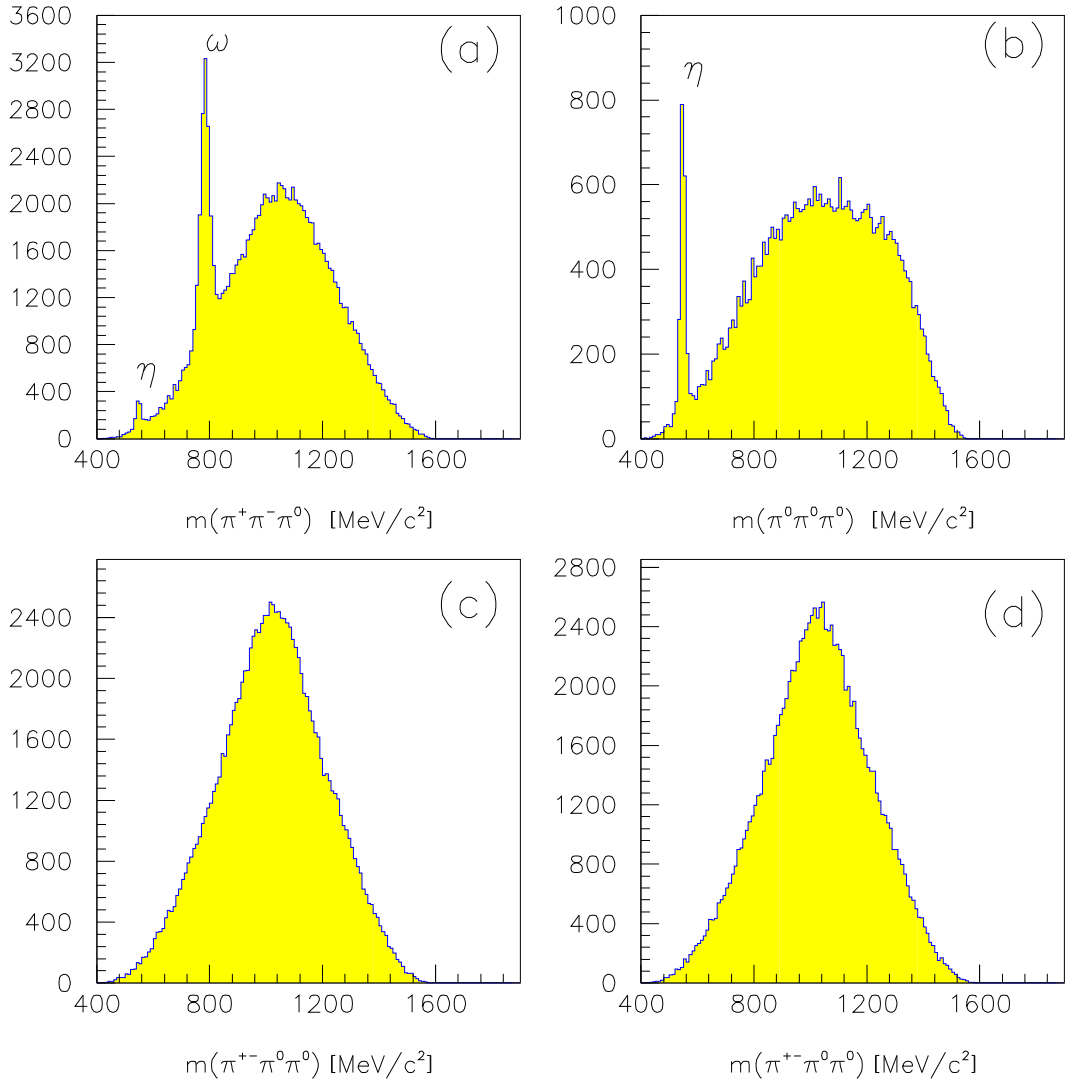

Figure 2.5: The four 3π invariant mass combinations. (**a**) shows $\pi^+\pi^-\pi^\circ$, where one sees the η and the ω, (three entries per event). (**b**) shows the single $3\pi^\circ$ combination per event. One only sees the η. **c** and **d** Show the $\pi^\pm\pi^\circ\pi^\circ$ invariant masses, (three entries per event). There is no obvious structure.

- $\phi(1020) \rightarrow \rho^\pm\pi^\mp \rightarrow \pi^+\pi^-\pi^\circ$
- $\phi(1020) \rightarrow \rho^\circ\pi^\circ \rightarrow \pi^+\pi^-\pi^\circ$
- $h_1(1170) \rightarrow \rho^\pm\pi^\mp \rightarrow \pi^+\pi^-\pi^\circ$

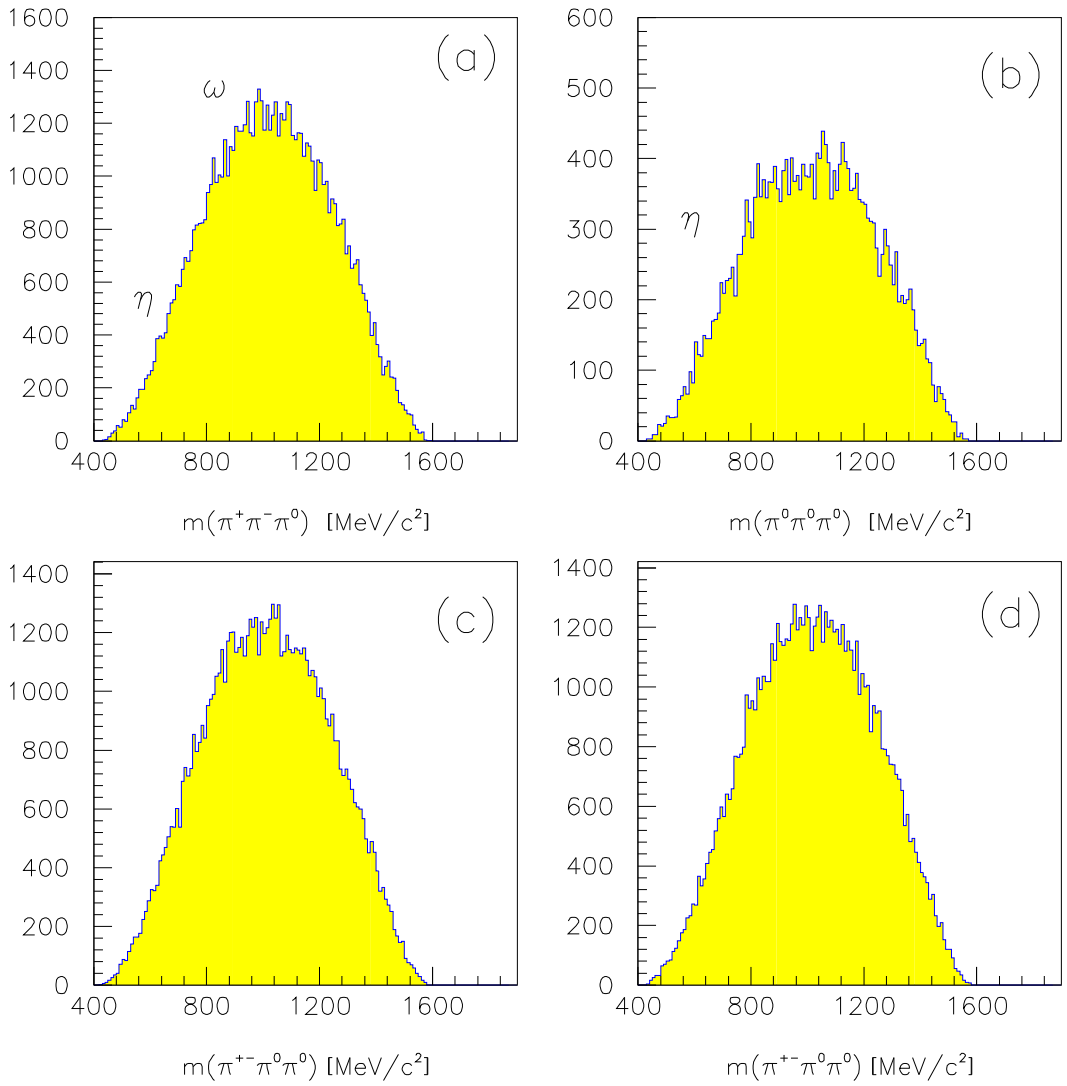

Figure 2.6: The four 3π invariant mass combinations for Monte Carlo. (**a**) shows $\pi^+\pi^-\pi^\circ$, where one sees the η and the ω, (three entries per event). (**b**) shows the single $3\pi^\circ$ combination per event. One only sees the η. **c** and **d** Show the $\pi^\pm\pi^\circ\pi^\circ$ invariant masses, (three entries per event). There is no obvious structure.

- $h_1(1170) \rightarrow \rho^\circ\pi^\circ \rightarrow \pi^+\pi^-\pi^\circ$
- $a_1^+(1260) \rightarrow \rho^{+\circ}\pi^{\circ+} \rightarrow \pi^+\pi^\circ\pi^\circ$
- $a_1^-(1260) \rightarrow \rho^{-\circ}\pi^{\circ-} \rightarrow \pi^-\pi^\circ\pi^\circ$
- $a_1^\circ(1260) \rightarrow \rho^\pm\pi^\mp \rightarrow \pi^+\pi^-\pi^\circ$
- $a_2^+(1320) \rightarrow \rho^{+\circ}\pi^{\circ+} \rightarrow \pi^+\pi^\circ\pi^\circ$
- $a_2^-(1320) \rightarrow \rho^{-\circ}\pi^{\circ-} \rightarrow \pi^-\pi^\circ\pi^\circ$
- $a_2^\circ(1320) \rightarrow \rho^\pm\pi^\mp \rightarrow \pi^+\pi^-\pi^\circ$
- $\omega(1390) \rightarrow \rho^\pm\pi^\mp \rightarrow \pi^+\pi^-\pi^\circ$
- $\omega(1390) \rightarrow \rho^\circ\pi^\circ \rightarrow \pi^+\pi^-\pi^\circ$

None of these final states should be seen in $3\pi^\circ$, and the ϕ, h_1 and $\omega(1390)$ would only be seen in $\pi^+\pi^-\pi^\circ$. In order to look for these, the 3π difference spectra have been formed, and are shown in figure 2.7. Again, we see quite clearly the prescence of both the η and the ω. I have also indicated in the various plots where we would expect to see the other objects. There is clearly no strong evidence for the ϕ, $a_1(1260)$, $a_2(1320)$ or $\omega(1390)$. However, we could not rule out the $h_1(1190)$.

In order to try and get a better feeling for these spectra, I have also presented similar Monte Carlo spectra. Figure 2.8 shows the spectra for $\pi^+\pi^-\pi^\circ\pi^\circ\pi^\circ$ phase space. Figure 2.9 shows the spectra for the $\omega\pi^\circ\pi^\circ$ sample, and figure 2.10 shows the spectra for the $\eta\pi^+\pi^-$ Monte Carlo sample. The combination of all of these plots leads me to conclude that other than the ω and η, there are no significant contributions from other 3π objects. In particular, the bump in the $h_1(1170)$ region can probably be simulated with a combination of phase space, and $\eta \rightarrow 3\pi^\circ$. To facilitate analysis, I will remove both the ω and the η using simple cuts in the invariant mass spectra. These cuts are described in section 3.1.

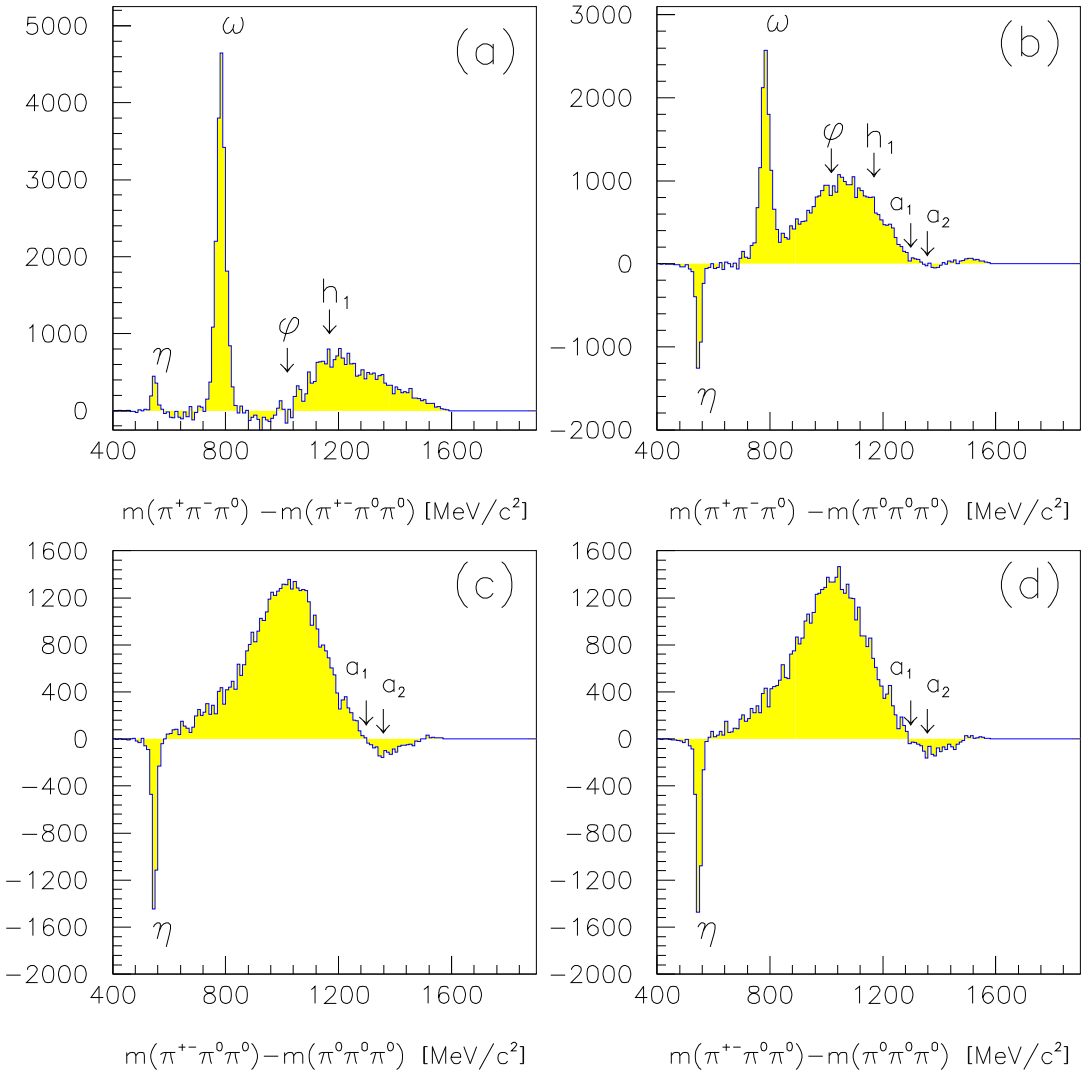

Figure 2.7: The four 3π invariant mass differences. These are weighted such that there is one positive entry per event. The arrows labled ϕ, h_1, a_1 and a_2 indicate where one would expect to see these resonances from their $\rho\pi$ decay modes.

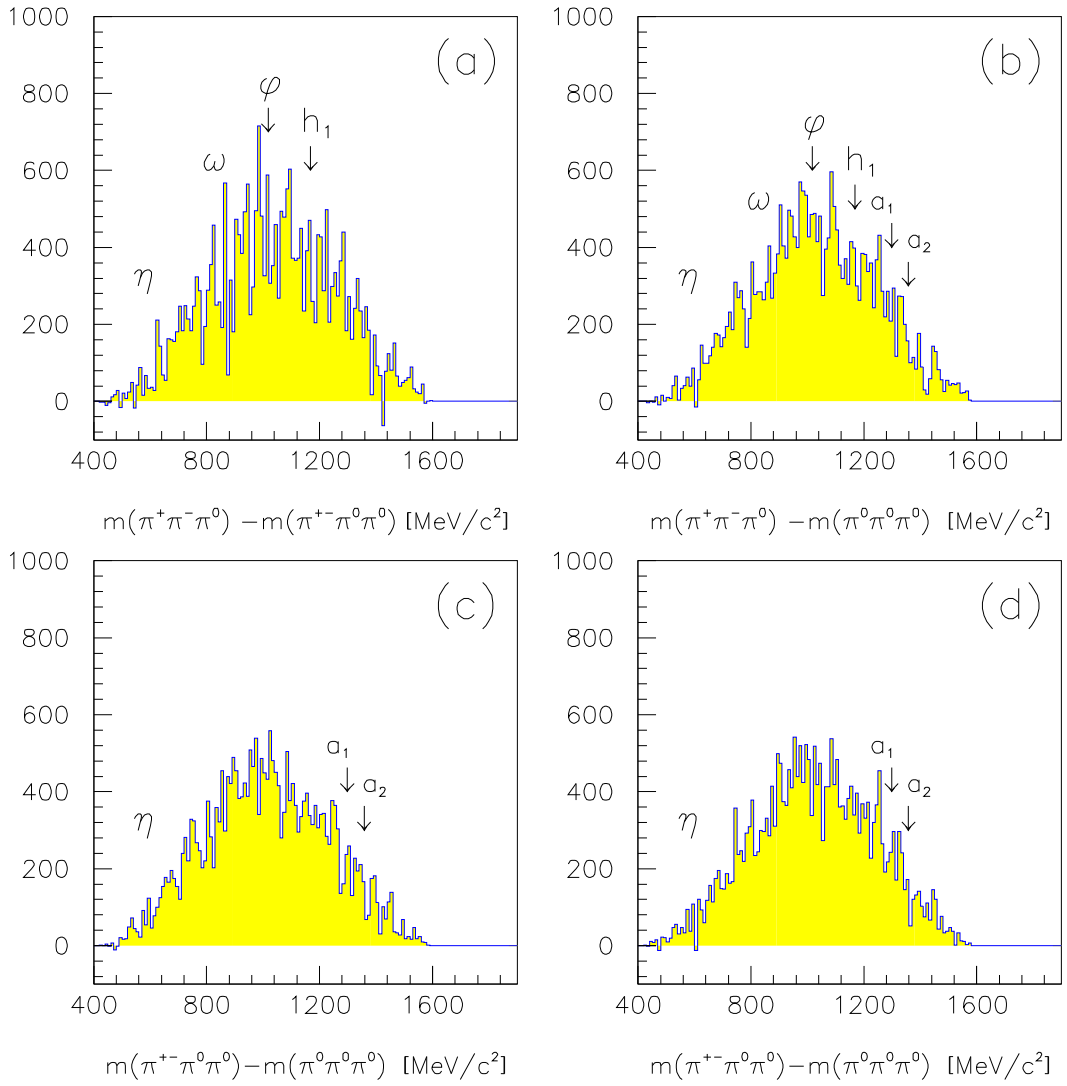

Figure 2.8: The four 3π invariant mass differences for Monte Carlo. These are weighted such that there is one positive entry per event. The arrows labled ϕ, h_1, a_1 and a_2 indicate where one would expect to see these resonances from their $\rho\pi$ decay modes.

Figure 2.9: The four 3π invariant mass differences for Monte Carlo $\omega\pi^\circ\pi^\circ$. These are weighted such that there is one positive entry per event. The arrows labled ϕ, h_1, a_1 and a_2 indicate where one would expect to see these mesons in their $\rho\pi$ decay modes.

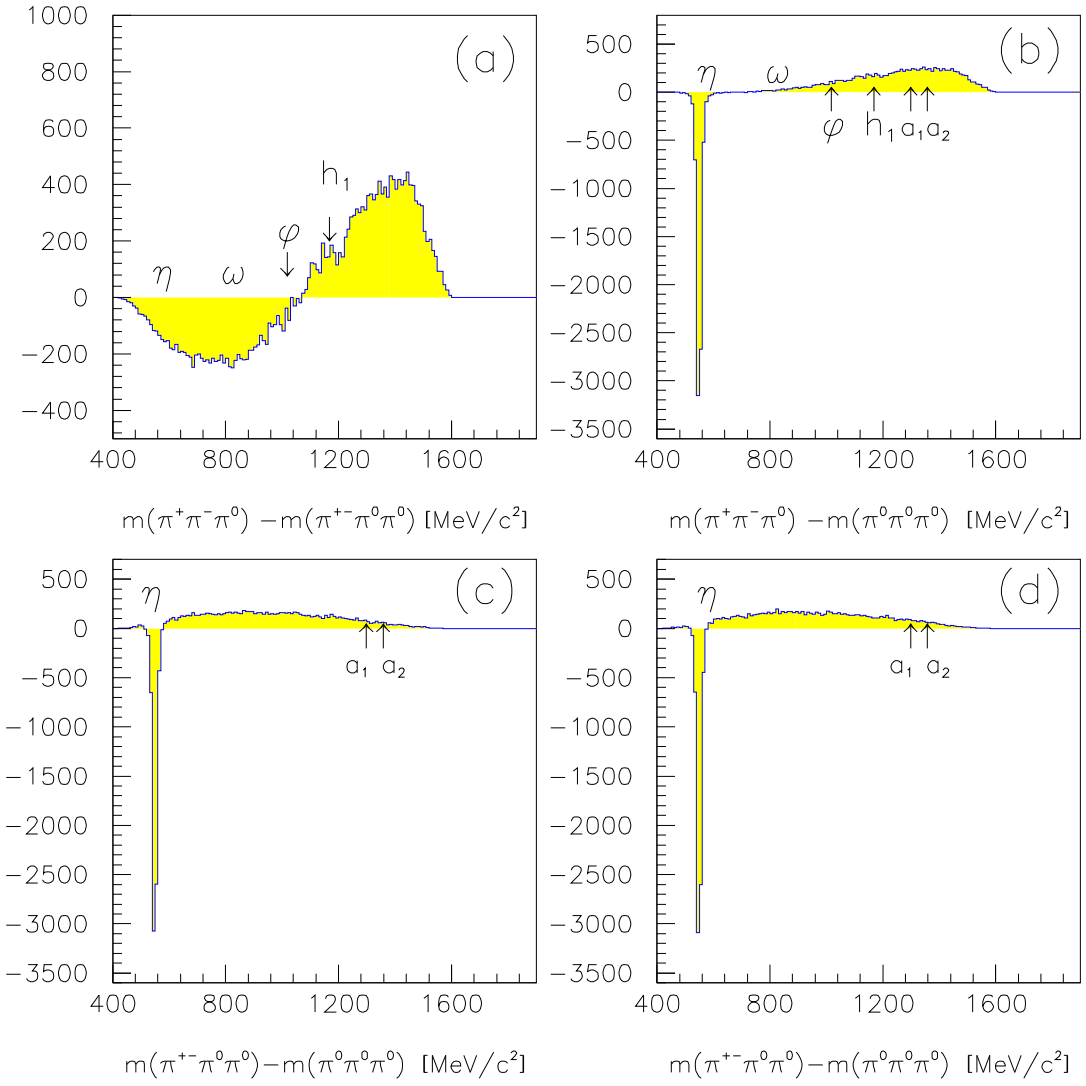

Figure 2.10: The four 3π invariant mass differences for Monte Carlo $\eta\pi^+\pi^-$. These are weighted such that there is one positive entry per event. The arrows labled ϕ, h_1, a_1 and a_2 indicate where one would expect to see these mesons in their $\rho\pi$ decay modes.

2.3 The 2π Invariant Masses

After removing the η and the ω from the data sample, we need to examine the 2π mass spectra. These plots are shown in figure 2.11. We see clear evidence for all three charge states of the $\rho(770)$, while at the indicated position of the $f_0(950)$, we see essentially nothing. Because of this, I will only consider two possible 2π objects, the $\rho(770)$, and the $(\pi\pi)$ S–Wave as given by the A.M.P. parametrization.

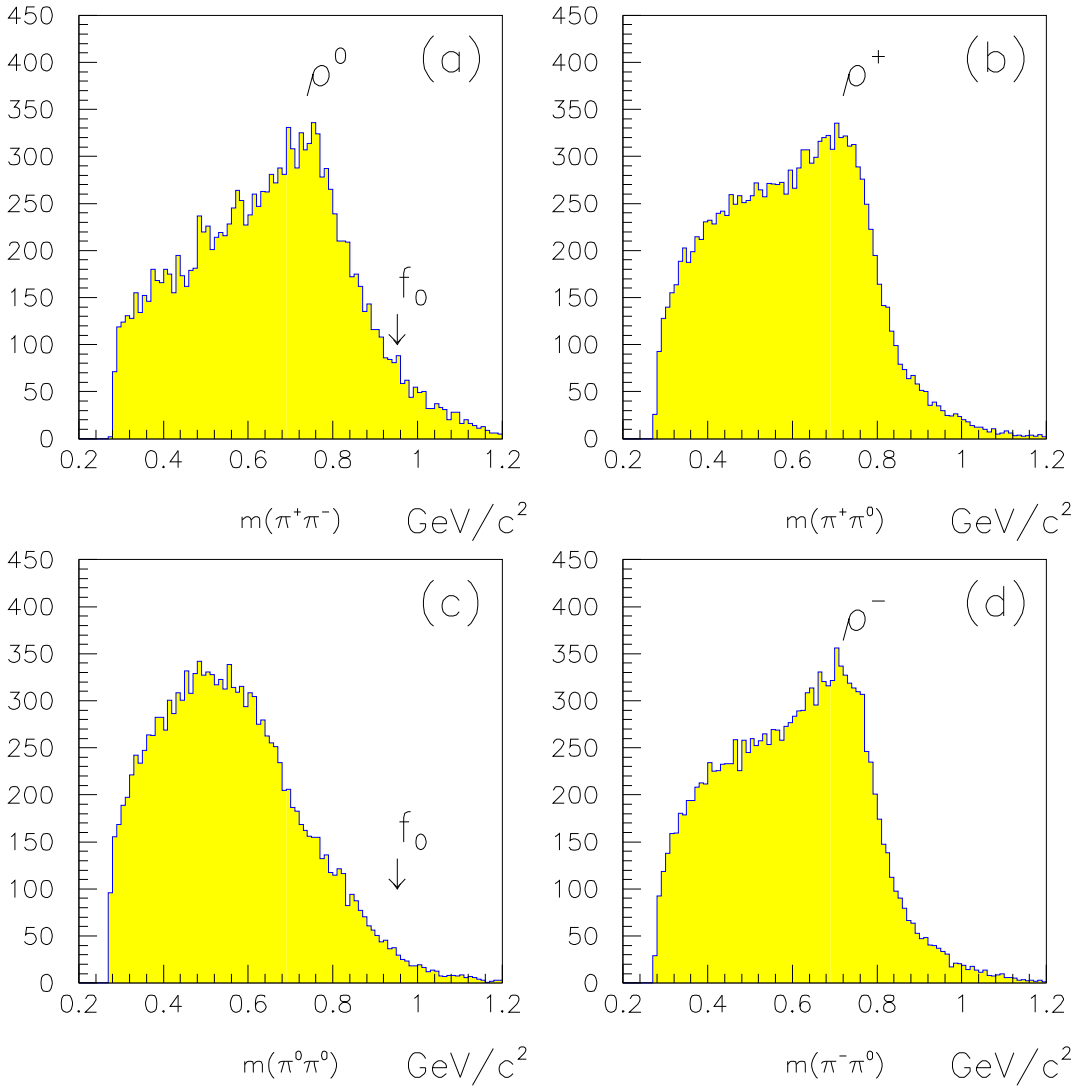

Figure 2.11: These figures show the four possible 2π invariant mass combinations. The ω and η decays to 3π's have been removed. The three charged states of the ρ are clearly seen. The arrows labled f_0 indicate where one should see the $f_0(950)$ in its 2π decay.

In order to try and see if the inermediate state $\rho^+\rho^-\pi^\circ$ does indeed contribute, we can plot the $\pi^+\pi^\circ$ invariant mass against the $\pi^-\pi^\circ$ invariant mass, (different π°'s are chosen for the two invariant masses). This plot leads to six entries per event, and is shown in figure 2.12. There is a clear enhancement in the $\rho\rho$ region of the plot. However, it is also clear that there is more than just $\rho\rho$ in the data; we need to consider $\rho\pi\pi\pi$ in addition to $\rho\rho\pi$.

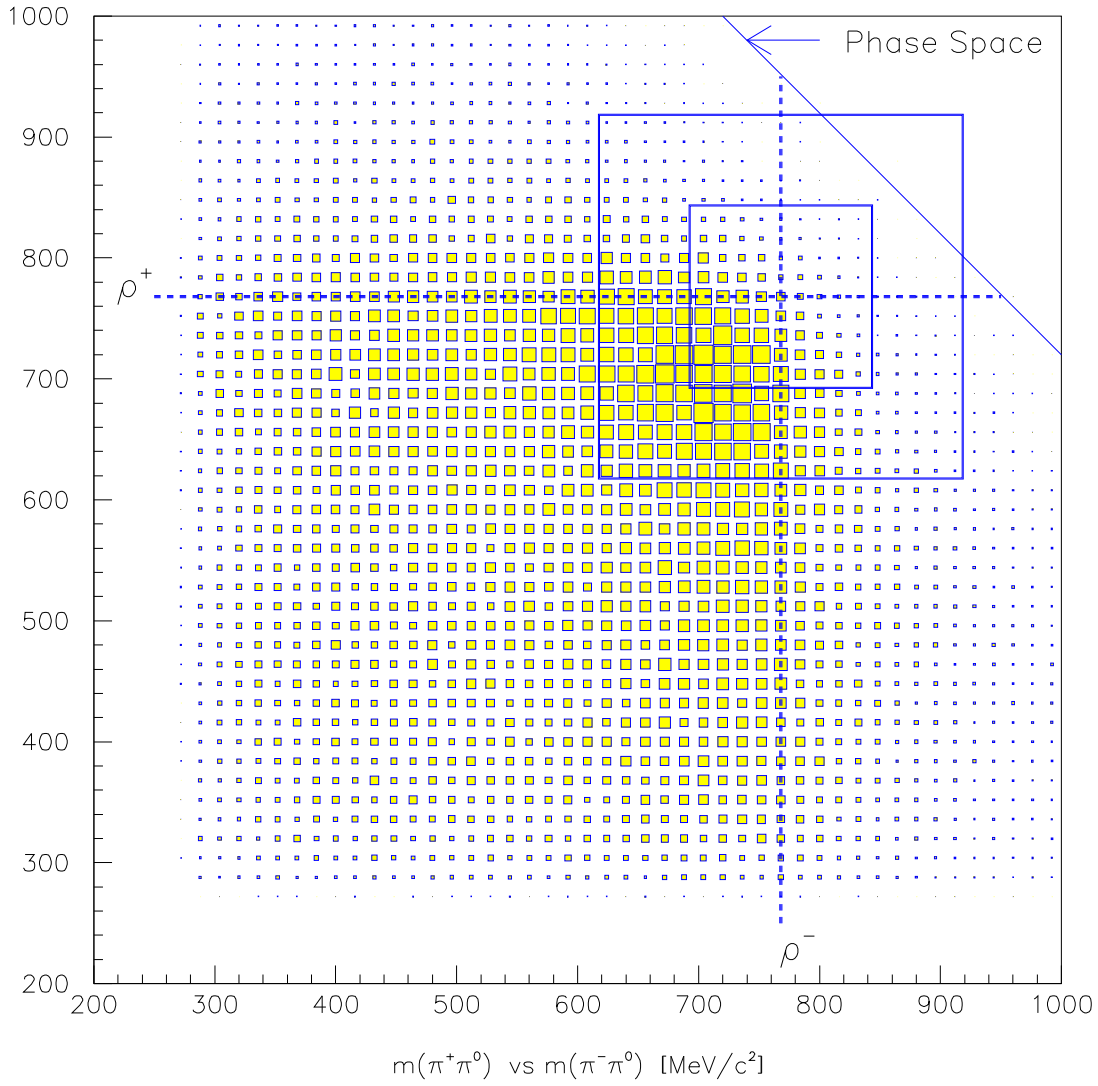

Figure 2.12: The $\pi^-\pi^\circ$ invariant mass plotted against the other two $\pi^+\pi^\circ$ invariant masses. There are six entries per event in this plot. The diagonal line in the upper right corner shows the approximate phasespace limit for these data. The nominal ρ^+ and ρ^- masses are shown with the dashed lines. The two boxes are centered on the $\rho(770)$ masses, and show a full width of 1Γ and 2Γ. Both ρ masses are supressed due to phasespace limits, but there is a clear enhancement in the $\rho^+\rho^-$ region.

2.4 The $\pi^+\pi^-\pi^\circ\pi^\circ\pi^\circ$ Branching Fraction

In part one of this document [1], I have derived a number of three body branching fractions. At this point, I will return to the branching ration point, and derive two fractions useful in this note. I start with the numbers in section 1 for both real and Monte Carlo data:

- 38,266 7–C fit $\pi^+\pi^-\pi^\circ\pi^\circ\pi^\circ$ events at a 15% confidence level cut. These events arise from a $\bar{p}$–stop sample of 3,346,403$\pm$ 50,915 events [1].
- 72997 7–C fit $\pi^+\pi^-\pi^\circ\pi^\circ\pi^\circ$ Monte Carlo events at a 15% confidence level cut. These events arise from 569,797 CBGEANT events.

The Monte Carlo events lead to a reconstruction efficiency for simple five π phase space of

$$\epsilon_{5\pi} = \frac{72997}{569797} = 0.1281 \pm 0.0005.$$

However, in [1], we have seen that the efficiency for final states involving narrow 3π objects are:

$$\begin{aligned} \epsilon_{\omega\pi\pi} &= 0.128812 \pm 0.003388 \\ \epsilon_{\eta\pi^\circ\pi^\circ} &= 0.120712 \pm 0.005713 \\ \epsilon_{\eta\pi^+\pi^-} &= 0.112023 \pm 0.006625 \end{aligned}$$

It also has been seen that the effect of broad resonances on the above three efficiencies is typically ± 0.005. We also recall that the $\eta \to 3\pi^\circ$ decay is problematic, and this may lead to the lower efficiency value. As such, if we only take the first three numbers, we can obtain an efficiency as the average:

$$\epsilon_{5\pi} = 0.126 \pm 0.005,$$

where the rather large error is due to the contributions of broad intermediate resonances. Given these numbers, we then compute that:

$$BR(\bar{p}p \to \pi^+\pi^-\pi^\circ\pi^\circ\pi^\circ) = 0.0908 \pm 0.0039 = 0.091 \pm 0.004 \quad (1)$$

Using this number, we can subtract the contributions from the $\omega\pi\pi$ and $\eta\pi\pi$ data. These numbers can be recomputed from the data in [1] to remove the uncertainty from the decays of the ω and η. As seen in $\pi^+\pi^-\pi^\circ\pi^\circ\pi^\circ$, we find:

- For $\omega\pi^\circ\pi^\circ$, we find 0.0213 ± 0.0008.
- For $\eta\pi^\circ\pi^\circ$,we find 0.00144 ± 0.00016.
- For $\eta\pi^+\pi^-$, we find 0.00445 ± 0.00033.

Summing the above three yields 0.0272 ± 0.0009, which we can subtract from 0.0908 ± 0.0039 to yield an ω and η free branching fraction of:

$$BR(\bar{p}p \to \pi^+\pi^-\pi^\circ\pi^\circ\pi^\circ = 0.064 \pm 0.004 \quad (2)$$

Alternatively, we can remove the η and ω from the $\pi^+\pi^-\pi^\circ\pi^\circ\pi^\circ$ sample by cutting at 3σ, (see section 3.1). This yields 23,220 real events, and 56,166 Monte Carlo events. We then use the Monte Carlo numbers to yield an efficeincy of:

$$\epsilon_{5\pi} = 0.09857 \pm 0.005,$$

where the larger error is used to account for intermediate resonances. Combining yields:

$$BR(\bar{p}p \to \pi^+\pi^-\pi^\circ\pi^\circ\pi^\circ) = 0.0704 \pm 0.0038. \quad (3)$$

These previous two numbers are consistent within errors. For all proceeding dicusion, I will take the simple average of them. I will however retain the full error due to the samples not being independent. This then yields an $\omega-$ η–free branching fraction of:

$$BR(\bar{p}p \to \pi^+\pi^-\pi^\circ\pi^\circ\pi^\circ) = 0.067 \pm 0.004. \tag{4}$$

This number will be used later in these analysis to estimate branching fractions into broad resonances.

3 The Fitting Procedure and Parametrization of the Data

3.1 Definition of the Problem

From the previous survey of the data, we will make the assumption that after the ω and η have been removed, all the data can be described via a reaction of the form of equation 5. We will also assume that for the B and C mesons, we will only use the $\rho(770)$ and the $\pi\pi$ s–wave parametrization, (A.M.P.).

$$\bar{p}p \quad \rightarrow \quad A\pi, A \rightarrow BC, B \rightarrow \pi\pi, C \rightarrow \pi\pi \tag{5}$$

To begin with, it is necessary to explain how we remove the ω and the η. In the case of the ω, the 3 $\pi^+\pi^-\pi^\circ$ invariant mass combinations are formed for each event. If at least one of these combinations is in a 3σ ω window defined as $m_\omega \pm$ 52.5 MeV, the event is rejected. For the η, the lone $3\pi^\circ$ invariant mass is first checked to see if it falls in a 3σ η window of $\pm$ 23.5 MeV around m_η. Then the 3 $\pi^+\pi^-\pi^\circ$ invariant masses are checked to see if at least one of them is also in the η window. If any of the above conditions is satisfied, the event is rejected. Rejecting all events which satisfy at least one of the above conditions leaves a sample of 23220 ω–, η–free $\pi^+\pi^-\pi^\circ\pi^\circ\pi^\circ$ events. A similar cut on the 72997 Monte Carlo events yields 56166 events. The higher acceptance for the Monte Carlo sample arise from the fact that there are no real ω's or η's in the Monte Carlo sample.

In order to describe the data, we need to define a set of coordinates. Given that we have 5 particles in the final state, 8 variables should be sufficient to completely describe the system. Five particles leads to 20 variables, however energy and momentum conservation reduce this to 16. Next, because we know the masses of the five particles, this reduces to 11. Finally, we are allowed to choose our coordinate system, this then reduces us to 8 variables. However, because there is no unique description of how we build A, B and C, there will be interference between the choices. For example, given that we say B is a ρ^+ and C is a ρ^-, then there are 3 ways we can form B from our pions, and for each of these, there are 2 ways to form C. We have six ways to put the event together. When we go to compute the helicity amplitude for the event, we need to compute all the angles relative to the **same** coordinate system. As such, once we have defined the coordinate system relative to one of the 6 solutions, we are stuck with it for the other 5 solutions. In this sense, we will need the 11 variables to describe the system, even though only 8 are truely significant.

So if we start in the $\bar{p}p$ rest frame, then clearly we need the mass of A, m_A. We also need the orientation of A relative to some coordinate system, $\cos\theta_A$ and ϕ_A. Now we can perform a rotation so the z–axis points along the direction of A, and boost into the A rest frame. Here, we now have two masses, m_B, and m_C, and two angles which orient the decay, $\cos\theta_B$ and ϕ_B.

Now we will need to move into the B and C rest frames. This is performed by first rotating the coordinate system so the z–axis lines up with the direction of motion, and then boosting. In the B rest frame, we need two angles to locate the resulting pions, $\cos\theta_1$ and ϕ_1. Similarly, in the C rest frame, we have the angles $\cos\theta_2$ and ϕ_2. From this we obtain the 11 varibles which describe or system.

$$(m_A, m_B, m_C, \cos\theta_A, \phi_A, \cos\theta_B, \phi_B, \cos\theta 1, \phi_1, \cos\theta_2, \phi_2) \tag{6}$$

If there is no ambiguity in putting the event back together, then it is always possible to choose $\theta_A = \phi_A = \phi_B = 0$.

We also note that for a given $\pi^+\pi^-\pi^\circ\pi^\circ\pi^\circ$ final state, there are 15 independent ways we can build A, B and C. In order to minimize later computation, I have defined an ntuple which contains the 11 variables for each of the 15 combinations, plus three additional variables (168 elements). This is computed once for each event, and then reused over and over by the fitting function.

3.2 The Likelihood Function

Because of the large number of dimensions needed to describe the $\pi^+\pi^-\pi^\circ\pi^\circ\pi^\circ$ final state, it is not possible to bin the data in any meaningful fashion. Even assuming only 5 bins per dimension, we would still have $5^8 = 390625$ bins. With only 23000 events, this would give an average of 0.06 events per bin, and nearly every bin would be an *edge bin*. Instead, we must treat the data in an unbinned fashion. In order to fit unbinned data, it is necessary to use a maximum likelihood method. Most of what I will now describe is detailed in references [8] and [9]. The necessary parts will be repeated here for completeness sake.

The likelihood funtion used in this analysis is defined in [8] as the *Standard Likelihood Method*. The likelihood function to be maximized is given as:

$$\mathcal{L} = \prod_{i=1}^{N} \frac{\mu_i}{\int \mu d\Omega} \tag{7}$$

where the product is taken over the N data points. The normalization integral over all phase space is normally computed via Monte Carlo methods. The usual procedure is to reduce the product to a sum by taking the logarithem of $\mathcal{L}$. The problem can then be reduced to minimizing the negative of the logarithem of the likelihood function:

$$-\ln\mathcal{L} = N \cdot \ln(\int \mu d\Omega) - \sum_{i=1}^{N} \ln\mu_i \tag{8}$$

Now let us look more closely at the weights μ_i. We can express these as $\mu_i = \xi_i \cdot \phi_i \cdot \epsilon_i$, where ϵ is the detector efficiency for the event, ϕ is the phase space weight of the event, and ξ is the dynamical weight of the event. Using this formalism, we can express equation 8 as:

$$-\ln\mathcal{L} = N \cdot \ln(\int \mu d\Omega) - \sum_{i=1}^{N} \ln\xi_i - \sum_{i=1}^{N} \ln(\phi_i \cdot \epsilon_i),$$

And given that we always perform the sum over the **same** events, the last sum will be a constant. As we are then minimizing equation 8, we can neglect a constant offset. However, in the case where we want to compare fits using different input samples, this term is necessary.

At this point, let us examine the normalization integral. This is normally computed by taking M Monte Carlo events, and evaulating the weight μ for each of them. In the case of Monte Carlo, the efficiency is known. It is 1 for the events that make it through the detector simulation, and 0 for the events which fail. The phase space factor is also known. In the case of a program like GENBOD[11], the weight is given for each event. Whereas for our typical CBGEANT[12], the events are generated according to phase space, so the weight is set to 1. In either case, we can define μ in such a way that

$$\sum_{j=1}^{M} \mu_j = \Omega_{tot},$$

where

$$\Omega_{tot} = \sum_{j=1}^{M} \phi_j$$

or then

$$\begin{aligned} \ln(\int \mu d\Omega) &= \ln(\frac{\Omega}{\Omega_{tot}}) + \ln(\sum_{j=1}^{M} \mu j) \\ &= \ln(\frac{\Omega}{\Omega_{tot}}) + \ln(\Omega_{tot}) \end{aligned}$$

which assuming that we use the **same** Monte Carlo events, is just a constant and can be neglected in the minimization procedure. This means the minimizing of equation 8 is equivalent to minimizing

$$-\ln \mathcal{L} \quad = \quad -\sum_{i=1}^{N} \ln \xi_i \tag{9}$$

Next we will examine the normalization. Typically our weights μ can be expressed as:

$$\mu_0 \quad = \quad \mid a_1 \cdot e^{-i\phi_1} \cdot w_1 + a_2 \cdot e^{-i\phi_2} \cdot w_2 \mid^2 \tag{10}$$

Where a_i are real constants, ϕ_i are phases and the w_i are complex weights. We will require that $\sum a_i^2 = 1$. In normalizing this, it is first necessary to normalize the complex weights w_i independently.

$$\Omega_{tot} \quad = \quad \alpha \cdot \sum_{j=1}^{M} \mid w_j \mid^2$$

which then yields an α for each w as:

$$\alpha \quad = \quad \frac{\Omega_{tot}}{\sum_{j=1}^{M} \mid w_j \mid^2}$$

This then means that we need to rewrite equation 10 as

$$\mu_1 \quad = \quad \mid a_1 \cdot e^{-i\phi_1} \cdot (w_1 \cdot \sqrt{\alpha_1}) + a_2 \cdot e^{-i\phi_2} \cdot (w_2 \cdot \sqrt{\alpha_2}) \mid^2$$

Finally, we need to require that the combined weight is normalized.

$$\Omega_{tot} \quad = \quad \beta \cdot \sum_{j=1}^{M} \mu_{1_j}$$

which then yields a β as:

$$\beta \quad = \quad \frac{\Omega_{tot}}{\sum_{j=1}^{M} \mu_{1_j}}$$

which yields our final expression for the normalized weight μ as given in equation 3.2

$$\mu \quad = \quad \mid a_1 \cdot e^{-i\phi_1} \cdot w_1 \cdot \sqrt{\beta \cdot \alpha_1} + a_2 \cdot e^{-i\phi_2} \cdot w_2 \cdot \sqrt{\beta \cdot \alpha_2} \mid^2 \tag{11}$$

It is important to note that every time we modify the dynamical weight, it is necessary to renormalize the funtion. We will see that if we want to leave the mass and width of resonances free, it is necessary to renormalize at every iteration. In the case where we fix these, wee need only normalize once at the start of the run.

3.3 Goodness of Fit

The major drawback of using a maximum likelihood fit is that there is no simple measure of the goodness of fit. In the limit of a large number of events, the quantity $2 \cdot \ln \mathcal{L}$ can be shown to be related to a χ^2, so taking the difference between $2 \cdot \ln \mathcal{L}$ for two different fits will lead to a $\Delta\chi^2$. However, going from this to an absolute χ^2/ndf is not trivial. In order to gauge the goodness of fits *by eye*, I have defined 31 projections from the 8–dimensional phase space. These are based on the 11 variables of equation 6 in section 3.1, and the 15 ways that it is possible to *reconstruct* each event. From these it is possible to define 31 unique projections. These include invariant masses

like $m(\pi^+\pi^-\pi^\circ\pi^\circ$ with three entries per event, $m(\pi^+\pi^-)$ with one entry per event, and then angles related to the decays.

For each of these 31 projections, it is possible to define a χ^2/ndf. We can then form a global pseudo–χ^2/ndf by summing these 31 indivdual ones. This of course uses the same information several times, and also does not take into account the correlations bewteen the variables. As such, we will very often see that the likelyhood tells us that the fit is better, while this pseudo–χ^2 tells us the fit is worse. However, this χ^2 can and does provide very valuable information about where a fit is having problems.

3.4 The Breit–Wigner Amplitudes

I take the standard Breit–Wigner form for an isobar of spin J.

$$BW(m;m_0,\Gamma_0,J) = \frac{m_0\cdot\Gamma_0}{m_0^2-m^2-i\cdot m_0\cdot\Gamma(m;m_0,\Gamma_0,J)}$$

with

$$\Gamma(m;m_0,\Gamma_0,J) = \Gamma_0\cdot\frac{m_0}{m}\cdot\frac{q}{q_0}\cdot\frac{F_J^2(q)}{F_J^2(q_0)}.$$

The Blatt–Weisskopf centrigugal–barrier functions are taken as:

$$\begin{aligned} F_0(q) &= 1 \\ F_1(q) &= \sqrt{\frac{2z}{z+1}} \\ F_2(q) &= \sqrt{\frac{13z^2}{(z-3)^2+9z}} \end{aligned}$$

where

$$z(q) = (q/p_R)^2$$

and $p_R = 0.1973$ GeV/c, corresponding to 1 fm. For $J=0$, then

$$\Gamma(m;m_0,\Gamma_0) = \Gamma_0\cdot\frac{m_0}{m}\cdot\frac{q}{q_0}$$

and for $J=1$

$$\Gamma(m;m_0,\Gamma_0) = \Gamma_0\cdot\frac{m_0}{m}\cdot\frac{q^3}{q_0^3}\cdot\frac{q_0^2+p_R^2}{q^2+p_R^2}$$

Finally, for $J=2$,

$$\Gamma(m;m_0,\Gamma_0) = \Gamma_0\cdot\frac{m_0}{m}\cdot\frac{q^5}{q_0^5}\cdot\frac{q_0^4+3\cdot q_0^2\cdot p_R^2+9\cdot p_R^4}{q^4+3\cdot q^2\cdot p_R^2+9\cdot p_R^4}.$$

In the case of a particle of mass m decaying to two daughters of mass m_1 and m_2,

$$q(m;m_1,m_2) = \frac{\sqrt{[m^2-(m_1+m_2)^2]\cdot[m^2-(m_1-m_2)^2]}}{2m}$$

This formula works fine for a massive object decaying into two stable objects. However, in the case where we consider one broad resonance decaying into two other broad resonances, this formula will break down. In this case, we do not use the masses of the daughter resonances for m_1 and m_2, but rather a combination of the grand daughter particle masses [10]. Suppose we have

$$m \to m_1 m_2 \to (m_a m_b)(m_c m_d)$$

then we define q as follows:

$$q(m; m_a, m_b, m_c, m_d) = \frac{\sqrt{[m^2 - (m_a + m_b + m_c + m_d)^2] \cdot [m^2 - (m_a + m_b - m_c - m_d)^2]}}{2m}$$

This formula will always provide a real value for q and q_0, meaning we can make a sensible interpretation for $\Gamma(m)$.

Throughout this paper, I refer to an object σ which *decays* into both $\pi^\circ\pi^\circ$ and $\pi^+\pi^-$. This σ refers to the $\pi\pi$ S-Wave parametrization of reference [14]. At this point, I use strictly the K1 parametrization. When a σ is implied, I have replaced the Breit–Wigner function with the following:

$$\mathcal{B}W(m_{\pi\pi}) = \frac{m_{\pi\pi}}{q} \cdot \frac{\eta(m_{\pi\pi}) \cdot \exp(2i\delta(m_{\pi\pi})) - 1}{2i}$$

where $m_{\pi\pi}$ is the 2π invariant mass, and η and δ are obtained from the K1 soultion to the $\pi\pi$ S–Wave scattering

3.5 Interference Between Decay Chains

For a fixed decay chain, there are usually several ways to build the intermediate particles A, B and C. If we consider A to be a neutral object decaying into $\rho^+\rho^-$, ($B = \rho^+$, $C = \rho^-$). Then there are three ways to build A from the $\pi^+\pi^-\pi^\circ\pi^\circ\pi^\circ$ final state, (leaving out a different π° each time). For each of these, there are then two ways to build the $\rho^+\rho^-$, depending on which π° is assigned to each particle. This leads to six combinations, all of which need to be included in the transition amplitude.

$$\mathcal{A} = \sum_{i=1}^{6} \left[\gamma_i \cdot h_i \cdot \prod_{j=1}^{3} BW_j(i) \right]$$

where h_i is the heicity amplitude for a given choice, and the product is over the corresponding Breit–Wigners of A, B and C. The factor γ_i is either 1 or -1, and the problem is to determine which.

These γ come from the isospin couplings of the system. We will consider that our object A is isospin 0, and is produced from a ${}^1S_0$ initial state. The G–parity of the $\pi^+\pi^-\pi^\circ\pi^\circ\pi^\circ$ final state is -1, which means that the G–parity of our ${}^1S_0$ initial state must also be -1. Also, $L = 0$ and $S = 0$. This means that $-1 = G({}^1S_0) = (-1)^{(L+S+I)}$, which then tells us that the initial state must be isospin 1, ($\mid 1, 0\rangle$). We must then couple this to a $\mid 0, 0\rangle$ object and a $\mid 1, 0\rangle$ object.

$$\begin{aligned} \mid 1, 0\rangle &= \langle 1, 0 \mid 0, 1, 0, 0\rangle \mid A\pi\rangle \\ {}^1S_0 &= \mid A\pi^\circ\rangle \end{aligned}$$

We then need to consider the A decaying to $\rho^+\rho^-$.

$$\begin{aligned} \mid 0, 0\rangle &= \langle 0, 0 \mid 1, 1, +1, -1\rangle \mid \rho^+\rho^-\rangle + \langle 0, 0 \mid 1, 1, -1, +1\rangle \mid \rho^-\rho^+\rangle + \langle 0, 0 \mid 1, 1, 0, 0\rangle \mid \rho^\circ\rho^\circ\rangle \\ A &= \frac{1}{\sqrt{3}} \mid \rho^+\rho^-\rangle + \frac{1}{\sqrt{3}} \mid \rho^-\rho^+\rangle - \frac{1}{\sqrt{3}} \mid \rho^\circ\rho^\circ\rangle \end{aligned}$$

Finally, we must consider the decays of the ρ^+ and ρ^-, (in this particular channel there is no ρ°).

$$\begin{aligned} \mid 1, +1\rangle &= \langle 1, +1 \mid 1, 1, +1, 0\rangle \mid \pi^+\pi^\circ\rangle + \langle 1, +1 \mid 1, 1, 0, +1\rangle \mid \pi^\circ\pi^+\rangle \\ \rho^+ &= \frac{1}{\sqrt{2}} \mid \pi^+\pi^\circ\rangle - \frac{1}{\sqrt{2}} \mid \pi^\circ\pi^+\rangle \end{aligned}$$

$$\begin{aligned} \mid 1, -1\rangle &= \langle 1, -1 \mid 1, 1, -1, 0\rangle \mid \pi^-\pi^\circ\rangle + \langle 1, -1 \mid 1, 1, 0, -1\rangle \mid \pi^\circ\pi^-\rangle \\ \rho^- &= -\frac{1}{\sqrt{2}} \mid \pi^-\pi^\circ\rangle + \frac{1}{\sqrt{2}} \mid \pi^\circ\pi^-\rangle \end{aligned}$$

We can then put all of this back together to form our initial state from our final state. Ignoring all the normalization terms,

$$\begin{aligned} {}^1S_0 &= -[(\pi^+\pi^\circ)(\pi^-\pi^\circ)]\pi^\circ \\ &= +[(\pi^+\pi^\circ)(\pi^\circ\pi^-)]\pi^\circ \\ &= +[(\pi^\circ\pi^+)(\pi^-\pi^\circ)]\pi^\circ \\ &= -[(\pi^\circ\pi^+)(\pi^\circ\pi^-)]\pi^\circ \end{aligned}$$

In order to determine the γ_i, we need to look carefully at what we call A, B and C. In this problem, I have always taken B to be the ρ^+, and the first daughter is always the π^+. Simlarly, C is always ρ^-, and the first daughter is always π^-. I also take B to always be the first daughter of A, and A to always be the first daughter of the ${}^1S_0$ initial state. This means that all 6 possible terms have the form $[(\pi^+\pi^\circ)(\pi^-\pi^\circ)]\pi^\circ$, so they all have the same sign for γ.

This is of course not always true. If we consider the ${}^3S_1$ initial state, then we can derive that this must be an isospin 0 state. If we then let A be an isospin 1 object, B is also an isospin 1 object, and C is an isospin 0 object, then we will find.

$$\begin{aligned} \mid 0,0\rangle &= \langle 0,0 \mid 1,1,+1,-1\rangle \mid A^+\pi^-\rangle + \langle 0,0 \mid 1,1,-1,+1\rangle \mid A^-\pi^+\rangle + \langle 0,0 \mid 1,1,0,0\rangle \mid A^\circ\pi^\circ\rangle \\ {}^3S_1 &= \frac{1}{\sqrt{3}} \mid A^+\pi^-\rangle + \frac{1}{\sqrt{3}} \mid A^-\pi^+\rangle - \frac{1}{\sqrt{3}} \mid A^\circ\pi^\circ\rangle \end{aligned}$$

For the A decaying to B,C, we have:

$$\begin{aligned} \mid 1,+1\rangle &= \langle 1,+1 \mid 1,0,+1,0\rangle \mid B^+C^\circ\rangle \\ A^+ &= \mid B^+C^\circ\rangle \end{aligned}$$

$$\begin{aligned} \mid 1,-1\rangle &= \langle 1,-1 \mid 1,0,-1,0\rangle \mid B^-C^\circ\rangle \\ A^- &= \mid B^-C^\circ\rangle \end{aligned}$$

$$\begin{aligned} \mid 1,0\rangle &= \langle 1,0 \mid 1,0,0,0\rangle \mid B^\circ C^\circ\rangle \\ A^\circ &= \mid B^\circ C^\circ\rangle \end{aligned}$$

If we now identify the B as the ρ, and C as σ,

$$\begin{aligned} \mid 1,+1\rangle &= \langle 1,+1 \mid 1,1,+1,0\rangle \mid \pi^+\pi^\circ\rangle + \langle 1,+1 \mid 1,1,0,+1\rangle \mid \pi^\circ\pi^+\rangle \\ \rho^+ &= \frac{1}{\sqrt{2}} \mid \pi^+\pi^\circ\rangle - \frac{1}{\sqrt{2}} \mid \pi^\circ\pi^+\rangle \end{aligned}$$

$$\begin{aligned} \mid 1,-1\rangle &= \langle 1,-1 \mid 1,1,-1,0\rangle \mid \pi^-\pi^\circ\rangle + \langle 1,-1 \mid 1,1,0,-1\rangle \mid \pi^\circ\pi^-\rangle \\ \rho^- &= -\frac{1}{\sqrt{2}} \mid \pi^-\pi^\circ\rangle + \frac{1}{\sqrt{2}} \mid \pi^\circ\pi^-\rangle \end{aligned}$$

$$\begin{aligned} \mid 1,0\rangle &= \langle 1,0 \mid 1,1,+1,-1\rangle \mid \pi^+\pi^-\rangle + \langle 1,0 \mid 1,1,-1,+1\rangle \mid \pi^-\pi^+\rangle \\ \rho^\circ &= \frac{1}{\sqrt{2}} \mid \pi^+\pi^-\rangle - \frac{1}{\sqrt{2}} \mid \pi^-\pi^+\rangle \end{aligned}$$

$$\begin{aligned} {}^3S_1 &= +[(\pi^+\pi^\circ)(\pi^\circ\pi^\circ)]\pi^- \\ &= -[(\pi^-\pi^\circ)(\pi^\circ\pi^\circ)]\pi^+ \\ &= -[(\pi^+\pi^-)(\pi^\circ\pi^\circ)]\pi^\circ \end{aligned}$$

In the manner in which I have defined the problem, all chains of the form $A^+\pi^-$ are written in the form of the first line. They therefore all have $\gamma = +1$. The $A^-\pi^+$ are all written in the form of the second line, so $\gamma = -1$. Finally, the $A^\circ\pi^\circ$ are all written as the third line; $\gamma = -1$.

3.6 The Helicity Amplitudes

All helicity amplitudes have been computed in the method described in reference ([13]). However, these have been worked out by hand, simplified, and then coded up in a very optimized way. The code has then been tested by comparing output with the Amsler's SPIN program [13]. In the following, I will always assume a reaction of the form:

$$\bar{p}p \quad \rightarrow \quad A\pi_1, A \rightarrow BC, B \rightarrow \pi_2\pi_3, C \rightarrow \pi_4\pi_5$$

I will also use the notation that L denotes the relative angular momentum between A and π_1 and S will denote their combined spin, (note that as the π has spin 0, S will always be the spin of A). I will then use l to denote the relative angular momentum between B and C, and s will denote their combined spin, (note that B and C are in all cases either ρ or σ, which means $s = 0, 1, 2$). I will also assume that no relative angular momenta larger than 2 are needed to describe the data. I will also make the simplifying assumption that all data can be described in terms of initial S–state annihilation. This means I will only consider the initial states $^1S_0$ and $^3S_1$. Also, given that we have five pions in the final state, we know that the overall G–parity must be negative, which means the quantum numbers of these two initial states are:

- $^1S_0$, $(I^G)J^{PC} = (1^-)0^{-+}$
- $^3S_1$, $(I^G)J^{PC} = (0^-)1^{--}$

3.6.1 $^1S_0 \rightarrow (0^+, 1^+, 2^+)0^{++}0^{-+}$

I have considered two possibilitites for the $0^{++} \rightarrow 4\pi$ decay.

- $0^{++} \rightarrow 0^{++}0^{++} \rightarrow (\pi^+\pi^-)(\pi^\circ\pi^\circ)$, for example $f_0 \rightarrow \sigma\sigma \rightarrow \pi^+\pi^-\pi^\circ\pi^\circ$.
- $0^{++} \rightarrow 1^-1^- \rightarrow (\pi^+\pi^\circ)(\pi^-\pi^\circ)$, for example $f_0 \rightarrow \rho^+\rho^- \rightarrow \pi^+\pi^\circ\pi^-\pi^\circ$.

In the first case, we have $L = 0$, $S = 0$ and $l = 0$, $s = 0$. In this decay, the 0^{++} must be an isospin 0 object. The helicity amplitude for this rather trivial case is

$$h = 1.$$

For the second case, I have $L = 0$, $S = 0$ and $l = 0$, $s = 0$. In this case, the 0^{++} object could have isospin 0, 1 or 2, but the z–component of isospin must be 0. At this point I only consider an isopsin 0 object. The helicity amplitude h is slightly more complicated.

$$h = \frac{1}{\sqrt{3}}\left[\sin\theta_1 \cdot \sin\theta_2 \cdot \cos(\phi_1 + \phi_2) - \cos\theta_1 \cdot \cos\theta_2\right]$$

3.6.2 $^1S_0 \rightarrow (0^+, 1^+, 2^+)2^{++}0^{-+}$

I have considered two possibilitites for the $2^{++} \rightarrow 4\pi$ decay,

- $2^{++} \rightarrow 0^{++}0^{++} \rightarrow (\pi^+\pi^-)(\pi^\circ\pi^\circ)$, for example $f_2 \rightarrow \sigma\sigma \rightarrow \pi^+\pi^-\pi^\circ\pi^\circ$.
- $2^{++} \rightarrow 1^-1^- \rightarrow (\pi^+\pi^\circ)(\pi^-\pi^\circ)$, for example $f_2 \rightarrow \rho^+\rho^- \rightarrow \pi^+\pi^\circ\pi^-\pi^\circ$.

In the first case, we have $L = 2$, $S = 2$ and $l = 2$, $s = 0$. In this mode, the isospin must be zero. The helicity amplitude is then given as:

$$h = \frac{1}{\sqrt{20}}\left(3 \cdot \cos^2\theta_b - 1\right)$$

For the second case, I have $L = 2$, $S = 2$ and $l = 0$, $s = 2$. Here the 2^{++} object can have isopsin 0, 1 or 2, but the z–component of isospin must be zero. I have considered only an isospin 0 object. The helicity amplitude is slightly more complicated, and given as

$$\begin{aligned} h &= \frac{1}{\sqrt{120}}\left(3 \cdot \cos^2\theta_b - 1\right) \cdot [\sin\theta_1 \cdot \sin\theta_2 \cdot \cos(\phi_1 - \phi_2) + 2 \cdot \cos\theta_1 \cos\theta_2] \\ &- \frac{3}{\sqrt{120}} \cdot \sin^2\theta_b \cdot \sin\theta_1 \cdot \sin\theta_2 \cdot \cos(\phi_1 - \phi_2) + \frac{3}{\sqrt{30}} \cdot \sin\theta_b \cos\theta_b \end{aligned}$$

3.6.3 $^1S_0 \to (0^+, 1^+, 2^+)1^-0^-$

Here I have considered one decay,

- $1^- \to 1^-0^{++} \to (\pi^\pm\pi^\circ)(\pi^\circ\pi^\circ)$, for example $\rho\prime^\pm \to \rho^\pm(770)\sigma \to \pi^\pm\pi^\circ\pi^\circ\pi^\circ$.

This can occur with $L = 1$, $S = 1$, and with $l = (0, 2)$, $s = 1$. For the case of $l = 0$, the helicity amplitude is given as:

$$h = \frac{1}{\sqrt{3}} \cdot (\sin\theta_b \cdot \sin\theta_1 \cdot \cos\phi_1 - \cos\theta_b \cdot \cos\theta_1)$$

and for the case of $l = 2$, this is expressed as:

$$h = \frac{1}{\sqrt{30}} \cdot (\sin\theta_b \cdot \sin\theta_1 \cdot \cos\phi_1 + 2 \cdot \cos\theta_b \cdot \cos\theta_1)$$

3.6.4 $^3S_1 \to (1^+)1^{--}0^{-+}$

Here I have considered two decays,

- $1^{--} \to 1^{--}0^{++} \to (\pi\pi)(\pi^\circ\pi^\circ)$, for example $\rho\prime \to \rho(770)\sigma \to \pi\pi\pi^\circ\pi^\circ$.
- $1^{--} \to 1^-1^- \to (\pi^+\pi^\circ)(\pi^-\pi^\circ)$, for example $\rho^\circ\prime \to \rho^+(770)\rho^-(770) \to \pi^+\pi^\circ\pi^-\pi^\circ$.

The first can occur with $L = 1$, $S = 1$, and with $l = (0, 2)$, $s = 1$. In this case, the returned helicity amplitude is a 3–element vector, (from the spin 1 initial state), (v_1, v_2, v_1^*). A very important simplification is to note that the third element of the vector is simply the complex–conjugate of the first.

$$\begin{aligned} v_1 &= \frac{1}{\sqrt{2}} \cdot e^{-i\cdot\phi_A} \cdot [Re(z_0) + i \cdot \cos\theta_A \cdot Im(z_0)] \\ v_2 &= -i \cdot \sin\theta_A \cdot Im(z_0) \end{aligned}$$

The constant z_0 is given for $l = 0$ and $l = 2$ as:

$$z_0[l=0] = \frac{1}{\sqrt{2}} \cdot e^{-i\cdot\phi_B}\left[\sin\theta_1\cos\theta_b \cdot \cos\phi_1 + \cos\theta_1 \cdot \sin\theta_b - i \cdot \sin\phi_1 \cdot \sin\theta_1\right]$$

$$z_0[l=2] = \frac{1}{\sqrt{20}} \cdot e^{-i\cdot\phi_B}\left[\sin\theta_1\cos\theta_b \cdot \cos\phi_1 - 2 \cdot \cos\theta_1 \cdot \sin\theta_b - i \cdot \sin\phi_1 \cdot \sin\theta_1\right]$$

The second can occur with $L = 1$, $S = 1$, and with $l = 1$, $s = (0, 1, 2)$. In this case, the returned helicity amplitude is a 3–element vector, (v_1, v_2, v_1^*). where the third element of the vector is simply the complex–conjugate of the first.

$$\begin{aligned} v_1 &= -\frac{1}{\sqrt{2}} \cdot e^{-i\cdot\phi_A} \cdot [Re(z_s) + i \cdot \cos\theta_A \cdot Im(z_s)] \\ v_2 &= i \cdot \sin\theta_A \cdot Im(z_s) \end{aligned}$$

The constant z_s is given for $s = (0, 1, 2)$ as:

$$\begin{aligned} z_0[s=0] &= \frac{-1}{\sqrt{6}} \cdot \sin\theta_b \cdot e^{-i\cdot\phi_B} [\cos\theta_1 \cdot \cos\theta_2 - \sin\theta_1 \cdot \sin\theta_2 \cdot \cos(\phi_1 + \phi_2)] \\ z_1[s=1] &= \frac{1}{\sqrt{8}} \cdot e^{-i\cdot\phi_B} \{\cos\theta_b \cdot [\sin\theta_1 \cdot \cos\theta_2 \cdot \cos\phi_1 + \cos\theta_1 \cdot \sin\theta_2 \cdot \cos\phi_2] \\ &- i \cdot [\sin\theta_1 \cdot \cos\theta_2 \cdot \sin\phi_1 - \cos\theta_1 \cdot \sin\theta_2 \cdot \sin\phi_2]\} \\ z_2[s=2] &= \frac{-1}{\sqrt{30}} \cdot \sin\theta_b \cdot e^{-i\cdot\phi_B} [2 \cdot \cos\theta_1 \cdot \cos\theta_2 + \sin\theta_1 \cdot \sin\theta_2 \cdot \cos(\phi_1 + \phi_2)] \\ &- \sqrt{\frac{3}{40}} \cdot e^{-i\cdot\phi_B} \{\cos\theta_b \cdot [\sin\theta_1 \cdot \cos\theta_2 \cdot \cos\phi_1 - \cos\theta_1 \cdot \sin\theta_2 \cdot \cos\phi_2] \\ &- i \cdot [\sin\theta_1 \cdot \cos\theta_2 \cdot \sin\phi_1 + \cos\theta_1 \cdot \sin\theta_2 \cdot \sin\phi_2]\} \end{aligned}$$

3.6.5 $^3S_1 \to (1^+)1^{+-}0^{-+}$

Here I have considered one decay,

- $1^{+-} \to 1^{--}0^{++} \to (\pi\pi)(\pi^\circ\pi^\circ)$, for example $b_1(1235) \to \rho(770)\sigma \to \pi\pi\pi^\circ\pi^\circ$.

This can occur with $L = (0, 2)$, $S = 1$, and with $l = s = 1$. As with the previous case, this helicity amplitude is also a 3 element vector. It is also true that the third element of the vector is just the complex conjugate of the first. This vector can then be written as.

$$\begin{aligned} v_1 &= e^{-i\cdot\phi_A} \cdot \left[Re(z_1) + i \cdot \cos\theta_A \cdot Im(z_1) + \frac{1}{\sqrt{2}} \cdot \sin\theta_A \cdot z_2\right] \\ v_2 &= z_2 \cdot \cos\theta_A - i \cdot \sqrt{2} \cdot \sin\theta_A \cdot Im(z_1) \end{aligned}$$

The values of z_1 and z_2 are given for $L = 0$ and $L = 2$ as:

$$\begin{aligned} z_1[L=0] &= \frac{1}{2} \cdot \sin\theta_1 \cdot e^{-i\cdot\phi_B} \cdot (cos\phi_1 - i \cdot \cos\theta_B \sin\phi_1) \\ z_1[L=2] &= \frac{1}{\sqrt{40}} \cdot \sin\theta_1 \cdot e^{-i\cdot\phi_B} \cdot (cos\phi_1 - i \cdot \cos\theta_B \cdot \sin\phi_1) \\ z_2[L=0] &= \frac{i}{\sqrt{2}} \cdot \sin\theta_1 \cdot \sin\theta_B \cdot \sin\phi_1 \\ z_2[L=2] &= \frac{-i}{\sqrt{5}} \cdot \sin\theta_1 \cdot \sin\theta_B \cdot \sin\phi_1 \end{aligned}$$

4 Systematic Tests of the Fitting Procedure

In this section, I will examine possible systematic problems in the fitting procedure. The procedure will consist of taking a 2'nd Monte Carlo sample, (different from the Monte Carlo fitting sample). To this 2'nd sample will be applied a dynamical weight, w. The original sample will then be used to *fit* the second sample under various conditions. The results can then be compared to the dynamical weights, and the effects of various conditions studied. Also included in this section will be a study of the effects of the probability cut on the fit results.

In order to do this, we must return to equation 7. If we had produced a Monte Carlo sample according to some *spin* hypothesis, and then fitted this second sample using a different sample, what would change? In reality, we apply a *spin* weight w to each event in the second sample. This then changes equation 7 to be:

$$\mathcal{L} = \prod_{i=1}^{N} \frac{\mu_i^{w_i}}{\int \mu d\Omega}$$

then equation 8 becomes:

$$-\ln \mathcal{L} = N \cdot \ln(\int \mu d\Omega) - \sum_{i=1}^{N} w_i \cdot \ln \mu_i$$

which as before, we could rewrite as:

$$-\ln \mathcal{L} = N \cdot \ln(\int \mu d\Omega) - \sum_{i=1}^{N} w_i \cdot \ln \xi_i - \sum_{i=1}^{N} w_i \cdot \ln(\phi_i \cdot \epsilon_i),$$

and the minimization equation, (9) is then:

$$-\ln \mathcal{L} = -\sum_{i=1}^{N} w_i \cdot \ln \xi_i$$

However, in order to compare fits made using different events, or events with different weights, one must carefully consider the term:

$$\sum_{i=1}^{N} w_i \cdot \ln(\phi_i).$$

4.1 The Dynamical Weights

For the dynamical weight of the 2'nd Monte Carlo sample, I have taken the following:

- ${}^1S_0(\bar{p}p) \rightarrow X(0^{++})\pi^\circ$, $X \rightarrow \rho^+\rho^-$, (see section 3.6.1).
- ${}^1S_0(\bar{p}p) \rightarrow \rho\prime\pi$, $\rho\prime \rightarrow \rho\sigma$, (see section 3.6.3).
- ${}^3S_1(\bar{p}p) \rightarrow \rho\prime\pi$, $\rho\prime \rightarrow \rho\sigma$, (see section 3.6.4).

This dynamical weight can be written as a term from the ${}^1S_0$ initial state , and one from the ${}^3S_1$ initial state, added incoherently.

$$w = f_{[1s0]} \cdot \mid A_{[1s0]} \mid^2 + (1 - f_{[1s0]}) \cdot \mid A_{[3s1]} \mid^2$$

where the contributions to the two initial states can be written as:

$$\begin{aligned} A_{[1s0]} &= a_x \cdot e^{-i\cdot\phi_x} \cdot A_{[x\rightarrow\rho\rho]} + a_\rho \cdot (1 - a^2_{[l=2]})^{\frac{1}{2}} \cdot A^0_{[l=0]} + a_\rho \cdot a_{[l=2]} \cdot e^{-i\cdot\phi} \cdot A^0_{[l=2]} \\ A_{[3s1]} &= (1 - a^2_{l=2})^{\frac{1}{2}} \cdot A^1_{[l=0]} + a_{[l=2]} \cdot e^{-i\cdot\phi} \cdot A^1_{[l=2]} \end{aligned}$$

For the dynamical weighting parameters, I have chosen the following values:

Parameter Name	*Value*
$m_X(0^{++})$	1350.00
$\Gamma_X(0^{++})$	300.00
$m_{\rho\prime}$	1450.00
$\Gamma_{\rho\prime}$	250.00
f_{1s0}	0.50000
a_X	0.95000
a_ρ	0.31225
$a_{l=2}$	0.10000
ϕ_X	1.00000
ϕ	3.14159

Table 4.1: Dynamical weight parameters for an $X(0^{++})$ and a $\rho\prime$.

4.1.1 Variations in the ω Cuts

In this section, I have examined what the effect on the fit is when one varies the ω–cut for the fitting sample, while holding the ω–cut on the input sample constant. In this study, the 2'nd Monte Carlo sample has had the ω removed using a 2.0σ cut. This sample has then been fit with three different samples, (1.0σ, 1.5σ and 2.0σ). The results are shown in table 4.2. For later reference, figure 4.1 shows four projections from this fit.

Parameter Name	*Weight*	*sample a*	*sample b*	*sample c*
$-2\ln\mathcal{L}$		-13411	-14070	-14743
χ^2/ndf		0.8855	0.9782	1.1242
$m_X(0^{++})$	1350.00	1332.20	1342.24	1347.22
$\Gamma_X(0^{++})$	300.00	301.49	296.25	283.80
$m_{\rho\prime}$	1450.00	1454.24	1451.15	1450.98
$\Gamma_{\rho\prime}$	250.00	261.78	269.36	250.70
f_{1s0}	0.50000	0.49799	0.49545	0.49455
a_X	0.95000	0.94215	0.94560	0.94830
a_ρ	0.31225	0.33519	0.32534	0.31737
$a_{l=2}$	0.10000	0.08342	0.11336	0.12115
ϕ_X	1.00000	0.90467	0.86802	0.76687
ϕ	3.14159	3.25197	3.12038	3.01285

Table 4.2: Fit results for an $X(0^{++})$ and a $\rho\prime$. The three sets of data correspond to different cuts used to remove the ω in the fitting sample. Sample **a** is cut at 2σ, sample **b** at 1.5σ, and sample **c** at 1σ.

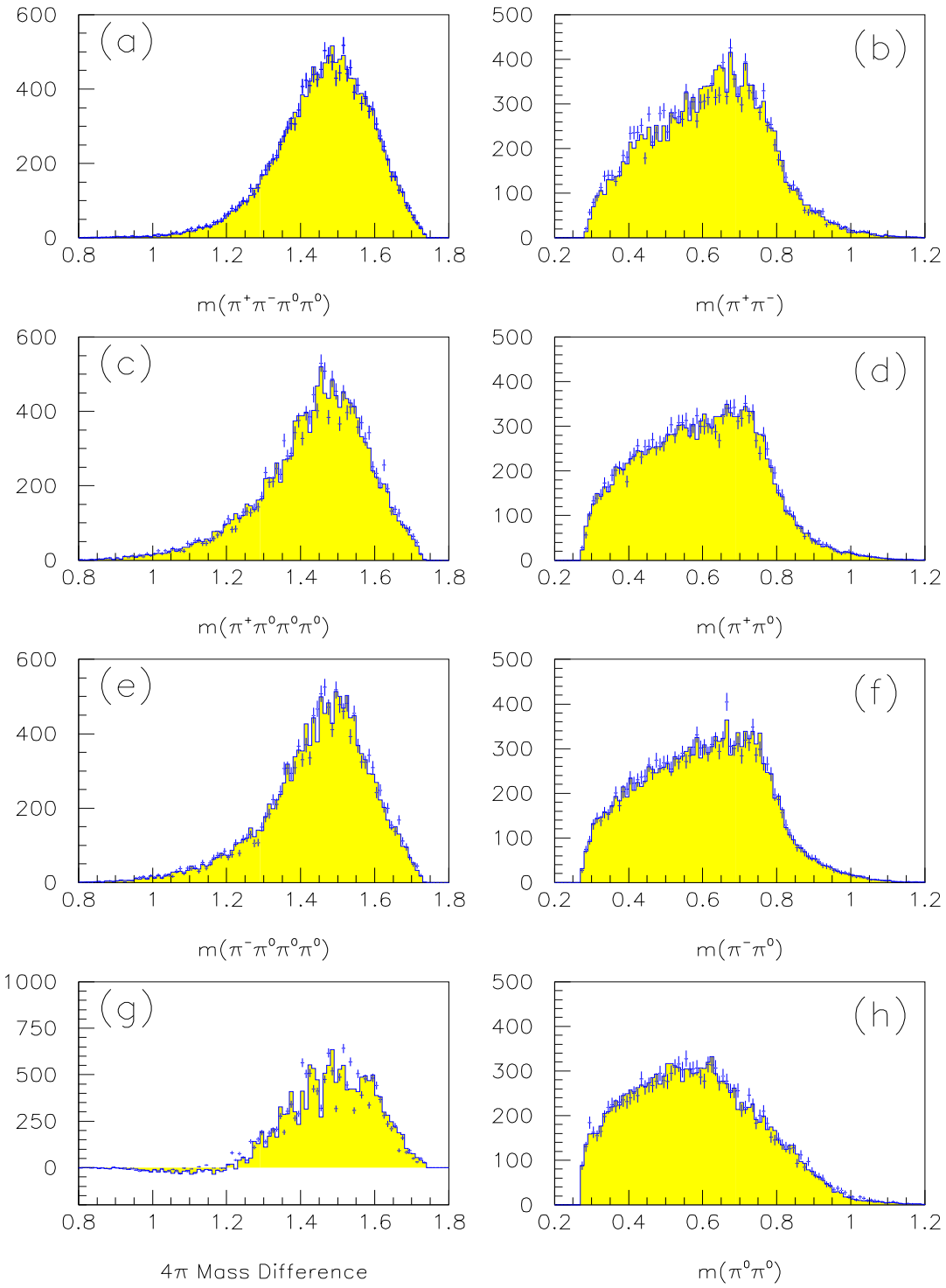

Figure 4.1: Mass projection fits from Monte Carlo to the $\rho\prime\pi$ and $X(0^{++})\pi$ hypothesis. The shaded regions are the fit results, while the points with error bars are the data. **a** shows the $\pi^+\pi^-\pi^0\pi^0$ invariant mass. **b** shows the $\pi^+\pi^-$ invariant mass. **c** and **e** show the $\pi^\pm 3\pi^0$ invariant masses. **d** and **f** show the $\pi^\pm\pi^0$ invariant masses. **g** shows the 4π mass differences, and **h** shows the $\pi^0\pi^0$ invariant mass.

4.1.2 Results using the wrong hypothesis

In this section, I have fitted the 2'nd Monte Carlo Sample with several wrong hypothesis. Given that the true result is 0^{++} and $\rho\prime$, I first looked at what the fit would do with a 2^{++} and $\rho\prime$ hypothesis. I then asked how much of this 2'nd hypothesis we could allow in addition to the true hypothesis. The results of these studies are shown in table 4.3. We see very clearly that the true hypothesis is favored by $\Delta \ln \mathcal{L}$ of 3595 – a very significant difference. We then see when we add an admixture of the 2^{++} hypothesis, we get an improvement in $\ln \mathcal{L}$ of 1 — an insignificant amount. When we then look more closely at this last test, we also see that the normalized strength of this 2^{++} addition is 0.00003 relative to 0.94326 for the 0^{++}, essentially zero! The fit has totally rejected this wrong hypothesis.

Parameter Name	0^{++} *Hyp.*	2^{++} *Hyp.*	0^{++} *and* 2^{++}
$-2\ln\mathcal{L}$	-13411	-9815.85	-13412
χ^2/ndf	0.8855	1.3090	0.8857
$m_X(0^{++})$	1332.20		1330.94
$\Gamma_X(0^{++})$	301.49		295.05
$m_X(2^{++})$		1248.03	2388.38
$\Gamma_X(2^{++})$		143.68	294.44
$m_{\rho\prime}$	1454.24	1535.89	1455.22
$\Gamma_{\rho\prime}$	261.78	390.17	262.24
f_{1s0}	0.49799	0.39104	0.49618
$a_{X(0)}$	0.94215		0.94326
$a_{X(2)}$		0.22975	0.00003
a_ρ	0.33519	0.97325	0.33207
$a_{l=2}$	0.08342	0.09990	0.08585
$\phi_{X(0)}$	0.90467		0.86040
$\phi_{X(2)}$		1.05869	4.17346
$\phi_{l=2}$	3.25197	1.97322	3.26507

Table 4.3: Fit results for an $X(0^{++})$ and a $\rho\prime$ dynamic weight fitted using various hypothesis. For comparison, the 0^{++} column is fit using the same hypothesis as the dynamical weight. The $X(2^{++})$ column then simply replaces the 0^{++} with a 2^{++} object.

In addition, I have performed the above fit using the 0^{++} , and a $\rho\prime$ that decays to $\rho^+\rho^-$, (as per section 3.6.4). (This decay of the $\rho\prime$ can not go from the ${}^1S_0$ initial state.) The results of the fit are shown in table 4.4, and it is seen to be significantly worse than the previous hypothesis.

4.2 Checks on the Confidence Level Cut

Another important question is the effects of the confidence level cut on the fit results. In these tests, the real data were fit using Monte Carlo sample *a* from the previous section. The confidence level cut was then varied from 15% up to 40%, and the results compared. These are shown in Table 4.5.

Parameter Name	0^{++} *Hyp.*
$-2\ln\mathcal{L}$	-8238.59
χ^2/ndf	8.3294
$m_X(0^{++})$	1320.69
$\Gamma_X(0^{++})$	270.70
$m_{\rho\prime}$	1255.07
$\Gamma_{\rho\prime}$	427.52
f_{1s0}	0.56436
$a_\rho(s=0)$	0.36619
$a_\rho(s=1)$	0.81861
$a_\rho(s=2)$	0.44247
$\phi_\rho(s=1)$	4.42166
$\phi_\rho(s-2)$	2.85399

Table 4.4: Fit results for an $X(0^{++})$ and a $\rho\prime$ dynamic weight fitted using the hypothesis that $\rho\prime \to \rho^+\rho^-$.

Parameter Name	*37% Cut*	*20% Cut*	*15% Cut*
$-2\ln\mathcal{L}$	-10433	-9866	-9837
χ^2/ndf	1.2572	1.2301	1.2223
$m_X(0^{++})$	1448.33	1449.37	1442.73
$\Gamma_X(0^{++})$	295.78	338.74	336.55
$m_{\rho\prime}$	683.71	692.61	674.46
$\Gamma_{\rho\prime}$	574.80	580.25	559.82
f_{1s0}	0.42987	0.42039	0.42248
a_X	0.84335	0.76988	0.84260
a_ρ	0.53736	0.63818	0.53854
$a_{l=2}$	0.19983	0.12777	0.15030
ϕ_X	1.47430	1.52883	1.43691
ϕ	4.95474	4.68411	4.71727

Table 4.5: Fit results for an $X(0^{++})$ and a $\rho\prime$. The three sets of data correspond to different confidence level cuts used to select the fitting sample.

5 Results of the Likelihood Fits

In this section, I will describe the results of many different fits. I will try to present the data in a fairly logical sequence, starting with fairly simple assumptions, and then proceeding to more complicated cases. In the case where I judge the fit to be rather poor, I will usually only quote the likelihood function, and the pseudo-χ^2. I will not give the actual parameters which minimize the fit.

5.1 Fits to a Single Intermediate State

The simplest assumption which one can make is to try and describe 100% of the data with only one decay channel. In table 5.1 I present the general results from this study. We can see that it essentially hopeless to describe these data purely in terms of a 0^{++} or a 2^{++} object. However, a description in terms of the $\rho\prime$ appears to be a big step in the right direction.

Description	$-2\ln\mathcal{L}$	χ^2/ndf	χ^2/ndf
$^1S_0 \to X(2^{++})\pi^\circ \to \rho^+\rho^- \to \pi^+\pi^-\pi^\circ\pi^\circ\pi^\circ$	7270.31	14957/2938	5.0910
$^1S_0 \to X(2^{++})\pi^\circ \to \sigma\sigma \to \pi^+\pi^-\pi^\circ\pi^\circ\pi^\circ$	13317.45	20746/2938	7.0614
$^1S_0 \to X(0^{++})\pi^\circ \to \rho^+\rho^- \to \pi^+\pi^-\pi^\circ\pi^\circ\pi^\circ$	3027.17	15592/2938	5.3069
$^1S_0 \to X(0^{++})\pi^\circ \to \sigma\sigma \to \pi^+\pi^-\pi^\circ\pi^\circ\pi^\circ$	-1977.88	14699/2938	5.0031
$^3S_1 \to b_1(1235)\pi \to \rho\sigma\pi \to \pi^+\pi^-\pi^\circ\pi^\circ\pi^\circ$	197.34	8352.7/2938	2.8430
$^1S_0 \to \rho\prime^\pm\pi^\mp$, $^3S_1 \to \rho\prime\pi$ $\rho\prime\pi \to \rho(770)\sigma\pi \to \pi^+\pi^-\pi^\circ\pi^\circ\pi^\circ$	-8193.21	5001.6/2938	1.7024

Table 5.1: A summary of the fit results to individual channels.

However, examining the fit parameters from the $\rho\prime$, (table 5.2), it is clear that this hypothesis cannot be totally correct. In particular, the mass seems rather low, 1136 MeV/c^2, and the width is far too large, 1497 MeV/c^c. Even so, this $\rho\prime$ seems to have many details favored by the data.

Parameter Name	
$-2\ln\mathcal{L}$	-8193.2
χ^2/ndf	1.7024
$m_{\rho\prime}$	1136.30
$\Gamma_{\rho\prime}$	1497.06
f_{1s0}	0.37576
$a_{l=2}$	0.05783
ϕ	4.80119

Table 5.2: Fit results for a $\rho\prime$ alone. The three sets of data are for the phase ϕ between the $l = 0$ and $l = 2$ decay of the $\rho\prime$, left free, fixed at 0 and fixed at π.

5.2 Fits to Two Intermediate States

5.2.1 $\rho\prime \rightarrow \rho\sigma$ and $X(0^{++}) \rightarrow \rho^+\rho^-$

Here we will try a $\rho\prime$ and a 0^{++} object together, (see sections 3.6.1, 3.6.3 and 3.6.4). The amplitude for this is:

$$w = f_{[1s0]} \cdot \mid A_{[1s0]} \mid^2 + (1 - f_{[1s0]}) \cdot \mid A_{[3s1]} \mid^2$$

where

$$\begin{aligned} A_{[1s0]} &= a_X \cdot e^{-i\cdot\phi_X} \cdot A_{[x\rightarrow\rho\rho]} + a_\rho \cdot (1 - a^2_{l=2})^{\frac{1}{2}} \cdot A^0_{[l=0]} + a_\rho \cdot a_{l=2} \cdot e^{-i\cdot\phi} \cdot A^0_{[l=2]} \\ A_{[3s1]} &= (1 - a^2_{l=2})^{\frac{1}{2}} \cdot A^1_{[l=0]} + a_{l=2} \cdot e^{-i\cdot\phi} \cdot A^1_{[l=2]} \end{aligned}$$

The results of this fit are shown in table 4.5 for varying confidence level cuts. Also shown in table 5.3 are similar results for different cuts on the Monte Carlo sample. In figure 5.1 are shown four mass projections from the 3σ fit. The most troublesome of these is the $\pi^+\pi^-$ invariant mass. The fit seems unable to reproduce the ρ° in the data sample, or rather it wants to produce it about 40 MeV below where it is seen in the data. The fit also selects a rather strange mass and width for the $\rho\prime$, (m = 680, Γ = 575). At first appearances, this looks like it could be the tail of the $\rho(770)$. However, for this to be the case, the decay of $\rho \rightarrow \rho\sigma$ would have to be of comparable strength to the $\rho \rightarrow \pi\pi$ decay. This cannot be true. As such, this is something which is not understood.

Parameter Name	3.5σ	3σ *Cut*	2σ *Cut*
$-2\ln\mathcal{L}$		-10433	-11836
χ^2/ndf		1.2572	1.5894
$m_X(0^{++})$		1448.33	1430.86
$\Gamma_X(0^{++})$		295.78	291.40
$m_{\rho\prime}$		683.71	809.61
$\Gamma_{\rho\prime}$		574.80	635.18
f_{1s0}		0.42987	0.42686
a_X		0.84335	0.88493
a_ρ		0.53736	0.46573
$a_{l=2}$		0.19983	0.15024
ϕ_X		1.47430	1.25760
ϕ		4.95474	4.95854

Table 5.3: Fit results for an $X(0^{++})$ and a $\rho\prime$. The three sets of data are for diiferent ω cuts on the Monte Carlo sample.

If we take the 3σ cut, (same as in data), as our standard, then we find there are problems in several of the projections. There are five projections whose χ^2/ndf is larger than 2: $\pi^+\pi^-\pi^\circ\pi^\circ$, $\pi^+3\pi^\circ$, $\pi^-3\pi^\circ$, $\pi^+\pi^-$ and one angular distribution. In addition, four projections have a χ^2/ndf larger than 1.3: $\pi^+\pi^\circ$, $\pi^-\pi^\circ$ and two angular distributions.

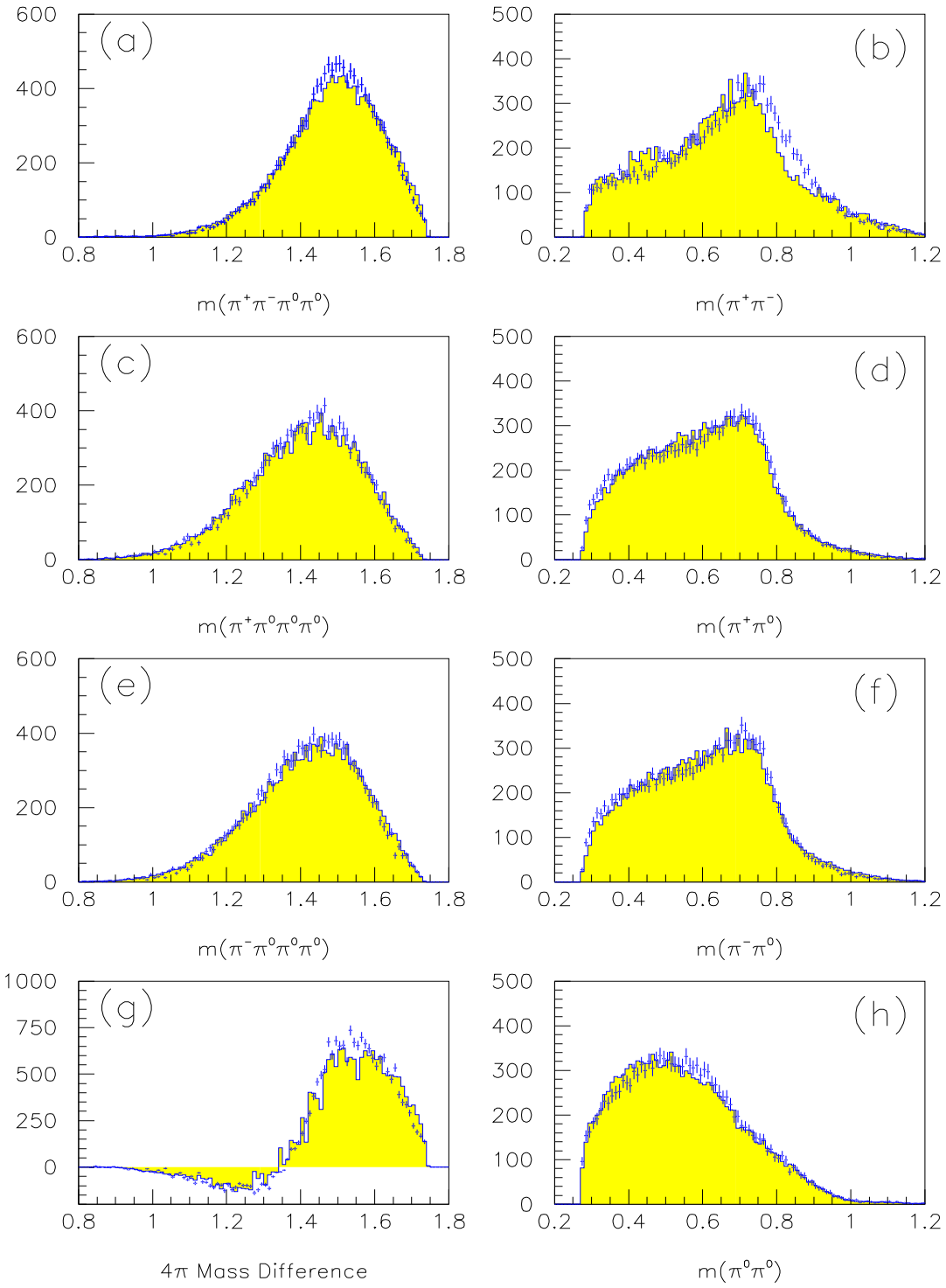

Figure 5.1: Mass projection fits to the $\rho\prime \to \rho\sigma$ and $X(0^{++}) \to \rho^+\rho^-$ hypothesis. The shaded regions are the fit results, while the points with error bars are the data. The fit has difficulty in the peak region of **a** and **b**, as well as not reproducing the 4π mass difference very well. There is also some problems in the $\pi^\circ\pi^{|circ}$ invariant mass, (**h**), and in the $\pi^\pm\pi^\circ$ invariant mass around 600 MEV/c^2.

5.2.2 $\rho\prime \to \rho\sigma$ and $X(0^{++}) \to \rho^+\rho^-$ & $\sigma\sigma$

In this section, I have considered the decay of the $X(0^{++})$ into $\sigma\sigma$, and into both $\rho\rho$ and $\sigma\sigma$. The general amplitude for this is obtained from sections 3.6.1, 3.6.3 and 3.6.4. It can be written as:

$$w = f_{[1s0]} \cdot \mid A_{[1s0]} \mid^2 + (1 - f_{[1s0]}) \cdot \mid A_{[3s1]} \mid^2$$

where

$$\begin{aligned} A_{[1s0]} &= a_{[x\to\rho\rho]} \cdot e^{-i\cdot\phi_{[x\to\rho\rho]}} \cdot A_{[x\to\rho\rho]} + a_{[x\to\sigma\sigma]} \cdot e^{-i\cdot\phi_{[x\to\sigma\sigma]}} \cdot A_{[x\to\sigma\sigma]} \\ &+ a_\rho \cdot (1 - a_{l=2}^2)^{\frac{1}{2}} \cdot A^0_{[l=0]} + a_\rho \cdot a_{l=2} \cdot e^{-i\cdot\phi} \cdot A^0_{[l=2]} \\ A_{[3s1]} &= (1 - a_{l=2}^2)^{\frac{1}{2}} \cdot A^1_{[l=0]} + a_{l=2} \cdot e^{-i\cdot\phi} \cdot A^1_{[l=2]} \end{aligned}$$

The results of this fit are shown in table 5.4. First of all, we see that the $\sigma\sigma$ decay alone gives a significantly worse fit than the $\rho\rho$ alone. However, as seen in figure 5.2 **b**, the $\sigma \to \pi^+\pi^-$ seems to interfere with $\rho^\circ \to \pi^+\pi^-$ in such a way as to significantly improve the overall $\pi^+\pi^-$ invariant mass. However, the $\pi^\pm\pi^\circ$ mass projections are worse. Given this progress, we next allow both decays. The results are given in column 4 of table 5.4, and we see a very significant improvement in the likelihood, ($\Delta\mathcal{L} \approx 900$). This second decay does not shift the mass, but does slightly broaden the 0^{++} object. This leads us to suspect that there may actually be two 0^{++} objects, one decaying to $\rho\rho$ and one decaying to $\sigma\sigma$, (see section 5.3.2). In figure 5.3 we see several mass projections from the case where both decays are allowed. Comparing this with the case of only $\rho\rho$, (figure 5.1), we see that the $\pi^+\pi^-$ and $\pi^\circ\pi^\circ$ invariant masses are better, but the $\pi^\pm\pi^\circ$ masses seem worse.

We can also estimate several branching fractions here. First, from only the $\rho\rho$ or $\sigma\sigma$ decays, we find:

$$\begin{aligned} BR(\bar{p}p \to f_0\pi^\circ \to \rho^+\rho^-\pi^\circ \to \pi^+\pi^-\pi^\circ\pi^\circ\pi^\circ) &\approx (0.067)\cdot(0.42987)\cdot(0.84335)^2 \approx 0.02048 \\ BR(\bar{p}p \to f_0\pi^\circ \to \sigma\sigma\pi^\circ \to \pi^+\pi^-\pi^\circ\pi^\circ\pi^\circ) &\approx (0.067)\cdot(0.44343)\cdot(0.48067)^2 \approx 0.00686 \end{aligned}$$

When we then allow both decays, we find:

$$\begin{aligned} BR(\bar{p}p \to f_0\pi^\circ \to \rho^+\rho^-\pi^\circ \to \pi^+\pi^-\pi^\circ\pi^\circ\pi^\circ) &\approx (0.067)\cdot(0.46998)\cdot(0.85178)^2 \approx 0.01999 \\ BR(\bar{p}p \to f_0\pi^\circ \to \sigma\sigma\pi^\circ \to \pi^+\pi^-\pi^\circ\pi^\circ\pi^\circ) &\approx (0.067)\cdot(0.46998)\cdot(0.47502)^2 \approx 0.00640 \end{aligned}$$

These are interestingly quite consistent, and lead us to conclude that both of these decays are allowed.

Parameter Name	$0^{++} \to \rho^+\rho^-$	$0^{++} \to \sigma\sigma$	$0^{++} \to \rho^+\rho^-$ & $\sigma\sigma$
$-2\ln\mathcal{L}$	-10433.5	$-9104.5.3$	-11330.1
χ^2/ndf	1.2572	1.6259	1.1179
$m_X(0^{++})$	1448.33	1502.44	1437.13
$\Gamma_X(0^{++})$	295.78	165.58	365.85
$m_{\rho\prime}$	683.71	1181.00	839.90
$\Gamma_{\rho\prime}$	574.80	901.16	705.94
f_{1s0}	0.42987	0.44343	0.47281
$a_{X\to 2\rho}$	0.84335		0.79444
$a_{X\to 2\sigma}$		0.48067	0.44953
$a_{\rho\prime}(^1s_0)$	0.53736	0.87690	0.40840
$a_{\rho\prime}(l=2)$	0.19983	0.08641	0.17118
$\phi_{X\to 2\rho}$	1.47430		1.51143
$\phi_{X\to 2\sigma}$		3.83105	4.39895
$\phi_{\rho\prime}(l=2)$	4.95474	4.56042	4.88303

Table 5.4: Fit results for an $X(0^{++})$ and a $\rho\prime$. The possible decay of the $X(0^{++})$ into $\sigma\sigma$ is studied. The $\rho\rho$ column is just the data from table 5.3. The $\sigma\sigma$ column allows only the $\sigma\sigma$ decay, and the last column allows both decays.

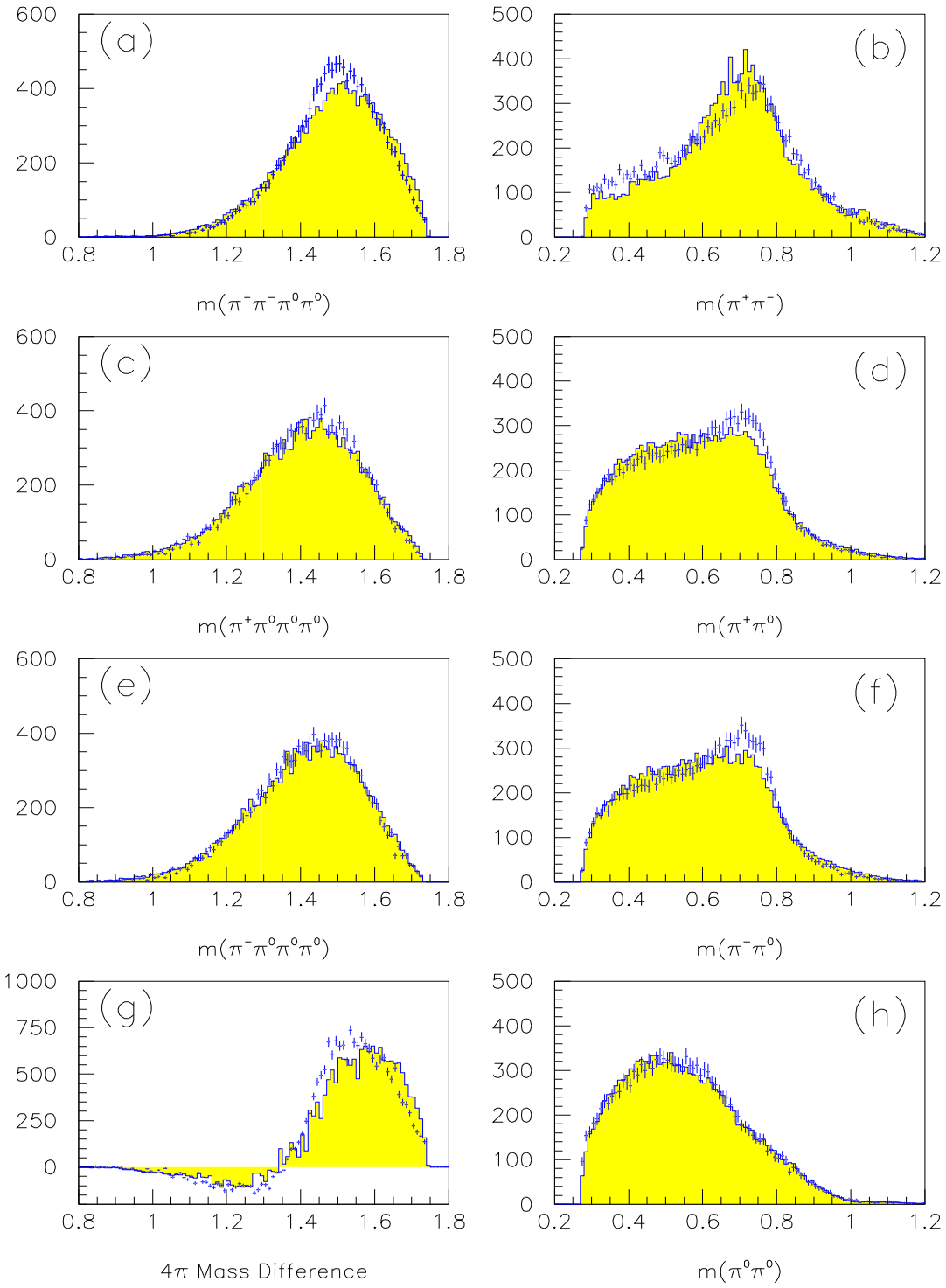

Figure 5.2: Mass projection fits to the $\rho\prime \to \rho\sigma$ and $X(0^{++}) \to \sigma\sigma$ hypothesis. The shaded regions are the fit results, while the points with error bars are the data. The fit has problems in **a**, **b**, **d**, **f**, and **g**. However, notice that in the $\pi^+\pi^-$ invariant mass, (**b**), the problems are quite a bit less than in the case where $X(0^{++}) \to \rho\rho$.

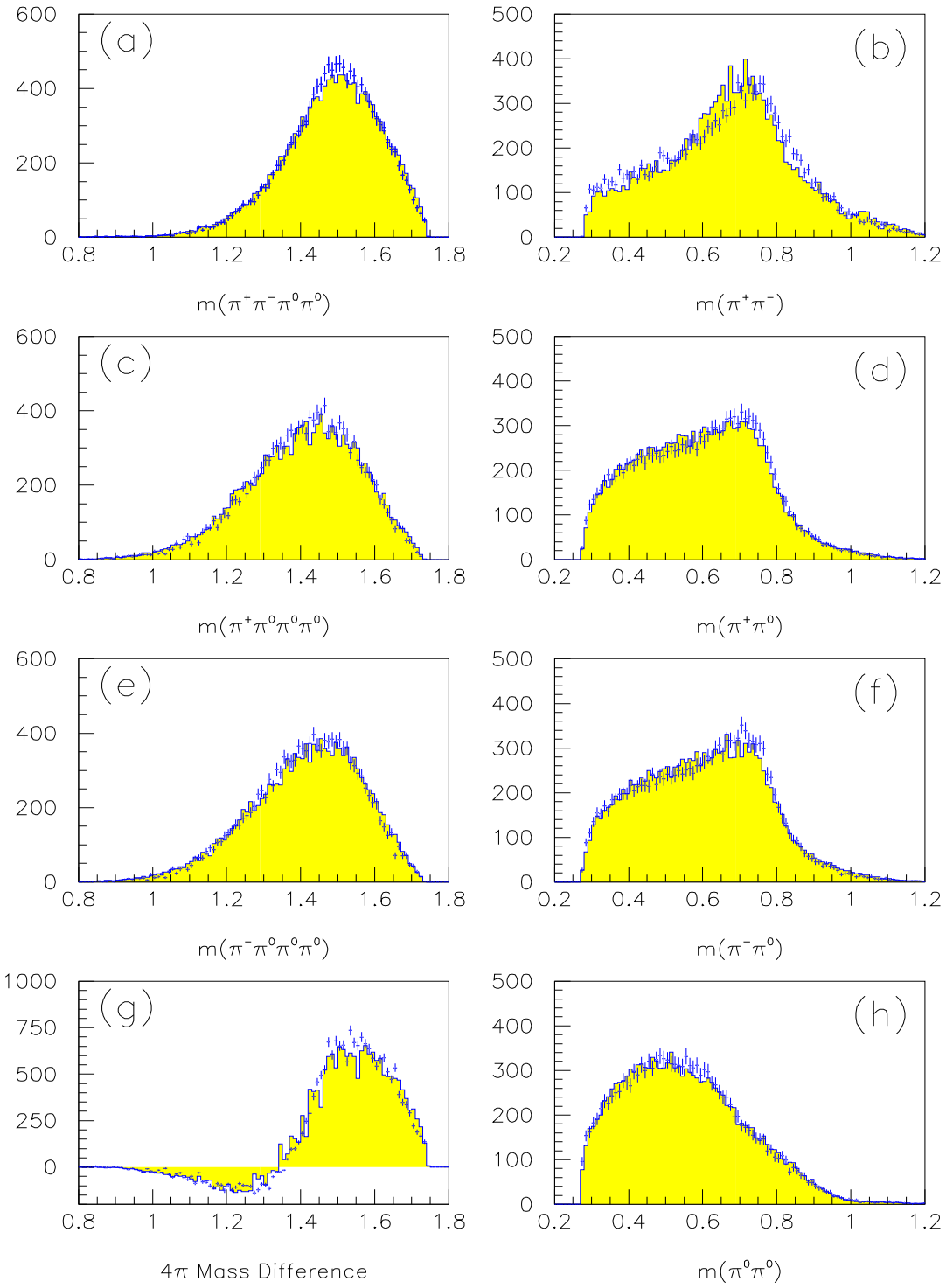

Figure 5.3: Mass projection fits to the $\rho\prime \rightarrow \rho\sigma$ and $X(0^{++}) \rightarrow \rho\rho$ & $\sigma\sigma$ hypothesis. The shaded regions are the fit results, while the points with error bars are the data. In comparison to $\rho\rho$ alone, this fit does much better in the $\pi^+\pi^-$ and $\pi^0\pi^0$ invariant masses, (**b** and **h**. There is also a slight improvement in the 4π mass differnece, (**g**). It still has the same sort of problmes in **a**, **d**, and **f**.

5.2.3 $\rho\prime \to \rho\sigma$ and $X(2^{++}) \to \rho^+\rho^-$

Here, we try a combination of a 2^{++} object decaying into $\rho^+\rho^-$ and the $\rho\prime$ decaying to $\rho\sigma$ from the previous section, (see sections 3.6.2, 3.6.3 and 3.6.4). The weight as used in this fit is given as:

$$w = f_{[1s0]} \cdot \mid A_{[1s0]} \mid^2 + (1 - f_{[1s0]}) \cdot \mid A_{[3s1]} \mid^2$$

where

$$\begin{aligned} A_{[1s0]} &= a_{x2} \cdot e^{-i\cdot\phi_{x2}} \cdot A_{[x2\to\rho\rho]} + a_{x0} \cdot e^{-i\cdot\phi_{x0}} \cdot A_{[x0\to\rho\rho]} \\ &+ a_\rho \cdot (1 - a_{l=2}^2)^{\frac{1}{2}} \cdot A^0_{[l=0]} + a_\rho \cdot a_{l=2} \cdot e^{-i\cdot\phi} \cdot A^0_{[l=2]} \\ A_{[3s1]} &= (1 - a_{l=2}^2)^{\frac{1}{2}} \cdot A^1_{[l=0]} + a_{l=2} \cdot e^{-i\cdot\phi} \cdot A^1_{[l=2]}. \end{aligned}$$

The results of this fit are shown in the 2^{++} column of table 5.5. This hypothesis is much worse than the 0^{++} hypothisis of section 5.2.1, ($\Delta \ln \mathcal{L} = 1301$), (column 0^{++} of table 5.5). In particular, there are nine projections whose χ^2/ndf is larger than 2: $\pi^+\pi^-\pi^\circ\pi^\circ$, $\pi^+3\pi^\circ$, $\pi^-3\pi^\circ$, $\pi^+\pi^-$, $\pi^+\pi^\circ$, $\pi^-\pi^\circ$, and three angular distributions. In addition, six angular distributions, and the $\pi^\circ\pi^\circ$ invariant mass have χ^2/ndf larger than 1.3. I do not consider this hypothesis a good description of the data.

However, it is interesting to determine how much of a 2^{++} object the fit of section 5.2.1 would accept. I have allowed a 0^{++} and a 2^{++} deacying to $\rho^+\rho^-$ in addition to the $\rho\prime$. These results for both a free mass and width of the 2^{++}, and for the mass and width fixed to 1520 and 120 respectively are also shown in table 5.5. We see that this combined hypothesis leads to a rather small improvement over the 0^{++} alone, ($\Delta \ln \mathcal{L} = 250$). We also see that there is about a 6% (0.25^2) admixture — at the border of significant.

Another interesting point is that when the mass and width of the 2^{++} object are left free, the fit chooses 1245 and 160 respectively — approximately the values for the $f_2(1270)$. However, fixing the mass and width at the $f_2(1520)$ values does not significantly change the outcome.

Parameter	*Mass Free*			*Mass Fixed*(†)
Name	0^{++}	2^{++}	2^{++} *and* 0^{++}	2^{++} *and* 0^{++}
$-2\ln\mathcal{L}$	−10433.5	−8462.95	−10647.0	−10626.8
χ^2/ndf	1.2572	1.8462	1.2931	1.2946
$m_X(0^{++})$	1448.33		1441.19	1445.77
$\Gamma_X(0^{++})$	295.78		352.86	339.05
$m_X(2^{++})$		1905.78	1245.82	1520.00†
$\Gamma_X(2^{++})$		129.51	159.16	120.00†
$m_{\rho\prime}$	683.71	587.56	765.21	766.41
$\Gamma_{\rho\prime}$	574.80	602.32	651.15	650.02
f_{1s0}	0.42987	0.36642	0.44561	0.44735
$a_{X(0)}$	0.84335		0.82006	0.82193
$a_{X(2)}$		0.19203	0.24509	0.25916
$a_{\rho\prime}$	0.53736	0.98139	0.51714	0.50722
$a_{l=2}$	0.19983	0.08425	0.16841	0.15151
$\phi_{X(0)}$	1.47430		1.69861	1.70649
$\phi_{X(2)}$		3.25741	5.14988	5.98813
$\phi_{l=2}$	4.95474	5.51420	5.04563	5.03565

Table 5.5: Fit results for an $X(0^{++})$ and a $\rho\prime$, $X(2^{++})$ and a $\rho\prime$, and $X(0^{++})$, $X(2^{++})$ and a $\rho\prime$. The last column had the mass and width of the 2^{++} fixed at 1520 and 120 respectively.

Given these results, we can make an estimate for the ratio of $X(2^{++}) \to \rho\rho$ to $X(2^{++}) \to \pi\pi$.

We get that:

$$BR(\bar{p}p(^1s_0) \to X_2(1520)\pi^\circ \to \rho^+\rho^-\pi^\circ) = (0.44735)\cdot(0.25916)^2\cdot(0.067) = 0.00201$$

where 0.44735 is the fraction of $^1S_0$ initial state, 0.25916 is the amplitude of $X_2 \to \rho^+\rho^-$, and 0.067 is the branching fraction to $\pi^+\pi^-3\pi^\circ$ excluding ω and η, (Equation 4). Isospin arguments then tell us that

$$BR(\bar{p}p(^1s_0) \to X_2(1520)\pi^\circ \to \rho\rho\pi^\circ) = 0.00302$$

From reference [16], we can find that:

$$BR(\bar{p}p(^1s_0) \to X_2(1520)\pi^\circ \to \pi^\circ\pi^\circ\pi^\circ) = (0.095)\cdot(0.01) = 0.00095$$

where 0.095 is the fraction of $^1S_0$ initial state going to X_2, and then decaying to $2\pi^\circ$, and 0.01 is roughly the branching fraction of $\bar{p}p$ into $2\pi^\circ$. Isospin arguments then tell us that

$$BR(\bar{p}p(^1s_0) \to X_2(1520)\pi^\circ \to \pi\pi\pi^\circ) = 0.00285$$

We can then form:

$$\frac{X_2 \to \rho\rho}{X_2 \to \pi\pi} = \frac{0.00302}{0.00285} =\sim 1.06.$$

In a similar light, we can assume that the 2^{++} object is all $f_2(1270)$, and that the 6.9% branching fraction of $f_2(1270)$ to $\pi^+\pi^-\pi^\circ\pi^\circ$ is all $\rho^+\rho^-$. We can then estimate that:

$$BR(\bar{p}p(^1s_0) \to f_2(1270)\pi^\circ \to \rho^+\rho^-\pi^\circ) = (0.44561)\cdot(0.24509)^2\cdot(0.067) = 0.00179$$

Using the 6.9%, we could then derive that:

$$BR(\bar{p}p(^1s_0) \to f_2(1270)\pi^\circ) = 0.039$$

This is far too large, and would clearly be seen in the $\bar{p}p \to \pi^+\pi^-\pi^\circ$ data — at about 30% !. As such, the identification of this 2^{++} object as the $f_2(1270)$ seems very unlikely.

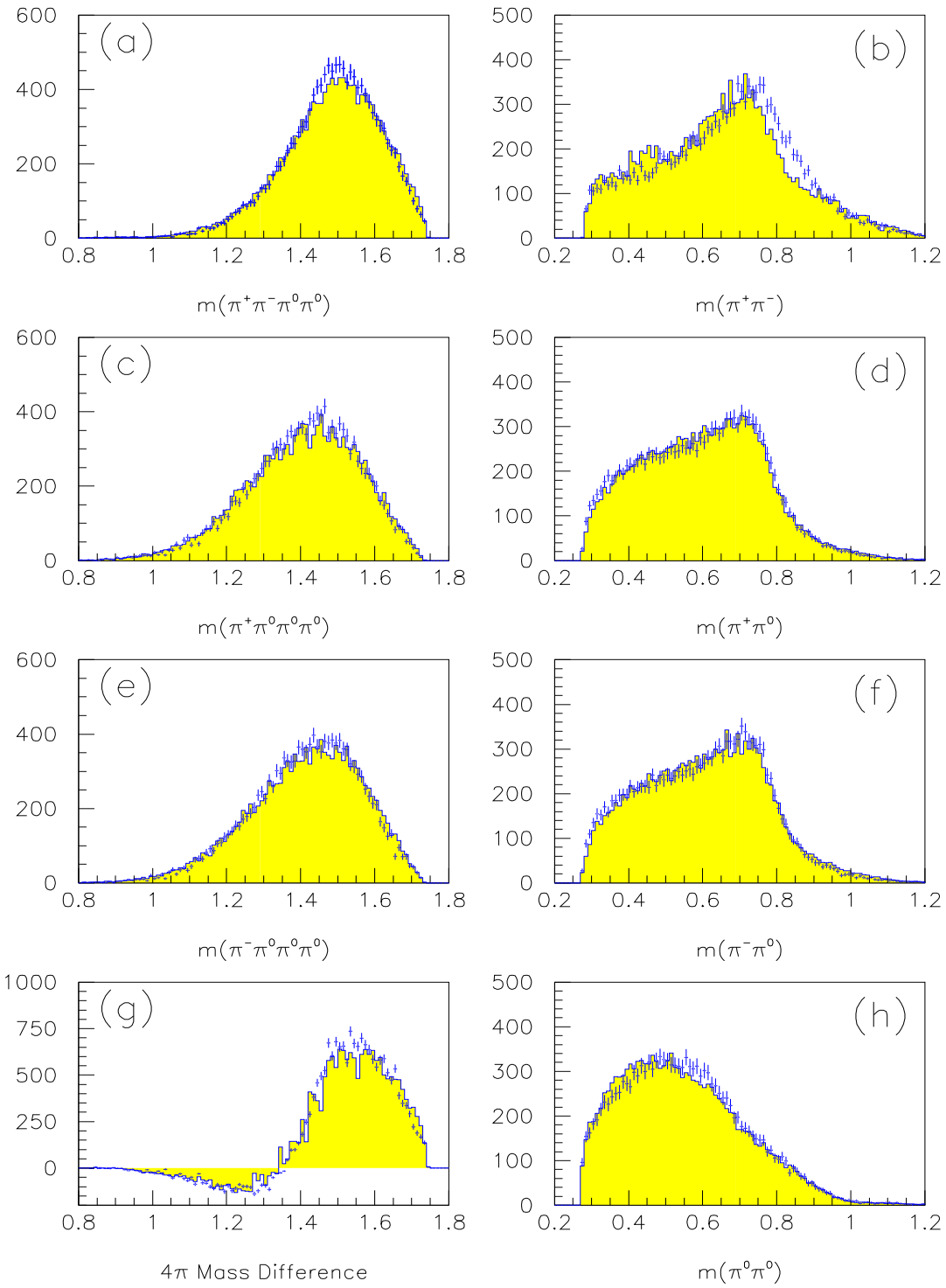

Figure 5.4: Mass projection fits to the $\rho\prime \to \rho\sigma$ $X(2^{++}) \to \rho^+\rho^-$ and $X(0^{++}) \to \rho^+\rho^-$ hypothesis. The shaded regions are the fit results, while the points with error bars are the data. The fit has problems in the peak regions of **a** and **b**. It also has trouble with the $\pi^{\pm}\pi^{circ}$ invariant masses in the 600 MeV/c^2 region, (**d** and **f**). Finally, there are pronlems in the $\pi^0\pi^0$ invariant mass, (**h**), and the 4π mass difference is not well reproduced, (**g**).

5.2.4 $b_1 \to \rho\sigma$ and $X(0^{++}) \to \rho^+\rho^-$ or $X(2^{++}) \to \rho^+\rho^-$

Here I consider a b_1, $((I^G)J^{PC} = (1^+)1^{+-})$, decaying into $\rho\sigma$, and either an $X(0^{++})$ or an $X(2^{++})$ decaying into $\rho^+\rho^-$. This is actually a relatively simple amplitude. The only ${}^1S_0$ contribution comes from the X, while the only ${}^3S_1$ contribution comes from the b_1. The weight for this hypothesis is:

$$w = f_{[1s0]} \cdot \mid A_{[1s0]} \mid^2 + (1 - f_{[1s0]}) \cdot \mid A_{[3s1]} \mid^2$$

where

$$A_{[1s0]} = a_{X0} \cdot A_{[x0 \to \rho\rho]} + a_{X2} \cdot e^{-i \cdot \phi_{X2}} \cdot A_{[x2 \to \rho\rho]}$$

$$A_{[3s1]} = (1 - a^2_{L=2})^{\frac{1}{2}} \cdot A^1_{[L=0]} + a_{L=2} \cdot e^{-i \cdot \phi_{[L=2]}} \cdot A^1_{[L=2]}$$

The results for the fits with both spins of X are shown in table 5.6. The 2^{++} hypothesis is significantly worse than the 0^{++} hypothesis, ($\Delta\mathcal{L} \approx 3000$). The 0^{++} hypothesis also gives worse results than that using the $\rho\prime \to \rho\sigma$ 5.2.1; it does however give better results in some of the projections. In

Parameter	$X(\to \rho^+\rho^-)$		
Name	$X(0^{++})$	$X(2^{++})$	*Both*
$-2\ln\mathcal{L}$	-8830.69	-5788.35	-9055.60
χ^2/ndf	1.1353	1.4545	1.1329
$m_X(0^{++})$	1437.61		1432.25
$\Gamma_X(0^{++})$	385.18		382.95
$m_X(2^{++})$		1495.83	1736.30
$\Gamma_X(2^{++})$		20.41	179.59
m_{b_1}	1344.75	1353.23	1332.15
Γ_{b_1}	442.76	387.43	479.87
f_{1s0}	0.44276	0.38743	0.49235
a_{X0}	1.00000	0.00000	0.95745
a_{X2}	0.00000	1.00000	0.28859
$a_{L=2}$	0.52704	0.56981	0.54679
ϕ_{X2}			5.24101
$\phi_{L=2}$	1.93482	1.82119	1.93096

Table 5.6: Fit results for a b_1 like object, $((I^G)J^{PC} = (1^+)1^{+-})$ decaying into $\rho\sigma$, and either an $X(0^{++})$ or an $X(2^{++})$ object decaying into $\rho^+\rho^-$.

figure 5.5 and 5.6 are shown several mass projections from these fits. The most interesting features, (in the 0^{++} data) are that the $\pi^+\pi^-\pi^\circ\pi^\circ$ invariant mass is very well reporduced, and the $\pi^+\pi^-$ invariant mass is much better reporduced than any of the previous fits. However, there are a number of problems.

In the 0^{++} case, there are five projections whose χ^2/ndf is larger than 2: $\pi^+3\pi^\circ$, $\pi^-3\pi^\circ$, $\pi^+\pi^-$, $\pi^+\pi^\circ$ and $\pi^-\pi^\circ$. There are also two angular distributions whose χ^2/ndf is larger than 1.3.

In the 2^{++} case, there are seven projections whose χ^2/ndf is larger than 2: $\pi^+3\pi^\circ$, $\pi^-3\pi^\circ$, $\pi^+\pi^-$, $\pi^+\pi^\circ$, $\pi^-\pi^\circ$ and two angular distributions. In addition, there are seven angular distributions whose χ^2/ndf is larger than 1.3.

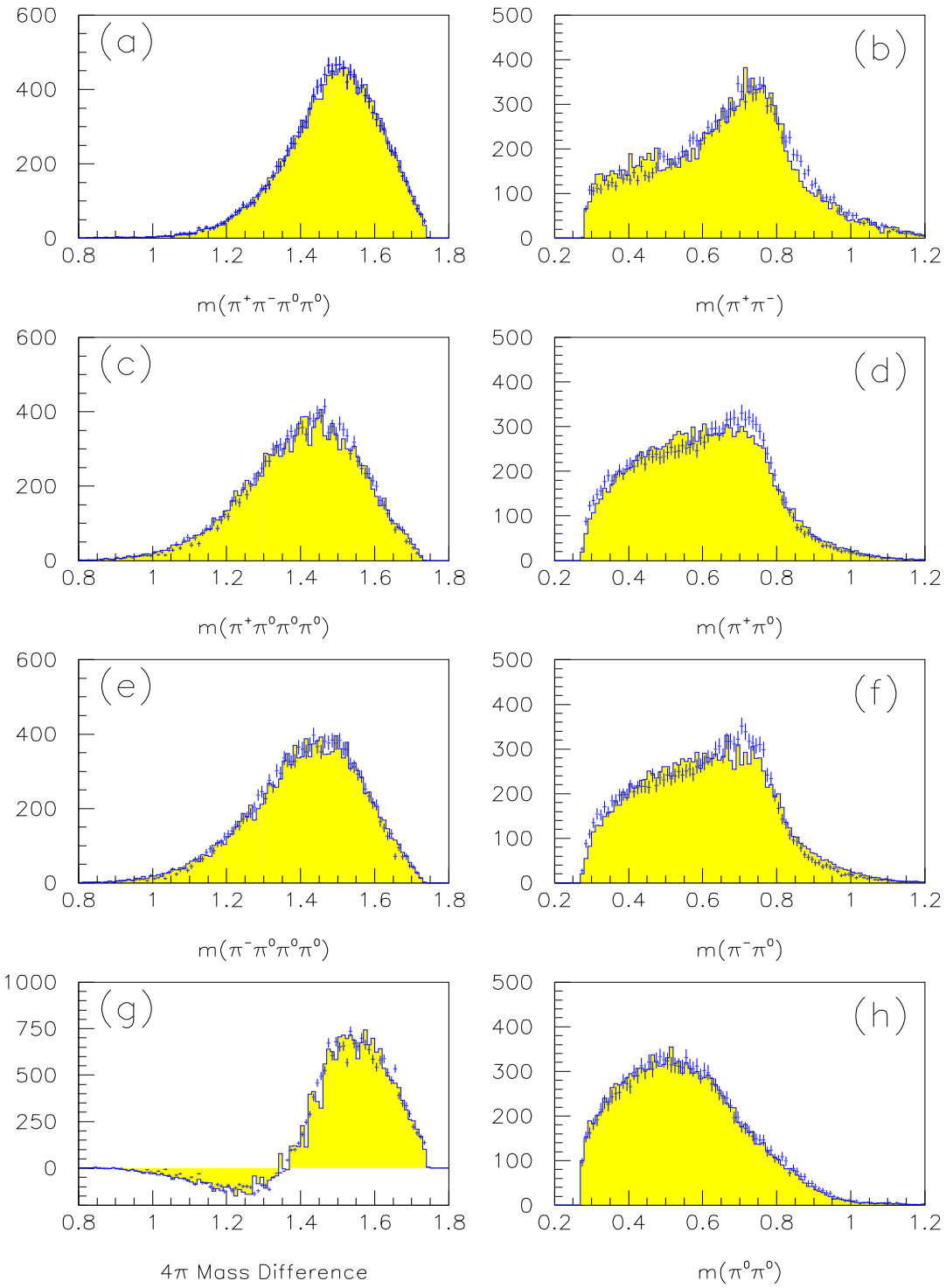

Figure 5.5: Mass projection fits to the $b_1 \to \rho\sigma$ and $X(0^{++}) \to \rho^+\rho^-$ hypothesis. The shaded regions are the fit results, while the points with error bars are the data. Note that the **a** is quite well reproduced by this fit. Also, event though there are still problmes in the $\pi^+\pi^-$ invariant mass, (**b**), the fit is quite a bit better than other fits. We also see that the $\pi^\circ\pi^\circ$ invariant mass, (**h**) and the 4π mass difference, (**g**) are rather well reproduced. The fit has serious problems in the $\pi^\pm\pi^\circ$ invariant masses, (**d** and **f**).

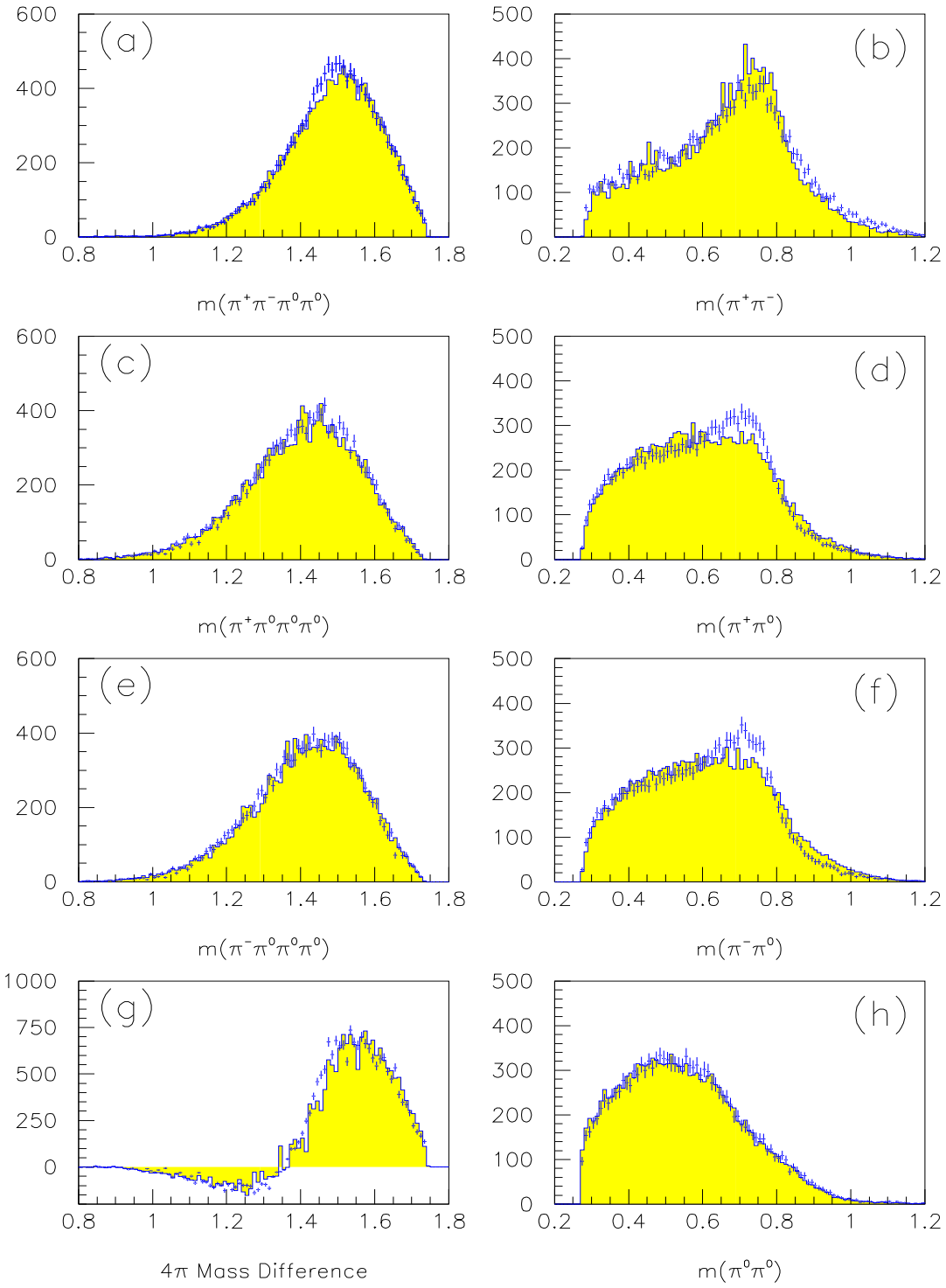

Figure 5.6: Mass projection fits to the $b_1 \to \rho\sigma$ and $X(2^{++}) \to \rho^+\rho^-$ hypothesis. The shaded regions are the fit results, while the points with error bars are the data. The fit has problems in **a**, **b**, **d**, **f** and **g**.

5.2.5 $\rho^\circ\prime \to \rho^+\rho^-$ and $X(0^{++}) \to \rho^+\rho^-$

In this section, we consider an alternate decay of the $\rho\prime$ into $\rho^+\rho^-$, (see section 3.6.4). The amplitude for this decay is given as:

$$w = f_{[1s0]} \cdot \mid A_{[1s0]} \mid^2 + (1 - f_{[1s0]}) \cdot \mid A_{[3s1]} \mid^2$$

where

$$A_{[1s0]} = A_{[x \to \rho\rho]}$$

$$\begin{aligned} A_{[3s1]} &= a_{\rho[s=0]} \cdot e^{-i \cdot \phi_{\rho[s=0]}} \cdot A(\rho)_{[s=0]} + a_{\rho[s=1]} \cdot e^{-i \cdot \phi_{\rho[s=1]}} \cdot A(\rho)_{[s=1]} \\ &+ a_{\rho[s=2]} \cdot e^{-i \cdot \phi_{\rho[s=2]}} \cdot A(\rho)_{[s=2]} \end{aligned}$$

The results for this fit are given in table 5.7. What is rather interesting about the $\rho^\circ\prime \to \rho^+\rho^-$ is that the fit chooses a reasonable mass and width for the $\rho\prime$, 1470 and 435 respectively. We can also see in figure 5.7 that the fit does a very nice job in several of the distributions. However, given that there is no ρ° anywhere in the fit, it is of course not possible for the fit to reproduce the observed ρ° in the data.

Parameter Name	$\rho\prime + X(0^{++})$
$-2 \ln \mathcal{L}$	-7658.2
χ^2/ndf	2.3364
$m_X(0^{++})$	1404.67
$\Gamma_X(0^{++})$	434.56
m_{ρ_2}	1471.36
Γ_{ρ_2}	434.55
f_{1s0}	0.35073
$a_{\rho_2}(s=0)$	0.57333
$a_{\rho_2}(s=1)$	0.50820
$a_{\rho_2}(s=2)$	0.64268
$\phi_{\rho_2}(s=0)$	3.23663
$\phi_{\rho_2}(s=1)$	0.60899
$\phi_{\rho_2}(s=2)$	5.37100

Table 5.7: Fit results for $\rho^\circ\prime \to \rho^+\rho^-$ and $X(0^{++}) \to \rho^+\rho^-$.

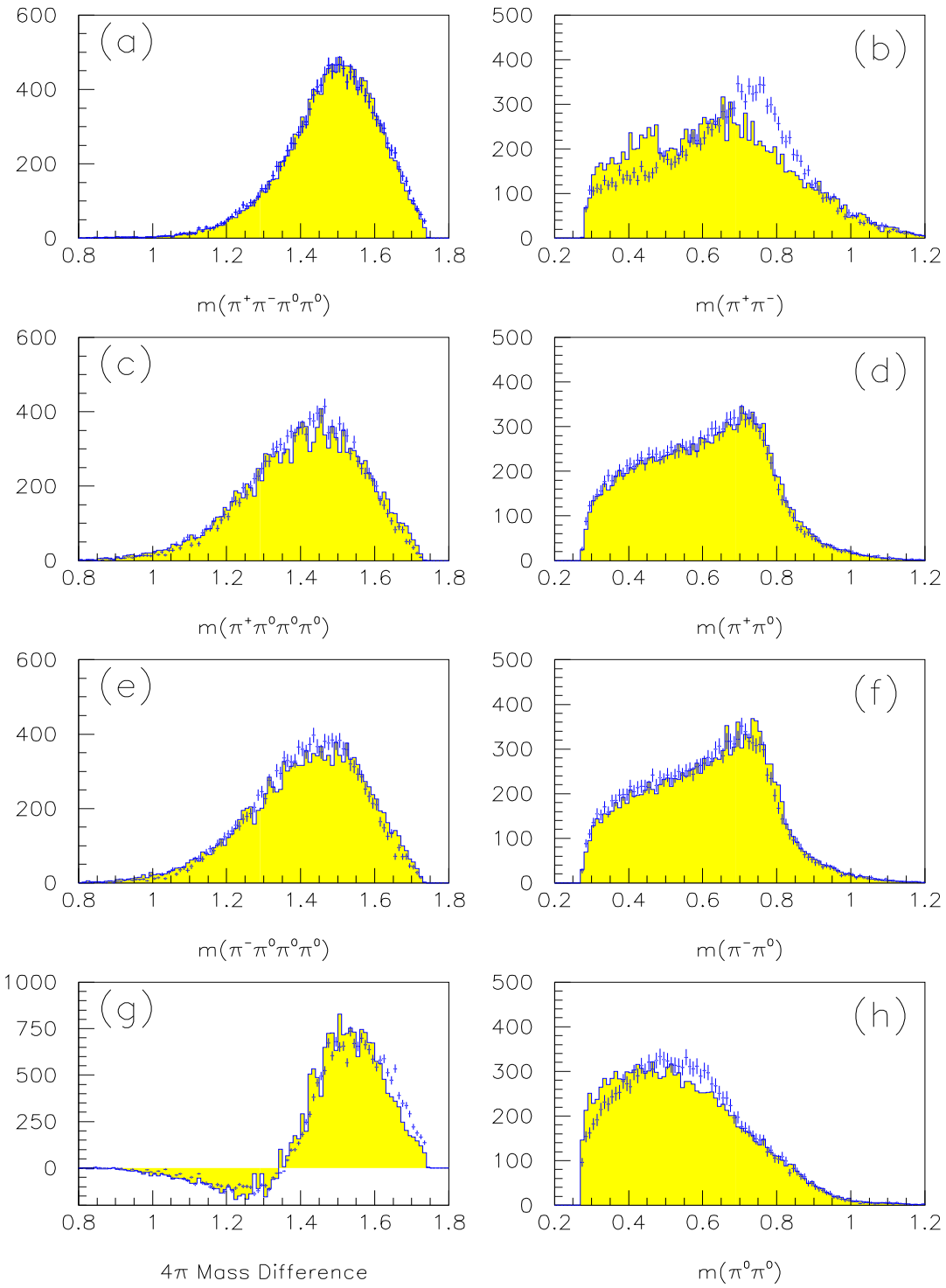

Figure 5.7: Mass projections to the $\rho^0\prime \to \rho^+\rho^-$ and $X(0^{++}) \to \rho^+\rho^-$ hypothesis. The shaded regions are the fit results, while the points with error bars are the data. The fit does rather well in **a**, and the $\pi^\pm\pi^\circ$ are repriduced very well, (**d** and **f**). The fit has real problems in the $\pi^+\pi^-$ invariant mass, (**b**), because there is no ρ° in the hypothesis. We also see that the 4π mass difference, (**g**), and the $\pi^\circ\pi^\circ$ invariant mass, (**h**) are not well reproduced.

5.3 Fits to More than Two Intermediate States

In the previous sections, we have learned a great deal about what the data like and dislike. We have also seen that the hypothesises tried are probably insufficient to completely explain the data. In this section, we will build more cmplicated hypothesis using those parts of the previous hypothesis that seem to give good results. Before starting, we should briefly review what we have learned.

- The data require a 0^{++} object produced from $^1S_0$ and decaying into $\rho^+\rho^-$, ($m_X \approx 1437$, $\Gamma_X \approx 352$). All hypothesises without this object give very poor results. We have summarized the properties in table 5.8.
- Replacing the 0^{++} object with a 2^{++} object is always disfavored by a very large amount. However, allowing an admixture of a 2^{++} object in addition to the 0^{++} object is allowed, and yields a small improvement in the fit.
- Considering only a 0^{++} object decaying into $\sigma\sigma$ is disfavored by the data, (section 5.2.2). However, as figure 5.2 shows, this hypothesis helps the low mass region of the $\pi^+\pi^-$ invariant mass, and goes a long way in solving the problems in the ρ° peak.
- Allowing both a $\sigma\sigma$ and a $\rho\rho$ decay of the 0^{++} is favored by the data. What is interesting is that only a $\sigma\sigma$ decay of the 0^{++} leads to an object of higher mass and narrower width. We will want to consider two 0^{++} objects, one decaying into $\rho^+\rho^-$, and the second into $\sigma\sigma$.
- The data seem to like a $J = 1$ object produced from $^3S_1$ and decaying into $\rho\sigma$. Identifying this as a $\rho\prime$ yields rather strange values for the mass and width, even though the likelihood of the fit is good. This identification also has problems explaining the $\pi^+\pi^-$ invariant mass, (figure 5.1).
- Identifying the $J = 1$ object as a b_1, (section 5.2.4) yields a significantly worse likelyhood, but oddly the pseudo–χ^2 is signifcantly better. This identification also does a much better job of reproducing the ρ° peak in the $\pi^+\pi^-$ invariant mass projection, (see figure 5.5), but has trouble reproducing the ρ^+ and ρ^- peaks.
- Identifying the $J = 1$ object as a $\rho\prime$, but only allowing a decay into $\rho^+\rho^-$, (section 5.2.5) yields a rather poor fit — but only because there is no ρ° in the hypothesis. The hypothesis does an excellent job with the ρ^+ and ρ^- peaks.

Section	*Comments*	*mass*	*width*	*B.F.*
4.2	20% C.L. Cut	1449.37	338.74	0.01669
4.2	15% C.L. Cut	1442.73	336.55	0.02010
5.2.1	3σ Cut	1448.33	295.78	0.02048
5.2.1	2σ Cut	1430.86	291.40	0.02240
5.2.2	$+\sigma\sigma$	1437.13	365.85	0.01999
5.2.3	$+X(2^{++})$	1441.19	352.86	0.02008
5.2.3	$+f_2(1560)$	1445.77	339.05	0.02025
5.2.4	b_1	1437.61	385.18	0.02966
5.2.4	$b_1 + X(2^{++})$	1432.25	382.95	0.03024
5.2.5	$\rho\prime_2$	1404.67	434.56	0.02350
Averages		1437 ± 13	352 ± 43	0.0223 ± 0.0044

Table 5.8: A summary of the mass, width and branching fraction for the 0^{++} object. The branching fraction is taken as $\bar{p}p$ into $f_0\pi^\circ$, with $f_\circ$ then decaying into $\rho^+\rho^-$.

5.3.1 $\rho_1\prime \to \rho\sigma$, $\rho_2\prime \to \rho^+\rho^-$ and $X(0^{++}) \to \rho^+\rho^-$

In this section, I take the second $\rho\prime$, ρ_2, decaying to $\rho^+\rho^-$ from section 5.2.5 and combine it with the orional $\rho\prime \to \rho\sigma$. This second ρ can only come from the $^3S_1$ initial state. Shown in table 5.9 are the fit results for the previous ρ and a 0^{++} object, (section 5.2.1). This new ρ, and a 0^{++} object, and both of these ρ's with the 0^{++} object. The amplitude for this decay is given as:

$$w = f_{[1s0]} \cdot \mid A_{[1s0]} \mid^2 + (1 - f_{[1s0]}) \cdot \mid A_{[3s1]} \mid^2$$

where

$$A_{[1s0]} = a_X \cdot e^{-i\cdot\phi_X} \cdot A_{[x\to\rho\rho]} + a_\rho \cdot (1 - a_{l=2}^2)^{\frac{1}{2}} \cdot A^0_{[l=0]} + a_\rho \cdot a_{l=2} \cdot e^{-i\cdot\phi} \cdot A^0_{[l=2]}$$

$$\begin{aligned} A_{[3s1]} &= a_{\rho 1} \cdot (1 - a_{l=2}^2)^{\frac{1}{2}} \cdot A^1_{[l=0]} + a_{\rho 1} \cdot a_{l=2} \cdot e^{-i\cdot\phi} \cdot A^1_{[l=2]} \\ &+ a_{\rho[s=0]} \cdot e^{-i\cdot\phi_{\rho[s=0]}} \cdot A(\rho)_{[s=0]} + a_{\rho[s=1]} \cdot e^{-i\cdot\phi_{\rho[s=1]}} \cdot A(\rho)_{[s=1]} \\ &+ a_{\rho[s=2]} \cdot e^{-i\cdot\phi_{\rho[s=2]}} \cdot A(\rho)_{[s=2]} \end{aligned}$$

In figure 5.8 are shown several mass projections for the hypothesis with both $\rho\prime$'s. The fit still exhibits many of the problems seen in section 5.2.1. It is also interesting that the fit has given rather strange mass and widths to the second $\rho\prime$, 850 and 1325 respectively. However, likelihood does look quite good for this fit. There are four projections whose χ^2/ndf is larger than 2: $\pi^+\pi^-\pi^\circ\pi^\circ$, $\pi^+3\pi^\circ$, $\pi^-3\pi^\circ$ and $\pi^+\pi^-$. In addition, one angular distribution, and the $\pi^+\pi^\circ$ and $\pi^-\pi^\circ$ invariant masses have a χ^2/ndf larger than 1.3.

Parameter Name	$\rho_1 + X(0^{++})$	$\rho_2 + X(0^{++})$	$\rho_1 + \rho_2 + X(0^{++})$
$-2\ln\mathcal{L}$	-10433.5	-7658.2	-11076.6
χ^2/ndf	1.2572	2.3364	1.2119
$m_X(0^{++})$	1448.33	1404.67	1436.18
$\Gamma_X(0^{++})$	295.78	434.56	393.77
m_{ρ_1}	683.71		697.76
Γ_{ρ_1}	574.80		693.14
m_{ρ_2}		1471.36	847.01
Γ_{ρ_2}		434.55	1326.57
f_{1s0}	0.42987	0.35073	0.35958
a_X	0.84335	1.00000	0.88928
$a_{\rho_1}(^1s_0)$	0.53736		0.45736
$a_{\rho_1}(^3s_1)$	1.00000		0.85557
$a_{\rho_1}(l=2)$	0.19983		0.25964
$a_{\rho_2}(s=0)$		0.57333	0.45794
$a_{\rho_2}(s=1)$		0.50820	0.06869
$a_{\rho_2}(s=2)$		0.64268	0.23146
ϕ_X	1.47430		1.73856
$\phi_{\rho_1}(l=2)$	4.95474		5.34310
$\phi_{\rho_2}(s=0)$		3.23663	3.23663
$\phi_{\rho_2}(s=1)$		0.60899	5.26187
$\phi_{\rho_2}(s=2)$		5.37100	5.16773

Table 5.9: Fit results for an $X(0^{++})$ two $\rho\prime$'s. ρ_1 is allowed to decay to $\rho\sigma$, while ρ_2 is allowed to decay to $\rho^+\rho^-$. The $X(0^{++})$ decays to $\rho^+\rho^-$.

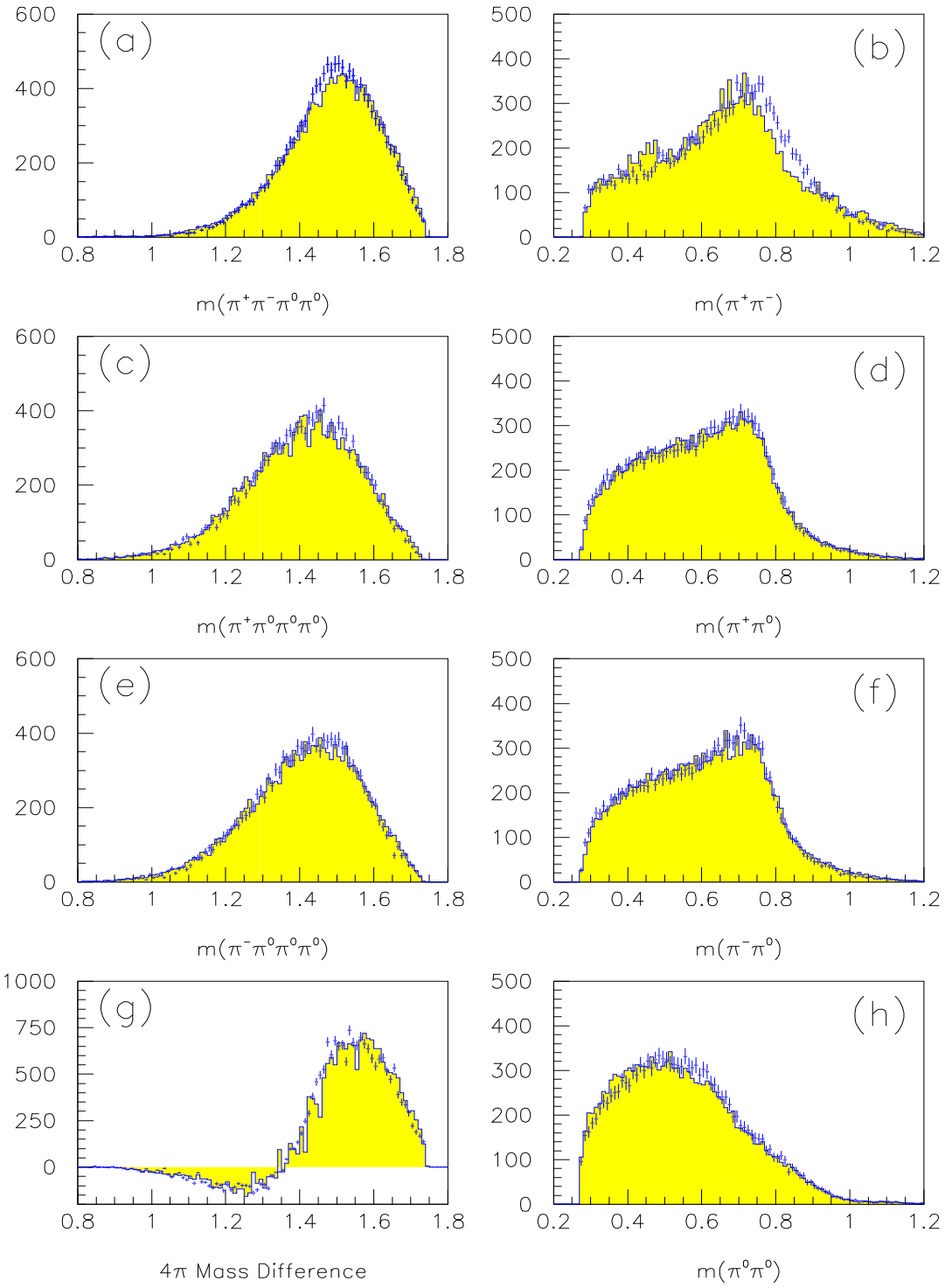

Figure 5.8: Mass projections to the $\rho_1 \to \rho\sigma$, $\rho_2^0 \to \rho^+\rho^-$ and $X(0^{++}) \to \rho^+\rho^-$ hypothesis. The shaded regions are the fit results, while the points with error bars are the data. The fit has problems in the peak region of **a** and **b**. We also see that the 4π mass difference, (**g**), and the $\pi^0\pi^0$ invariant mass, (**h**) are not well reproduced.

5.3.2 $\rho\prime \to \rho\sigma$, $X(0^{++}) \to \rho^+\rho^-$ and $f_0 \to \rho^+\rho^-$ or $\sigma\sigma$

In section 5.3.2 we allowed both a 0^{++} and a 2^{++} in addition to the $\rho\prime \to \rho\sigma$. In this section, I allow a second $X(0^{++})$ object with possible decays into either $\sigma\sigma$ or $\rho\rho$. The amplitude for this process is:

$$w = f_{[1s0]} \cdot \mid A_{[1s0]} \mid^2 + (1 - f_{[1s0]}) \cdot \mid A_{[3s1]} \mid^2$$

where

$$\begin{aligned} A_{[1s0]} &= a_{[x\to\rho\rho]} \cdot e^{-i\cdot\phi_{[x\to\rho\rho]}} \cdot A_{[x\to\rho\rho]} + a_{[f\to2\sigma]} \cdot e^{-i\cdot\phi_{[f\to2\sigma]}} \cdot A_{[f\to2\sigma]} + a_{[f\to2\rho]} \cdot e^{-i\cdot\phi_{[f\to2\rho]}} \cdot A_{[f\to2\rho]} \\ &+ a_\rho \cdot (1 - a_{l=2}^2)^{\frac{1}{2}} \cdot A^0_{[l=0]} + a_\rho \cdot a_{l=2} \cdot e^{-i\cdot\phi} \cdot A^0_{[l=2]} \\ A_{[3s1]} &= (1 - a_{l=2}^2)^{\frac{1}{2}} \cdot A^1_{[l=0]} + a_{l=2} \cdot e^{-i\cdot\phi} \cdot A^1_{[l=2]} \end{aligned}$$

The results of this study are given in table 5.10. The most intersesting result is that the fit likes a second 0^{++} object decaying into $\sigma\sigma$, ($\Delta\mathcal{L} \approx 930$), (column 3 of table 5.10). However, this object appears to be nearly degenerate in mass to the 0^{++} decaying into $\rho\rho$, but quite a bit narrower. Recall that in section 5.2.2 we considered a single 0^{++} object decaying to both $\rho\rho$ and $\sigma\sigma$; the fit totally rejected the latter decay. When we allow only a $\rho\rho$ decay of this second object, (column 4 of table reftab:rho2X0, the fit does not improve very much, and the mass and width of the new object don't make sense.

In addition, we can fix the mass and width of this second object to that of the $f_0(1560)$ [17]. In this case, the $\rho\rho$ decay mode is completely rejected, (column 6), while the $\sigma\sigma$ decay mode gives a fit which is only slightly worse, (comumn 5). Several mass projections from this last fit are shown in figure 5.9.

Parameter	*No 2'nd*	*Mass Free*		*Mass Fixed*(†)	
Name	$f_0(1560)$	$f_0 \to \sigma\sigma$	$f_0 \to \rho^+\rho^-$	$f_0 \to \sigma\sigma$	$f_0 \to \rho^+\rho^-$
$-2\ln\mathcal{L}$	-10433.5	-11361.5	-10647.6	-11252.5	-10532.7
χ^2/ndf	1.2572	1.1108	1.2787	1.1151	1.2591
$m_X(0^{++})$	1448.33	1445.76	1453.51	1415.77	1464.85
$\Gamma_X(0^{++})$	295.78	434.74	306.24	431.26	294.43
$m_f(0^{++})$		1458.30	631.72	$1560.00^\dagger$	$1560.00^\dagger$
$\Gamma_f(0^{++})$		204.74	297.49	$245.00^\dagger$	$245.00^\dagger$
$m_{\rho\prime}$	683.71	826.59	553.53	838.50	705.39
$\Gamma_{\rho\prime}$	574.80	602.84	21.11	566.55	562.12
f_{1s0}	0.42987	0.47345	0.41777	0.47453	0.43231
$a_{X\to2\rho}$	0.84335	0.80648	0.85061	0.79804	0.84821
$a_{f\to2\rho}$			0.36491		$1.65\cdot10^{-6}$
$a_{f\to2\sigma}$		0.44459		0.43918	
$a_{\rho\prime}(^1s_0)$	0.53736	0.38978	0.37891	0.41261	0.52966
$a_{\rho\prime}(l=2)$	0.19983	0.20199	0.24316	0.20882	0.21378
$\phi_{X\to2\rho}$	1.47430	1.74668	1.80923	1.66755	1.53132
$\phi_{f\to2\rho}$			6.04079		1.07916
$\phi_{f\to2\sigma}$		4.51338		5.08160	
$\phi_{\rho\prime}(l=2)$	4.95474	4.93293	5.07875	4.95519	4.99335

Table 5.10: Fit results for two $X(0^{++})$'s and a $\rho\prime$. The possible decay of the second $X(0^{++})$ into $\sigma\sigma$ and $\rho\rho$ is studied.

However, given the fact that the two 0^{++} masses are so close, it is most likely that the two objects are one in the same. Recall from section 5.2.2 where we allowed the $X(0^{++})$ to decay to

both $\rho^+\rho^-$ and $\sigma\sigma$. There we measured:

$$BR(\bar{p}p \to f_0\pi^\circ \to \rho^+\rho^-\pi^\circ \to \pi^+\pi^-\pi^\circ\pi^\circ\pi^\circ) \approx (0.067)\cdot(0.46998)\cdot(0.85178)^2 \approx 0.01999$$

Which we can compare with:

$$BR(\bar{p}p \to f_0\pi^\circ \to \rho^+\rho^-\pi^\circ \to \pi^+\pi^-\pi^\circ\pi^\circ\pi^\circ) \approx (0.067)\cdot(0.47345)\cdot(0.80648)^2 \approx 0.02063.$$

For the $\sigma\sigma$,

$$BR(\bar{p}p \to f_0\pi^\circ \to \sigma\sigma\pi^\circ \to \pi^+\pi^-\pi^\circ\pi^\circ\pi^\circ) \approx (0.067)\cdot(0.46998)\cdot(0.47502)^2 \approx 0.00640$$

Which we can compare with:

$$BR(\bar{p}p \to f_0\pi^\circ \to \sigma\sigma\pi^\circ \to \pi^+\pi^-\pi^\circ\pi^\circ\pi^\circ) \approx (0.067)\cdot(0.47345)\cdot(0.44459)^2 \approx 0.00627.$$

We also see that the relative phase between the two decays in section 5.2.2 is 2.88752, while in this section we find 2.76670. I think given the existing data, we must assume that there is only one 0^{++} object, which decays to both $\rho\rho$ and $\sigma\sigma$. Using simple isospin arguments, we could then derive that:

$$\frac{BR(f_0 \to \rho\rho)}{BR(f_0 \to \sigma\sigma)} \approx 2.08$$

and, that assuming f_0 only decays to $\rho\rho$ and $\sigma\sigma$, then:

$$BR\,[\bar{p}p \to f_0\pi^\circ] \approx 0.044$$

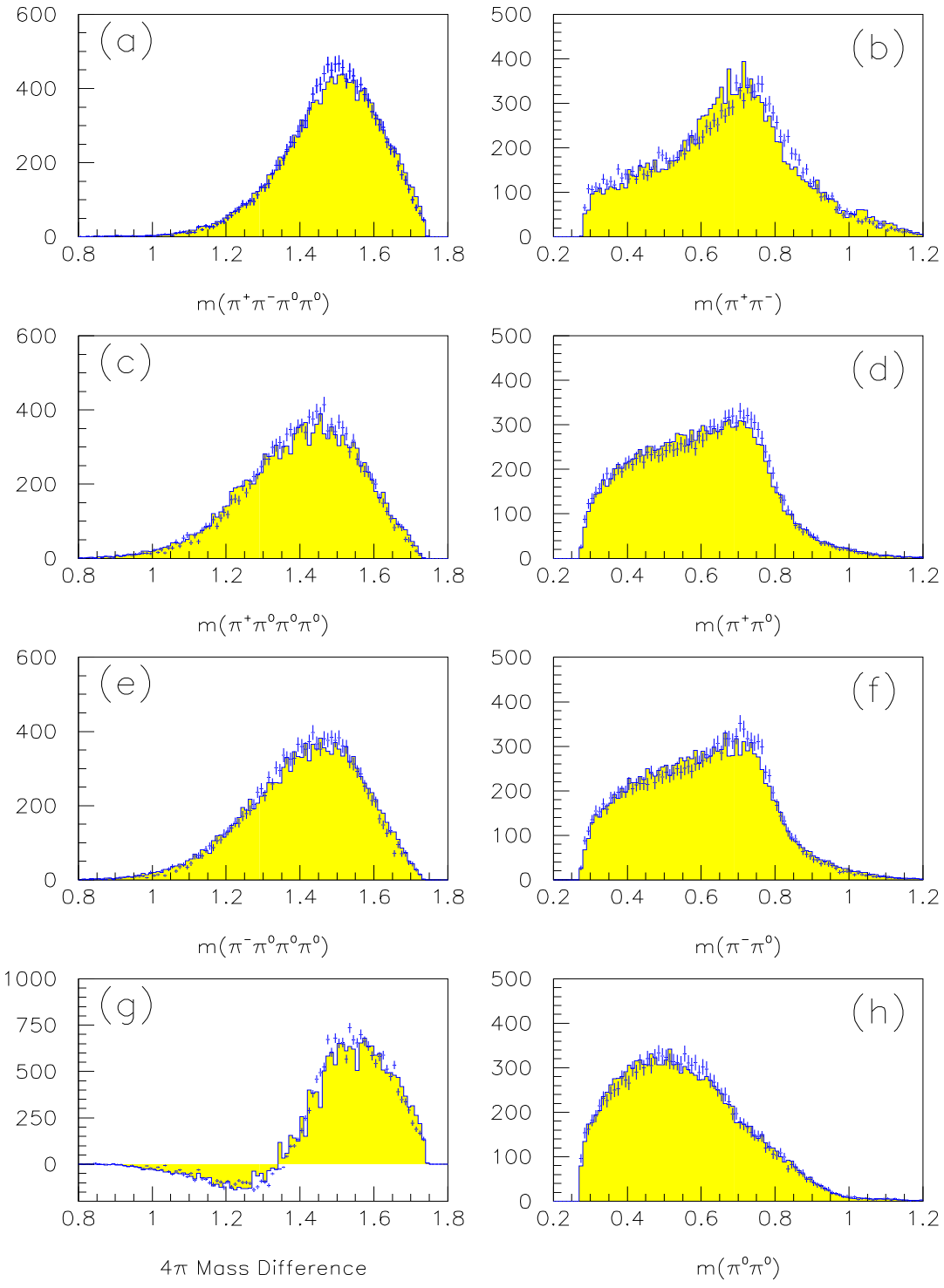

Figure 5.9: Fit results for an $\rho\prime \to \rho\sigma$, $X(0^{++}) \to \rho^+\rho^-$ and $f_0(1560) \to \sigma\sigma$. The fit has problems in the peak reigion of **a**, and **b**. There is also some trouble reproducing the $\pi^{\pm}\pi^{\circ}$ invariant mass, (**d** and **f**).

5.3.3 $b_1 \to \rho\sigma$ and $X(0^{++}) \to \rho^+\rho^-$ and $X(0^{++}) \to \sigma\sigma$

Based on the success of the $\sigma\sigma$ decay of the $X(0^{++})$ from section 5.2.2, I now consider a b_1, $((I^G)J^{PC} = (1^+)1^{+-})$, decaying into $\rho\sigma$, and an $X(0^{++})$ decaying into both $\rho^+\rho^-$ and $\sigma\sigma$. This is actually a relatively simple amplitude. The only $^1S_0$ contribution comes from the X, while the only $^3S_1$ contribution comes from the b_1. The weight for this hypothesis is:

$$w = f_{[1s0]} \cdot \mid A_{[1s0]} \mid^2 + (1 - f_{[1s0]}) \cdot \mid A_{[3s1]} \mid^2$$

where

$$A_{[1s0]} = a_{X\to\sigma\sigma} \cdot e^{-i\cdot\phi_{X\to\sigma\sigma}} \cdot A_{[X\to\sigma\sigma]} + a_{X\to\rho\rho} \cdot A_{[X\to\rho\rho]}$$

$$A_{[3s1]} = (1 - a^2_{L=2})^{\frac{1}{2}} \cdot A^1_{[L=0]} + a_{L=2} \cdot e^{-i\cdot\phi} \cdot A^1_{[L=2]}$$

The results for the fit are shown in table 5.11, and several mass projections are shown in figure 5.10. As seen in the figure, the $\rho^\pm$ are not fit very well, however, the entrie $\pi^+\pi^-$ invariant mass seems nicely reproduced. What is rather bothersome is the fact that the mass and width of the b_1 come out quite a bit off from their accepted values, mass 1300 MeV/c^2 and width 520 MeV/c^2.

In addition to this we can also take a second 0^{++} object, which we allow to decay only into $\sigma\sigma$. The results for this fit are shown in column 5 of table 5.11, and mass projections are seen in figure 5.11. What is interesting is that the mass of the f_0 comes out nearly the same as the X_0, but its width is much narrower — 165 versus 461. Also, the fit is not that much better than the fit where the same 0^{++} has both decays. As such, it is difficult to conclude that there is a second 0^{++} object.

Parameter	$X(0^{++})$ Decays Into:				f_0
Name	$\rho\rho$	$\sigma\sigma$	*Both*	*fixed* †	$\sigma\sigma$
$-2\ln\mathcal{L}$	−8830.69		−9231.75	−8374.33	−9282.94
χ^2/ndf	1.1353		1.1434	1.3707	1.1202
$m_X(0^{++})$	1437.61		1414.43	1410.74	1416.93
$\Gamma_X(0^{++})$	385.18		387.66	365.30	461.47
m_{f0}					1444.95
Γ_{f0}					165.25
m_{b_1}	1344.75		1312.53	1232†	1309.89
Γ_{b_1}	442.76		520.93	155†	497.03
f_{1s0}	0.44276		0.49310	0.55987	0.49750
$a_{X\to\rho\rho}$	1.00000		0.95049	0.92495	0.95489
$a_{X\to\sigma\sigma}$			0.31077	0.38009	
$a_{f0\to\sigma\sigma}$					0.29697
$a_{L=2}$	0.52704		0.54119	0.41193	0.59309
$\phi_{X\to\sigma\sigma}$			3.26956	3.46807	
$\phi_{f0\to\sigma\sigma}$					3.32860
$\phi_{L=2}$	1.93482		1.86294	2.22020	1.82203

Table 5.11: Fit results for a $b_1 \to \rho\sigma$ and $X(0^{++}) \to \rho^+\rho^-$. In addition, both $X(0^{++}) \to \sigma\sigma$ and $f_0 \to \sigma\sigma$ are tried.

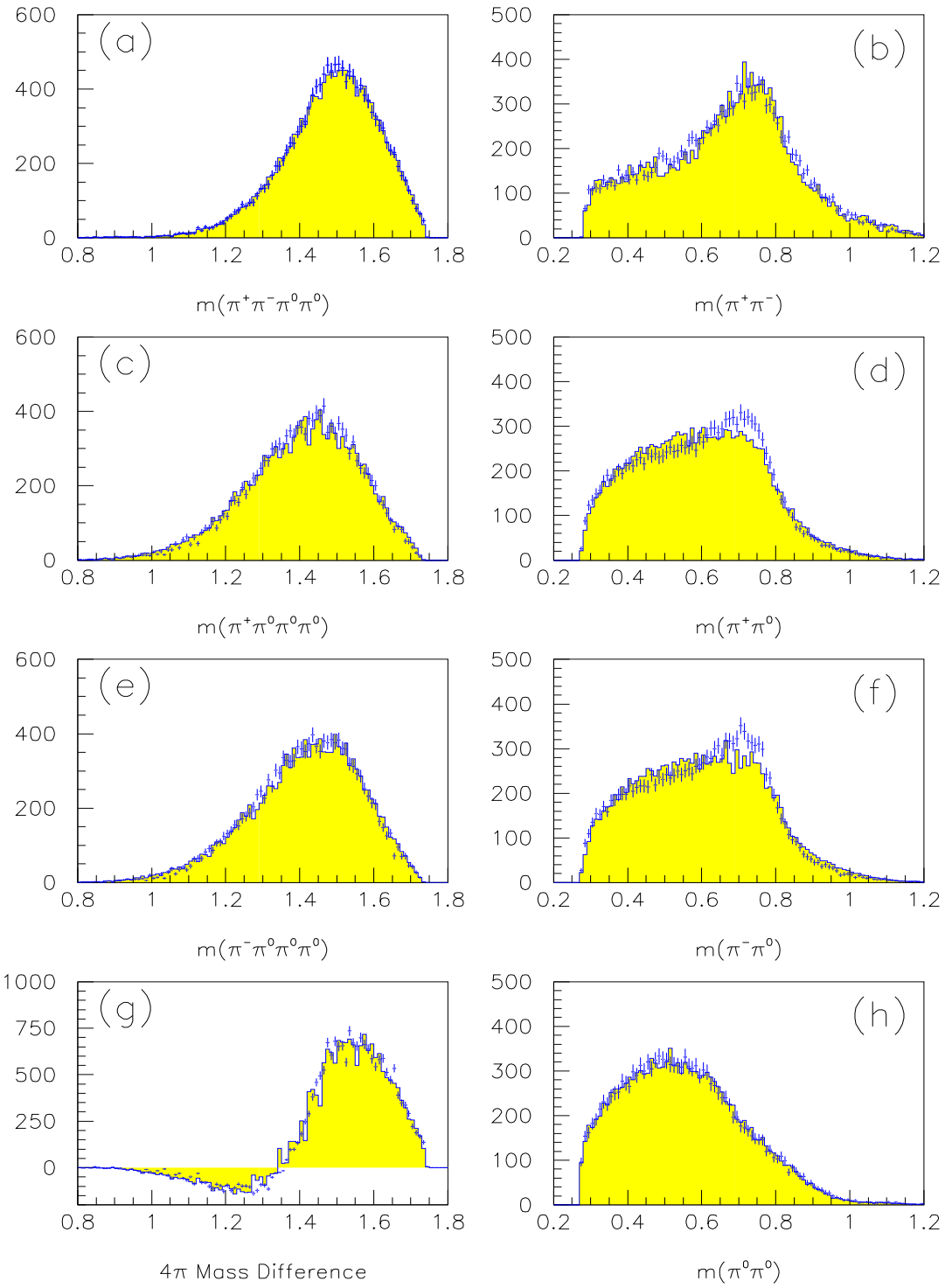

Figure 5.10: Mass projections to the $b_1 \to \rho\sigma$ and $X(0^{++}) \to \rho^+\rho^-$ & $\sigma\sigma$ hypothesis. The shaded regions are the fit results, while the points with error bars are the data. There seem to be problems in the $\pi^\pm\pi^\circ$ invariant masses, (**d** and **f**); the fit really does not reproduce the $\rho^\pm$ very well. However, all other projections appear quite good.

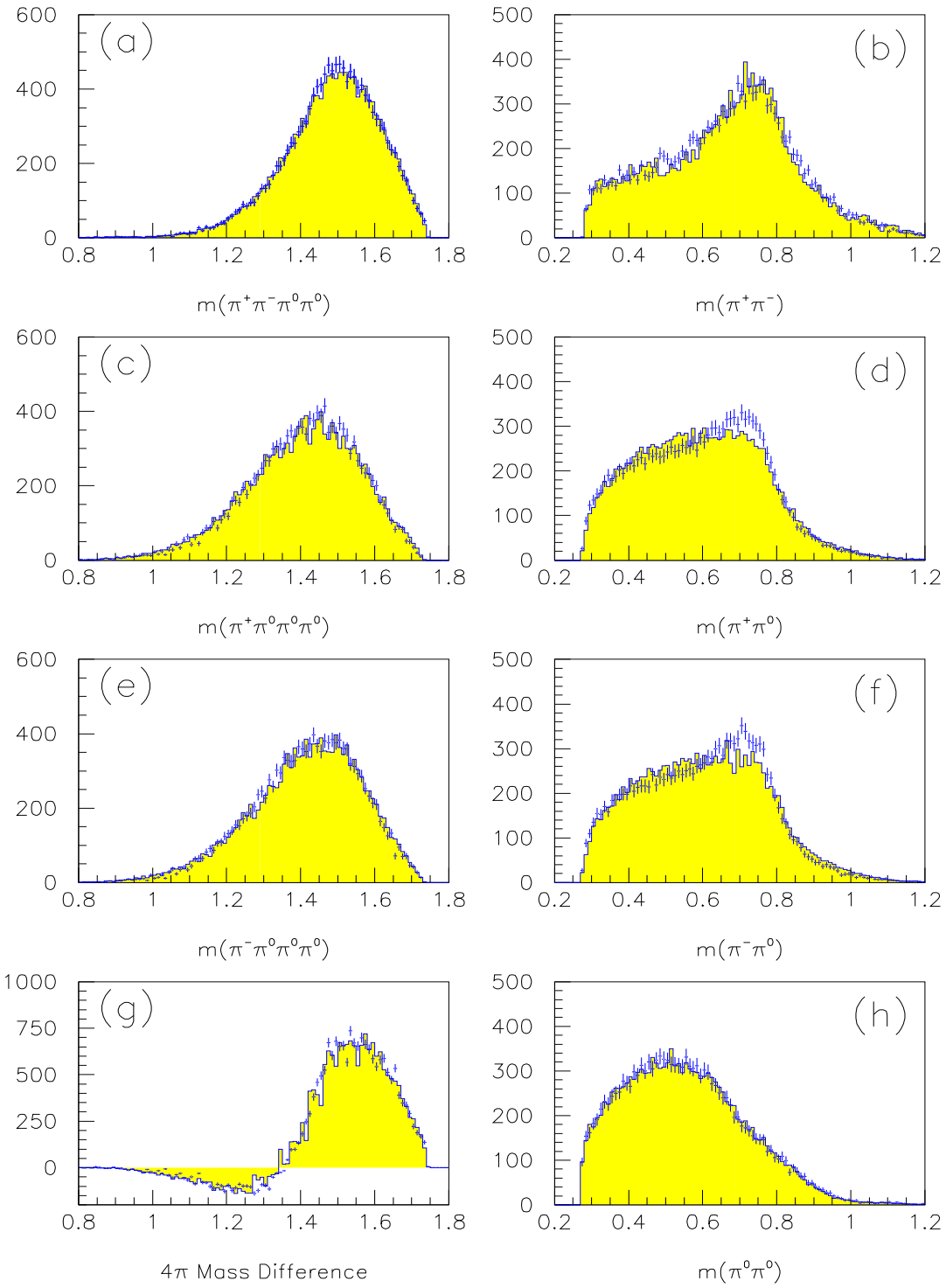

Figure 5.11: Mass projections to the $b_1 \to \rho\sigma$ and $X(0^{++}) \to \rho^+\rho^-$ and $f_0 \to \sigma\sigma$ hypothesis. The shaded regions are the fit results, while the points with error bars are the data. There seem to be problems in the $\pi^\pm\pi^\circ$ invariant masses, (**d** and **f**); the fit really does not reproduce the $\rho^\pm$ very well. However, all other projections appear quite good.

5.3.4 $b_1 \to \rho\sigma$, $\rho\prime \to \rho^+\rho^-$ and $X(0^{++}) \to \rho^+\rho^-$

We have seen earlier that a $\rho\prime$ decaying to $\rho^+\rho^-$, and a b_1 decaying to $\rho\sigma$ are both able to reproduce very well many of the features in the data, but individually they fail in specific projections. What is interesting is that one they tend to complement each other. The amplitude for the three included amplitudes is given as:

$$w = f_{[1s0]} \cdot \mid A_{[1s0]} \mid^2 + (1 - f_{[1s0]}) \cdot \mid A_{[3s1]} \mid^2$$

where

$$A_{[1s0]} = A_{[x \to \rho\rho]}$$

$$\begin{aligned} A_{[3s1]} &= a_{b1} \cdot (1 - a_{l=2}^2)^{\frac{1}{2}} \cdot A(b_1)^1_{[l=0]} \\ &+ a_{b1} \cdot a_{l=2} \cdot e^{-i \cdot \phi_{b1}} \cdot A(b_1)^1_{[l=2]} \\ &+ a_{\rho[s=0]} \cdot e^{-i \cdot \phi_{\rho[s=0]}} \cdot A(\rho)_{[s=0]} \\ &+ a_{\rho[s=1]} \cdot e^{-i \cdot \phi_{\rho[s=1]}} \cdot A(\rho)_{[s=1]} \\ &+ a_{\rho[s=2]} \cdot e^{-i \cdot \phi_{\rho[s=2]}} \cdot A(\rho)_{[s=2]} \end{aligned}$$

The results of this fit are given in table 5.12, and several mass projections can be seen in figure 5.12.

Parameter	*Mass Free*			*Mass Fixed*(†)
Name	$b_1 + X(0^{++})$	$\rho + X(0^{++})$	$b_1 + \rho + X(0^{++})$	$b_1 + \rho + X(0^{++})$
$-2 \ln \mathcal{L}$	-8830.7	-7658.2	-10232.1	-9628.4
χ^2/ndf	1.1353	2.3364	1.1518	1.3025
$m_X(0^{++})$	1437.61	1404.67	1354.97	1356.29
$\Gamma_X(0^{++})$	385.18	434.56	400.88	415.56
m_{b_1}	1344.78		1200.12	$1232^\dagger$
Γ_{b1}	442.76		1121.75	$155^\dagger$
m_ρ		1471.36	1495.07	1431.87
Γ_ρ		434.55	289.90	293.62
f_{1s0}	0.46412	0.35073	0.35640	0.34966
a_{b_1}	1.00000		0.75956	0.66700
$a_{b_1}(l=2)$	0.52704		0.34615	0.41510
$a_\rho(s=0)$		0.57333	0.41780	0.52218
$a_\rho(s=1)$		0.50820	0.09805	0.08836
$a_\rho(s=2)$		0.64268	0.48878	0.52018
$\phi_{b_1}(l=2)$	1.93482		2.04452	2.20155
$\phi_\rho(s=0)$		3.92245	3.82701	4.20950
$\phi_\rho(s=1)$		1.29480	0.23941	0.20171
$\phi_\rho(s=2)$		6.05682	5.83854	6.14483

Table 5.12: Fit results for an $X(0^{++})$, b_1 and $\rho\prime$. b_1 is produced from ${}^3s_1$ and is allowed to decay to $\rho\sigma$. The $\rho\prime$ is produced from ${}^3s_1$ and decays into $\rho^+\rho^-$. The $X(0^{++})$ is produced from ${}^1s_0$, and decays into $\rho^+\rho^-$.

In general the fit is not bad, it just has a rather large number of free parameters, (21). There are four projections whose χ^2/ndf is larger than 2: $\pi^+3\pi^\circ$, $\pi^-3\pi^\circ$, $\pi^+\pi^-$, and one angular distribution. In addition, there are three angular distributions whose χ^2/ndf is larger than 1.3.

In addition, we can fix the mass and width of the $b_1(1235)$ to their PDG values, ($m_b = 1232$, $\Gamma_b = 155$). The results of this are given in the last column of table 5.12. We see that the fit is not as

good as the free fit, but is not terrible. This fit leads to three projections whose χ^2/ndf are larger than 2: $\pi^+3\pi^\circ$, $\pi^-3\pi^\circ$ and $\pi^+\pi^-$. There are also seven projections with χ^2/ndf larger than 1.3: $\pi^+\pi^\circ$, $\pi^-\pi^\circ$, and 5 angular distributions.

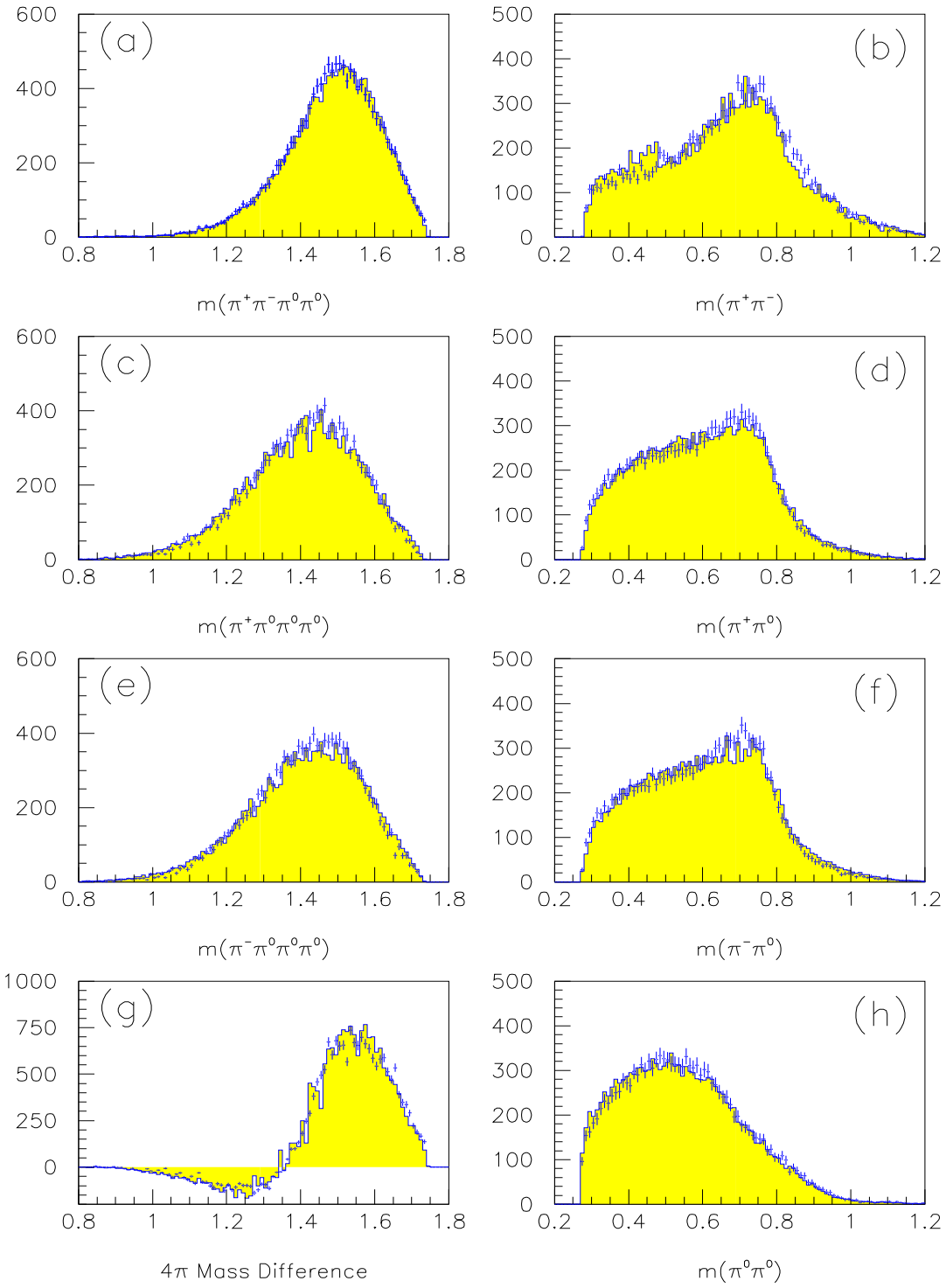

Figure 5.12: Fit results for an $X(0^{++})$, b_1 and $\rho\prime$. b_1 is produced from ${}^3s_1$ and is allowed to decay to $\rho\sigma$. The $\rho\prime$ is produced from ${}^3s_1$ and decays into $\rho^+\rho^-$. The $X(0^{++})$ is produced from ${}^1s_0$, and decays into $\rho^+\rho^-$. The fit has problems in **b**, **d** and **f**. However, the problems appear quite a bit less than previous fits.

5.3.5 $b_1 \to \rho\sigma$, $\rho\prime \to \rho^+\rho^-$, $X(0^{++}) \to \rho^+\rho^-$ & $\sigma\sigma$

Here we take the amplitude of section 5.3.4 as a staring point, and allow a second 0^{++} object, f_0 to decay to $\sigma\sigma$. The amplitude for this is given as:

$$w = f_{[1s0]} \cdot \mid A_{[1s0]} \mid^2 + (1 - f_{[1s0]}) \cdot \mid A_{[3s1]} \mid^2$$

where

$$\begin{aligned}
A_{[1s0]} &= a_{x\to\rho\rho} \cdot A_{[x\to\rho\rho]} + a_{x\to\sigma\sigma} \cdot e^{-i\cdot\phi_{x\to\sigma\sigma}} \cdot A_{[x\to\sigma\sigma]} \\
\\
A_{[3s1]} &= a_{b1} \cdot (1 - a_{l=2}^2)^{\frac{1}{2}} \cdot A(b_1)^1_{[l=0]} \\
&+ a_{b1} \cdot a_{l=2} \cdot e^{-i\cdot\phi_{b1}} \cdot A(b_1)^1_{[l=2]} \\
&+ a_{\rho[s=0]} \cdot e^{-i\cdot\phi_{\rho[s=0]}} \cdot A(\rho)_{[s=0]} \\
&+ a_{\rho[s=1]} \cdot e^{-i\cdot\phi_{\rho[s=1]}} \cdot A(\rho)_{[s=1]} \\
&+ a_{\rho[s=2]} \cdot e^{-i\cdot\phi_{\rho[s=2]}} \cdot A(\rho)_{[s=2]}
\end{aligned}$$

The results of this fit are shown in table 5.13, and several mass projections are shown in figure 5.13.

Parameter Name	*Mass Free* $b_1 + \rho\prime + X(0)$		*Mass Fixed*(†)
	$\rho\rho$	$\rho\rho\&\sigma\sigma$	$\rho\rho\&\sigma\sigma$
$-2\ln\mathcal{L}$	-10232.1	-10351.8	-9954.5
χ^2/ndf	1.1518	1.0597	1.1758
$m_X(0^{++})$	1354.97	1415.09	1391.06
$\Gamma_X(0^{++})$	400.88	391.85	397.27
m_{b_1}	1200.12	1277.40	1232†
Γ_{b1}	1121.75	483.60	155†
m_ρ	1495.07	1524.45	1438.36
Γ_ρ	289.90	493.09	461.13
f_{1s0}	0.35640	0.44901	0.41555
$a_{x\to\rho\rho}$	1.0	0.96448	0.90983
$a_{x\to\sigma\sigma}$		0.26416	0.41497
a_{b_1}	0.75956	0.78698	0.66681
$a_{b_1}(l=2)$	0.34615	0.49930	0.45814
$a_\rho(s=0)$	0.41780	0.37665	0.48058
$a_\rho(s=1)$	0.09805	0.07100	0.12817
$a_\rho(s=2)$	0.48878	0.48348	0.55497
$\phi_{x\to\sigma\sigma}$		3.50866	3.51733
$\phi_{b_1}(l=2)$	2.04452	1.90223	2.12105
$\phi_\rho(s=0)$	3.82701	4.32288	4.43104
$\phi_\rho(s=1)$	0.23941	0.51046	0.89814
$\phi_\rho(s=2)$	5.83854	6.20256	0.06700

Table 5.13: Fit results for an $X(0^{++})$, b_1 and $\rho\prime$. b_1 is produced from ${}^3s_1$ and is allowed to decay to $\rho\sigma$. The $\rho\prime$ is produced from ${}^3s_1$ and decays into $\rho^+\rho^-$. The $X(0^{++})$ is produced from ${}^1s_0$, and decays into both $\rho^+\rho^-$ and $\sigma\sigma$.

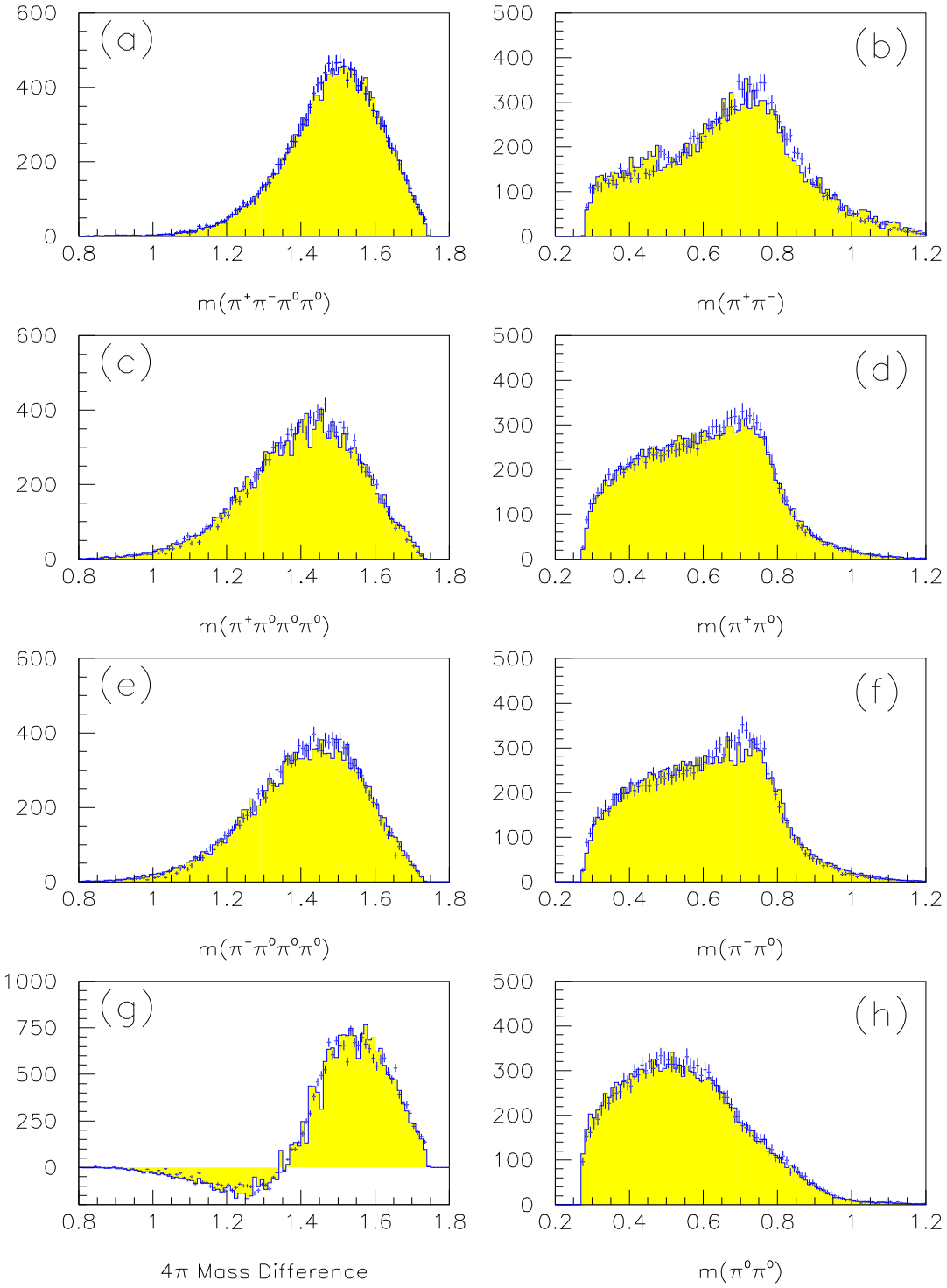

Figure 5.13: Fit results for $b_1 \to \rho\sigma$, $\rho^0\prime \to \rho^+\rho^-$, $X(0^{++}) \to \rho^+\rho^-$ & $\sigma\sigma$. The b_1 and $\rho\prime$ are produced from ${}^3s_1$ while the $X(0^{++})$ is produced from ${}^1s_0$.

5.3.6 $b_1 \to \rho\sigma$, $\rho\prime \to \rho^+\rho^-$, $X(0^{++}) \to \rho^+\rho^-$ and $f_0(1560) \to \sigma\sigma$

Here we take the amplitude of section 5.3.4 as a staring point, and allow a second 0^{++} object, f_0 to decay to $\sigma\sigma$. The amplitude for this is given as:

$$w = f_{[1s0]} \cdot \mid A_{[1s0]} \mid^2 + (1 - f_{[1s0]}) \cdot \mid A_{[3s1]} \mid^2$$

where

$$A_{[1s0]} = a_x \cdot A_{[x \to \rho\rho]} + a_{f0} \cdot e^{-i \cdot \phi_{f0}} \cdot A_{[f0 \to \sigma\sigma]}$$

$$\begin{aligned} A_{[3s1]} &= a_{b1} \cdot (1 - a_{l=2}^2)^{\frac{1}{2}} \cdot A(b_1)^1_{[l=0]} \\ &+ a_{b1} \cdot a_{l=2} \cdot e^{-i \cdot \phi_{b1}} \cdot A(b_1)^1_{[l=2]} \\ &+ a_{\rho[s=0]} \cdot e^{-i \cdot \phi_{\rho[s=0]}} \cdot A(\rho)_{[s=0]} \\ &+ a_{\rho[s=1]} \cdot e^{-i \cdot \phi_{\rho[s=1]}} \cdot A(\rho)_{[s=1]} \\ &+ a_{\rho[s=2]} \cdot e^{-i \cdot \phi_{\rho[s=2]}} \cdot A(\rho)_{[s=2]} \end{aligned}$$

Parameter	*Mass Free* $b_1 + \rho\prime$		*Mass Fixed*(†) $b_1 + \rho\prime$	
Name	$+X(0^{++})$	$+X(0^{++}) + f_0$	$+X(0^{++})$	$+X(0^{++}) + f_0$
$-2\ln\mathcal{L}$	-10232.1	-10509.4	-9628.4	-10467.8
χ^2/ndf	1.1518	1.0666	1.3025	1.0610
$m_X(0^{++})$	1354.97	1347.43	1356.29	1342.98
$\Gamma_X(0^{++})$	400.88	446.51	415.56	486.61
m_{f0}		1419.80		1560.†
Γ_{f0}		368.80		245.†
m_{b_1}	1200.12	1250.75	1232.†	1273.11
Γ_{b1}	1121.75	925.71	155.†	817.07
m_ρ	1495.07	1500.04	1431.87	1473.31
Γ_ρ	289.90	491.49	293.62	628.12
f_{1s0}	0.35640	0.39748	0.34966	0.39052
a_x		0.95424		0.95988
a_{f0}		0.29904		0.28040
a_{b_1}	0.75956	0.77173	0.66700	0.75990
$a_{b_1}(l=2)$	0.34615	0.30898	0.41510	0.32987
$a_\rho(s=0)$	0.41780	0.39198	0.52218	0.41584
$a_\rho(s=1)$	0.09805	0.14934	0.08836	0.09607
$a_\rho(s=2)$	0.48878	0.47802	0.52018	0.49031
ϕ_{f0}		3.48267		4.20081
$\phi_{b_1}(l=2)$	2.04452	2.08402	2.20155	2.13540
$\phi_\rho(s=0)$	3.82701	3.89479	4.20950	3.87131
$\phi_\rho(s=1)$	0.23941	0.54872	0.20171	0.43425
$\phi_\rho(s=2)$	5.83854	5.79657	6.14483	5.76399

Table 5.14: Fit results for an $X(0^{++})$, b_1 and $\rho\prime$. b_1 is produced from $^3s_1$ and is allowed to decay to $\rho\sigma$. The $\rho\prime$ is produced from $^3s_1$ and decays into $\rho^+\rho^-$. The $X(0^{++})$ is produced from $^1s_0$, and decays into $\rho^+\rho^-$.

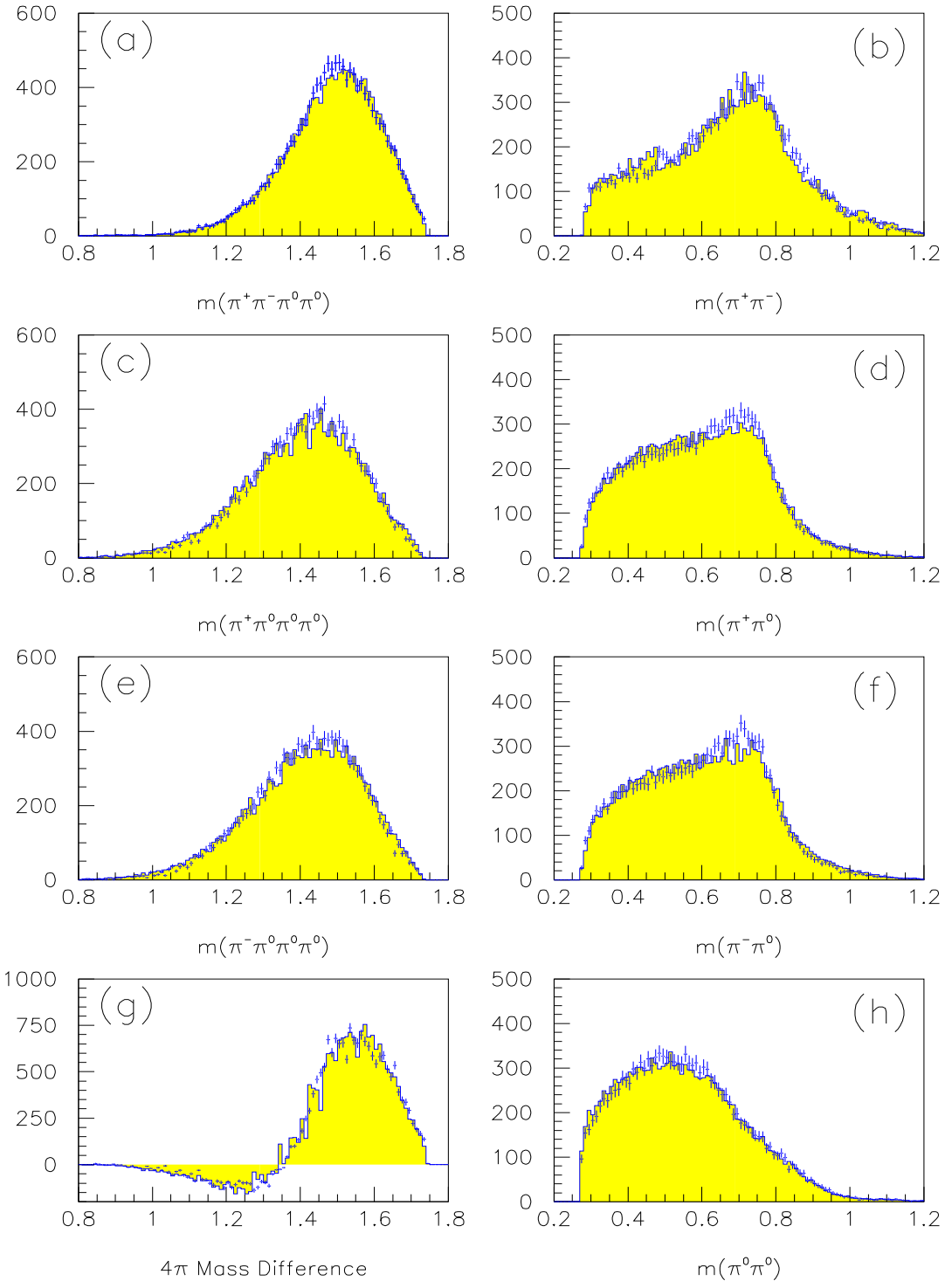

Figure 5.14: Fit results for $b_1 \to \rho\sigma$, $\rho' \to \rho^+\rho^-$, $X(0^{++}) \to \rho^+\rho^-$ and $f_0(1560) \to \sigma\sigma$. The b_1 and ρ' are produced from $^3s_1$ while the two 0^{++} objects are produced from $^1s_0$. The fit has trouble in the low mass region of the $\pi^+\pi^-$ invariant mass, **b**.

5.3.7 $b_1 \to \rho\sigma$, $\rho\prime \to \rho^+\rho^-$, $X(0^{++}) \to \rho^+\rho^-$ and $f_2(1520) \to \rho^+\rho^-$

Here we take the amplitude of section 5.3.4 as a staring point, and allow a 2^{++} object, f_2 to decay to $\rho^+\rho^-$. The amplitude for this is given as:

$$w = f_{[1s0]} \cdot \mid A_{[1s0]} \mid^2 + (1 - f_{[1s0]}) \cdot \mid A_{[3s1]} \mid^2$$

where

$$A_{[1s0]} = a_x \cdot A_{[x\to\rho\rho]} a_{f2} \cdot e^{-i\cdot\phi_{f2}} \cdot A_{[f2\to\rho\rho]}$$

$$\begin{aligned} A_{[3s1]} &= a_{b1} \cdot (1 - a_{l=2}^2)^{\frac{1}{2}} \cdot A(b_1)^1_{[l=0]} \\ &+ a_{b1} \cdot a_{l=2} \cdot e^{-i\cdot\phi_{b1}} \cdot A(b_1)^1_{[l=2]} \\ &+ a_{\rho[s=0]} \cdot e^{-i\cdot\phi_{\rho[s=0]}} \cdot A(\rho)_{[s=0]} \\ &+ a_{\rho[s=1]} \cdot e^{-i\cdot\phi_{\rho[s=1]}} \cdot A(\rho)_{[s=1]} \\ &+ a_{\rho[s=2]} \cdot e^{-i\cdot\phi_{\rho[s=2]}} \cdot A(\rho)_{[s=2]} \end{aligned}$$

Parameter	*Mass Free* $b_1 + \rho\prime$		*Mass Fixed*(†) $b_1 + \rho\prime$	
Name	$+X(0^{++})$	$+X(0^{++}) + f_2$	$+X(0^{++})$	$+X(0^{++}) + f_2$
$-2\ln\mathcal{L}$	-10232.1	-10527.3	-9628.4	-10516.4
χ^2/ndf	1.1518	1.0765	1.3025	1.0922
$m_X(0^{++})$	1354.97	1418.19	1356.29	1410.68
$\Gamma_X(0^{++})$	400.88	288.18	415.56	302.87
m_{f2}		2243.92		1520.†
Γ_{f2}		127.99		120.†
m_{b_1}	1200.12	1308.45	1232.†	1346.54
Γ_{b1}	1121.75	1376.32	155.†	1753.13
m_ρ	1495.07	1535.38	1431.87	1519.22
Γ_ρ	289.90	494.22	293.62	495.32
f_{1s0}	0.35640	0.38332	0.34966	0.37972
a_x		0.94007		0.94662
a_{f2}		0.34098		0.32236
a_{b_1}	0.75956	0.74817	0.66700	0.74387
$a_{b_1}(l=2)$	0.34615	0.32329	0.41510	0.33409
$a_\rho(s=0)$	0.41780	0.45702	0.52218	0.45429
$a_\rho(s=1)$	0.09805	0.08690	0.08836	0.09664
$a_\rho(s=2)$	0.48878	0.47311	0.52018	0.48056
ϕ_{f2}		5.79558		5.72279
$\phi_{b_1}(l=2)$	2.04452	2.09831	2.20155	2.03225
$\phi_\rho(s=0)$	3.82701	3.80653	4.20950	3.65623
$\phi_\rho(s=1)$	0.23941	0.28098	0.20171	0.41374
$\phi_\rho(s=2)$	5.83854	5.84446	6.14483	5.71767

Table 5.15: Fit results for an $X(0^{++})$, b_1 and $\rho\prime$. b_1 is produced from $^3s_1$ and is allowed to decay to $\rho\sigma$. The $\rho\prime$ is produced from $^3s_1$ and decays into $\rho^+\rho^-$. The $X(0^{++})$ is produced from $^1s_0$, and decays into $\rho^+\rho^-$.

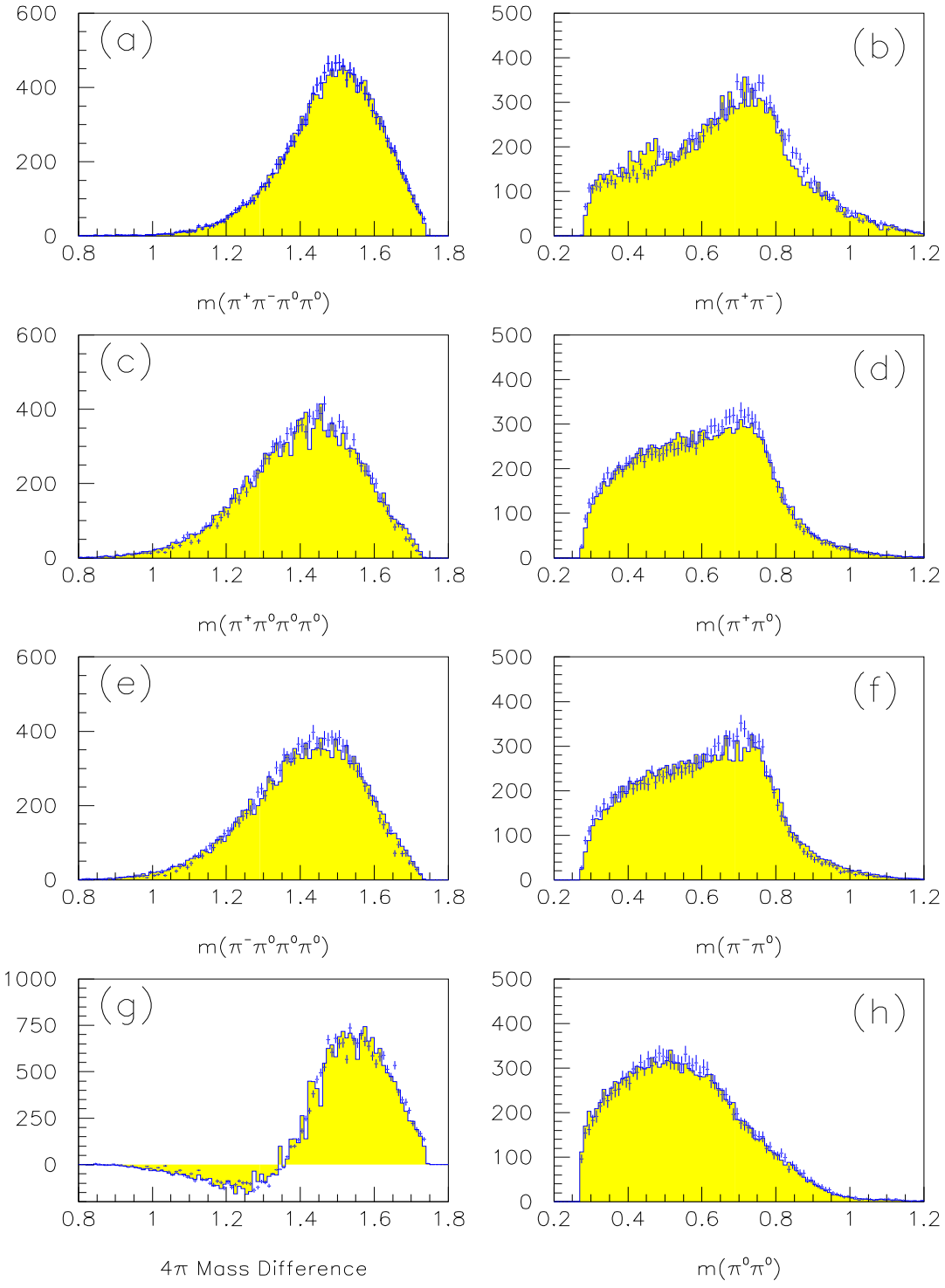

Figure 5.15: Fit results for $b_1 \to \rho\sigma$, $\rho^0\prime \to \rho^+\rho^-$, $X(0^{++}) \to \rho^+\rho^-$ and $f_2(1520) \to \rho\rho$. The b_1 and $\rho\prime$ are produced from $^3s_1$ while the two 0^{++} objects are produced from $^1s_0$. The fit has trouble in the low mass region of the $\pi^+\pi^-$ invariant mass, **b**. It also has problems in **a**, **f**, **g** and **h**.

6 Summary

First of all, we measure the branching fraction into $\pi^+\pi^-\pi^\circ\pi^\circ\pi^\circ$.

$$BR(\bar{p}p \to \pi^+\pi^-\pi^\circ\pi^\circ\pi^\circ) = 0.091 \pm 0.004$$

and we can then determine that after we have excluded the ω and η from the final state, that:

$$BR(\bar{p}p \to \pi^+\pi^-\pi^\circ\pi^\circ\pi^\circ) = 0.067 \pm 0.004.$$

We have also carried out a rather complicated spin parity analysis of the full $\pi^+\pi^-\pi^\circ\pi^\circ\pi^\circ$ final state. Even though we cannot completely identify everything in the $\pi^+\pi^-\pi^\circ\pi^\circ\pi^\circ$ final state, there are several strutures that seem indisputable. Firstly, the dominant structure in $\rho^+\rho^-$ is an isoscaler $J^{PC} = 0^{++}$ object, ($f_0(1440)$).

$$\begin{aligned} m_{f0} &= 1437 \pm 13 MeV/c^2 \\ \Gamma_{f0} &= 352 \pm 43 MeV/c^2 \end{aligned}$$

In addition, we also see strong evidence for the $\sigma\sigma$ deacy of $f_0(1440)$, (table reftab:x02d). Using isospin arguments, we can derive that:

$$\frac{BR(f_0 \to \rho\rho)}{BR(f_0 \to \sigma\sigma)} \approx 2.08$$

We also can derive the following branching fractions:

$$\begin{aligned} BR(\bar{p}p \to f_0\pi^\circ \to \rho^+\rho^-\pi^\circ \to \pi^+\pi^-\pi^\circ\pi^\circ\pi^\circ) &\approx 0.0223 \\ BR(\bar{p}p \to f_0\pi^\circ \to \sigma\sigma\pi^\circ \to \pi^+\pi^-\pi^\circ\pi^\circ\pi^\circ) &\approx 0.00640 \end{aligned}$$

Section	*Comments*	*mass*	*width*	*B.F.* $\rho^+\rho^-$	*B.F.* $\sigma\sigma$
5.2.2	$\rho\prime$	1437.13	365.85	0.01999	0.00640
5.3.3	b_1	1414.43	387.86	0.02985	0.00319
5.3.5	$b_1\rho$	1415.09	391.85	0.02798	0.00210

Table 6.1: A summary of the mass, width and branching fraction for the 0^{++} object decaying into both $\rho\rho$ and $\sigma\sigma$.

We also find that the data slightly favor two 0^{++} objects. One decaying into $\rho^+\rho^-$, and the second decaying into $\sigma\sigma$. A summary of these results are shown in table 6.2. We have seen that the results are not very sensitive to the mass and width of this second object. We also see that the inclusion of a $b_1 \to \rho\sigma$ tends to reduce the need for this second object.

We have also looked for a $J^{PC} = 2^{++}$ object decaying to $\rho^+\rho^-$. We find no clear signal for this object, but the data are consistent with some small admixture. However, the results have a much larger scatter than that for the 0^{++} of above, (see table 6.3). As such it is rather difficult to conclude there is really a 2^{++} contribution. However, when we force the mass and width to 1520 MeV/c^2 and 120 MeV/c^2, we find that the data are consistent with the following, (assuming only initial S states):

$$BR\left[\bar{p}p \to f_2(1520)\pi^\circ \to \rho^+\rho^-\pi^\circ\right] \approx 0.0020.$$

Then using the results on $^1s_0$ production of the f_2 from our $3\pi^\circ$ analysis [16] we estimate that:

$$\frac{X_2 \to \rho\rho}{X_2 \to \pi\pi} = \frac{0.00302}{0.00285} =\sim 1.06.$$

Section	*Comments*	*mass*	*width*	*B.F.*
5.3.2	f_0 free	1458.30	204.74	0.00627
5.3.2	f_0 fixed	1560†	245†	0.00613
5.3.3	f_0 free	1444.95	165.25	0.00294
5.3.3	f_0 fixed	1560†	245†	
5.3.6	f_0 free	1419.80	368.80	0.00238
5.3.6	f_0 fixed	1560†	245†	0.00206

Table 6.2: A summary of the mass, width and branching fraction for a 2'nd 0^{++} object. The branching fraction is taken as $\bar{p}p$ into $f_0\pi^\circ$, with f_0 then decaying into $\sigma\sigma$. One σ then decays to $\pi^+\pi^-$, and the second to $\pi^\circ\pi^\circ$.

However, this result depends very strongly on numbers in the $3\pi^\circ$ analysis that may change with the higher statistics currently being analyzed. This search for the $f_2(1520)$ in $\rho\rho$ probably needs to wait for data from a gas target.

Finally, it appears that most, (55% — 65%) of the $\pi^+\pi^-\pi^\circ\pi^\circ\pi^\circ$ final state comes from the $^3S_1$ initial state, and proceeds through an isovector, $J = 1$ object. Unfortunately, it is not certain what this isovector object is. We have tried $\rho\prime \to \rho\sigma$, $b_1 \to \rho\sigma$, and $\rho^\circ\prime \to \rho^+\rho^-$, as well as combinations of these. Even though the data can be described reasonable well, the mass and widths found for these objects do not normally make much sense. In particular, for the $\rho\prime \to \rho\sigma$, we always find a mass of about 700 MeV/c^2 and a width of 700 MeV/c^2. However, atributing this to the tail of the normal $\rho(770)$ would imply the 4π and 2π decays of the $\rho(770)$ are of similar size. For the $b_1 \to \rho\sigma$, we find a mass of about 1300 MeV/c^2 and a width of 400 — 500 MeV/c^2. Finally, for the $\rho^\circ\prime \to \rho^+\rho^-$ we find resonably sensible numbers. A mass of 1400 — 1550 MeV/c^2 and a width of 300 — 500 MeV/c^2 seem acceptable. However this is insuffucient to explain the data. In terms of obtaining nearly sensible masses and widths, this latter two $J = 1$ hypothesis seem the most promising. It may eventually turn out that we are required to allow a small contribution for initial P states, but until now this has not been attempted.

Section	*Comments*	*mass*	*width*	*B.F.*
5.2.3	free	1245.82	159.16	0.00179
5.2.3	fixed	1520†	120†	0.00201
5.2.4	b_1	1736.30	179.59	0.00275
5.3.7	ρb_1	2243.92	127.99	0.00298
5.3.7	ρb_1	1520†	120†	0.00264

Table 6.3: A summary of the mass, width and branching fraction for the 2^{++} object. The branching fraction is taken as $\bar{p}p$ into $f_2\pi^\circ$, with f_2 then decaying into $\rho^+\rho^-$.

A Angular Distributions

In this section, I present 24 angular distributions from the fit in section 5.2.2, ($\rho\prime \rightarrow \rho\sigma$, and $X(0^{++}) \rightarrow \rho^+\rho^-$ & $\sigma\sigma$). Figure A.1 shows eight projections of angles from the deacy of the 4π object A into the two 2π objects B and C. The angles are computed in the rest frame of A. Note the cryptic captions. **a** and **b** assume a neutral A, $(\pi^+\pi^-\pi^\circ\pi^\circ)$ decaying into a neutral B, $(\pi^+\pi^-)$, and a neutral C, (π°). **c** and **d** assume a neutral A, $(\pi^+\pi^-\pi^\circ\pi^\circ)$ decaying into a charged B, $(\pi^+\pi^\circ)$ and a charged C, $(\pi^-\pi^\circ)$. **e** and **f** assume a postively charged A , $(\pi^+3\pi^\circ)$ deacaying into a positevely cahrged B, $(\pi^+\pi^\circ)$, and a neutral C, $(\pi^\circ\pi^\circ)$. Finally, **g** and **h** assume a negatively charged A, $(\pi^-3\pi^\circ)$ deacying to a negative B, $(\pi^-\pi^\circ)$ and a neutral C, $(\pi^\circ\pi^\circ)$.

Figure A.2 shows eight projections of angles from the decay of the B into $\pi\pi$. The angles are in the rest frame of the B. The eight cases correspond to the cases described above.

Figure A.3 shows eight projections of angles from the decay of the C into $\pi\pi$. The angles are in the rest frame of the C. The eight cases correspond to the cases described above.

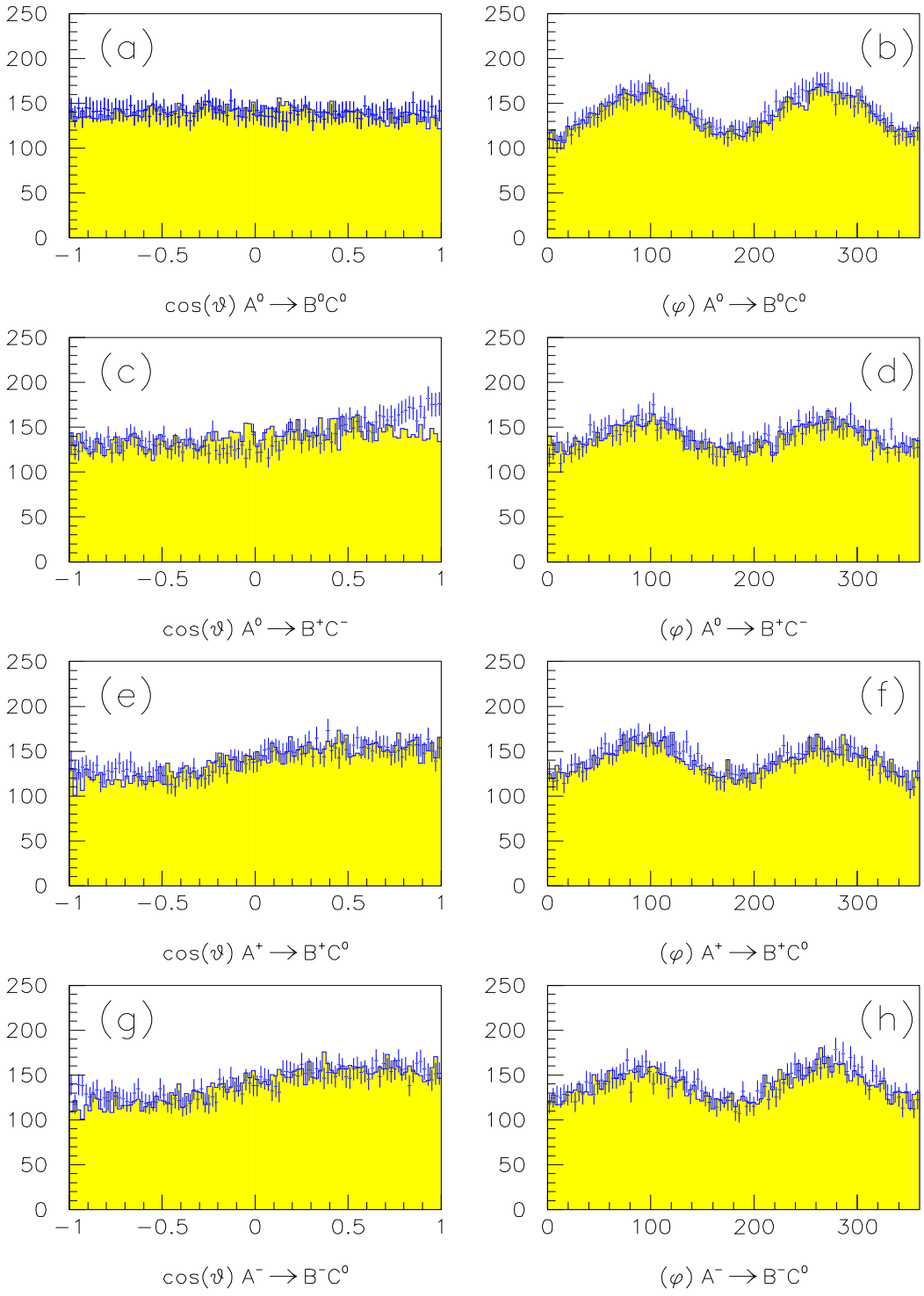

Figure A.1: Angular distributions for $A \to BC$.

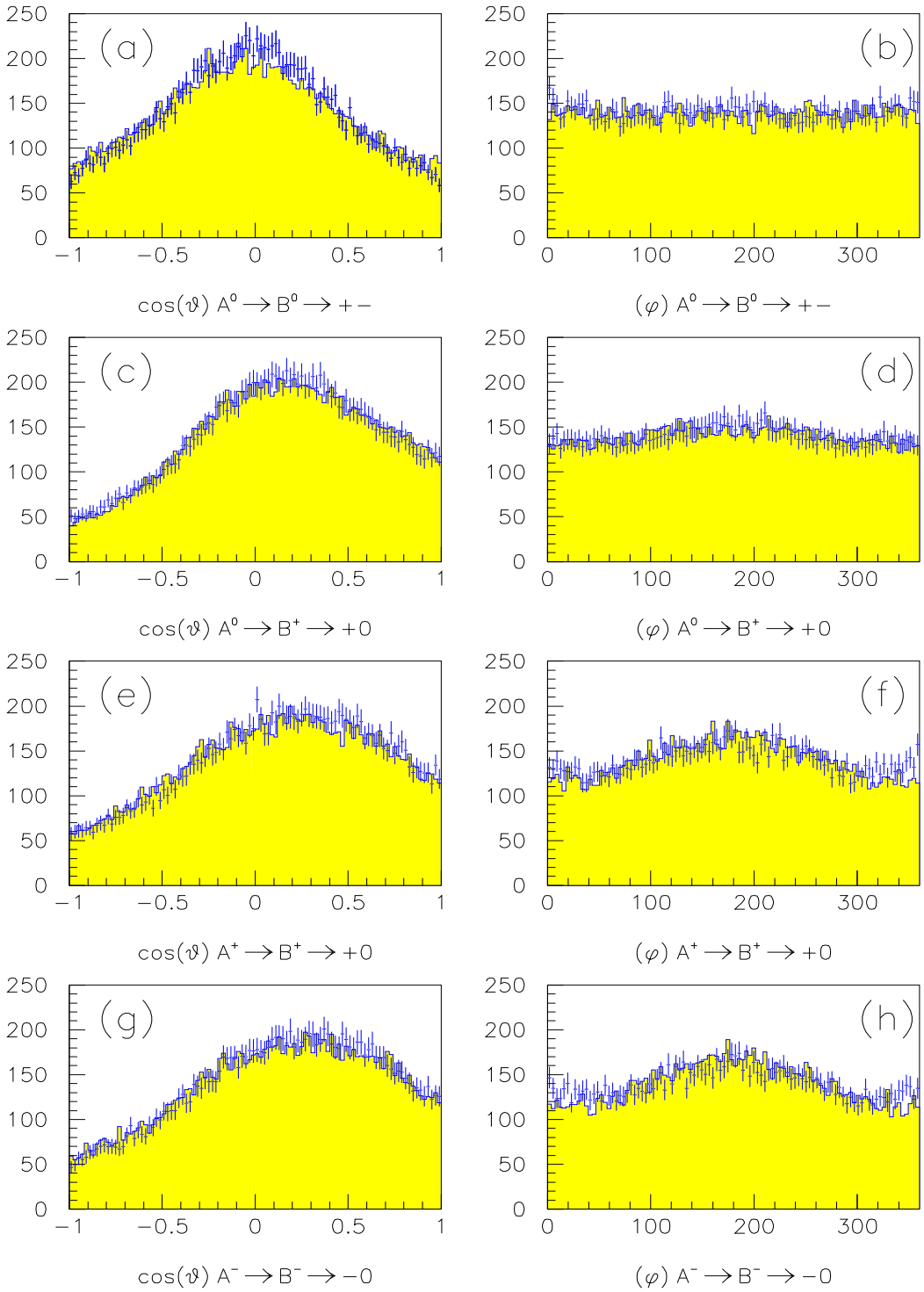

Figure A.2: Angular distributions for $B \to \pi\pi$.

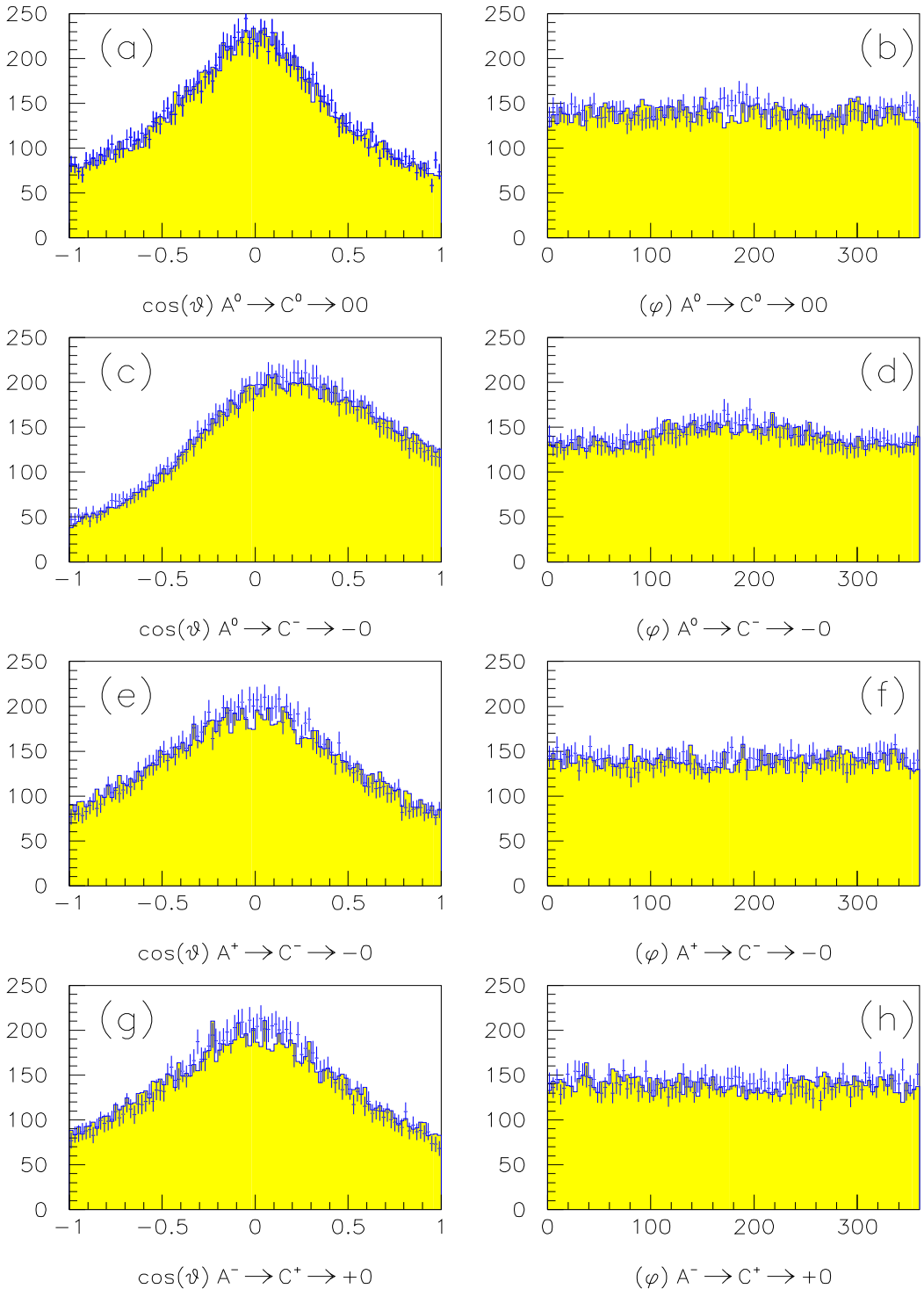

Figure A.3: Angular distributions for $C \to \pi\pi$.

References

[1] C. A. Meyer, **The analysis of $\bar{p}p \to \pi^+\pi^-\pi^\circ\pi^\circ\pi^\circ$ in the $\pi^+\pi^-6\gamma$ Final State. Part 1: $\omega\pi^\circ\pi^\circ$, $\eta\pi^\circ\pi^\circ$ and $\eta\pi^+\pi^-$**, CB–Note 197, (1992).

[2] C. Baltay, P. Franzini, G. Lütjens, J. C. Severiens, D. Tycko and D. Zanello, **Phys. Rev. 145**, 1103, (1966).

[3] C. Defoix and P. Espigat, **Experimental Analysis of the Reaction $\bar{p}p \to \pi^+\pi^-\pi^+\pi^-\pi^\circ$ at Rest (Non–ω° Events). Evidence for a $\rho^\circ\rho^\circ$ Effect Around 1440 MeV.** CERN–74–18, p.28, (1974).

[4] A. Bettini *et al.*, **Nuovo Cimento 42A**, 695, (1966).

[5] D. Bridges, I. Daftari and T. E. Kalogeropoulos, **Phys. Rev. Lett. 56**, 214, (1986) and **Phys. Rev. Lett. 57**, 1534, (1986).

[6] H. Albrecht, *et. al.*, The ARGUS Collaboration, **Phys. Lett. B217**, 205, (1989); **Phys. Lett B276**, 535, (1991).

[7] Mario Gaspero, **Soviet J. of Nucl. Phys. 55**, 795, (1992).

[8] Kay Könogsmann, **Fits to Unbinned Data**, CB–Note 195, May 1992.

[9] C. Amsler, **Likelihood Fitting**, CB–Note 1xx, May 1992.

[10] M. Locher, Private communication.

[11] **GENBOD N–Body Monte Carlo Generator**, Cern Program Library W515.

[12] R. Bossingham, **LEAR Crystal Barrel Experiment, PS197 Monte Carlo Software, CBGEANT 4.06/02**, CB–Note 169, (1992).

[13] C. Amsler and J. C. Bizot, **Comp. Phys. Comm. 30**, 21, (1983).

[14] K. L. Au *et al.*, **Phys. Rev. D35**, 1633, (1987).

[15] S. U. Chung, **Formulas for Partial–Wave Analysis**, BNL Report, April 1989.

[16] E. Aker *et. al.*, The Crystal Barrel Collaboration, **Phys. Lett. B260** 249, (1991).

[17] C. Amsler *et al.*, The Crystal Barrel Collaboration, **Phys. Lett. B291**, 347, (1992).